Infrared fibers

Guangming Tao,[1] Heike Ebendorff-Heidepriem,[2] Alexander M. Stolyarov,[3] Sylvain Danto,[4] John V. Badding,[5] Yoel Fink,[6] John Ballato,[7] and Ayman F. Abouraddy[1,*]

[1]CREOL, The College of Optics & Photonics, University of Central Florida, 4000 Central Florida Blvd., Orlando, Florida 32816, USA

[2]Institute of Photonics and Advanced Sensing, School of Chemistry and Physics, ARC Centre of Excellence for Nanoscale BioPhotonics, The University of Adelaide, Adelaide SA 5005, Australia

[3]MIT Lincoln Laboratory, Massachusetts Institute of Technology, 244 Wood St., Lexington, Massachusetts 02420, USA

[4]ICMCB/CNRS University of Bordeaux, 87 Avenue du Dr. Schweitzer, 33608 Pessac, France

[5]Department of Chemistry, Department of Physics & Astronomy, Pennsylvania State University, University Park, State College, Pennsylvania 16802, USA

[6]Research Laboratory of Electronics, Massachusetts Institute of Technology, 77 Massachusetts Ave., Cambridge, Massachusetts 02139, USA

[7]Center for Optical Materials Science and Engineering Technologies (COMSET), Department of Materials Science & Engineering, Clemson University, 101 Sikes Ave., Clemson, South Carolina 29634, USA

*Corresponding author: raddy@creol.ucf.edu

Received October 7, 2014; revised April 7, 2015; accepted April 8, 2015; published June 15, 2015 (Doc. ID 224556)

Infrared (IR) fibers offer a versatile approach to guiding and manipulating light in the IR spectrum, which is becoming increasingly more prominent in a variety of scientific disciplines and technological applications. Despite well-established efforts on the fabrication of IR fibers in past decades, a number of remarkable breakthroughs have recently rejuvenated the field—just as related areas in IR optical technology are reaching maturation. In this review, we describe both the history and recent developments in the design and fabrication of IR fibers, including IR glass and single-crystal fibers, multimaterial fibers, and fibers that exploit the transparency window of traditional crystalline semiconductors. This interdisciplinary review will be of interest to researchers in optics and photonics, materials science, and electrical engineering.

OCIS codes: (060.2310) Fiber optics; (060.2390) Fiber optics, infrared; (060.2400) Fiber properties; (060.4005) Microstructured fibers; (160.2290) Fiber materials; (190.4370) Nonlinear optics, fibers
http://dx.doi.org/10.1364/AOP.7.000379

1. Introduction. 381
2. Infrared Materials. 385
3. Criteria for Drawing an Infrared Fiber. 389
4. Infrared Fiber Fabrication Methodologies. 392
4.1. Preform-to-Fiber Approaches. 393
4.1a. Step-Index Fibers. 393
4.1b. IR Microstructure Fibers. 397
4.2. Non-Preform-Based Approaches. 398
5. Heavy Metal Oxide Glass Infrared Fibers 400
5.1. Tellurite Glass Infrared Fibers. 400
5.2. (Lead)–Germanate and Tungsten–Tellurite-Glass Infrared Fiber. . 403
6. Fluoride Glass Infrared Fibers 404
6.1. ZBLAN Glass Fibers. 405
6.2. Fluoroindate Glass Fibers. 406
7. Chalcogenide Glass Infrared Fibers. 408
7.1. Current Status of Optical Losses in Chalcogenide Glass Fiber . . 410
7.2. Enhancement of Mechanical Robustness. 411
7.3. Multimaterial Infrared Chalcogenide Glass Fibers. 412
7.4. Chalcogenide Glass Infrared Microstructure Fibers. 414
8. Multimaterial Infrared Fibers. 415
8.1. Hollow-Core Multimaterial Photonic Bandgap Infrared Fibers. . . 416
8.2. Thermally Drawn Crystalline Semiconductor Infrared Fibers. . . . 418
8.3. Chemically Deposited Crystalline Semiconductor Infrared Fibers. 419
9. Other Infrared Fibers 421
9.1. Hollow-Core Silica Infrared Fibers. 421
9.2. Hollow Metallic Infrared Fibers. 422
9.3. Crystalline Infrared Fibers by Hot Extrusion 423
9.4. Hybrid Infrared Fibers by Pressure-Assisted Melt Filling 424
10. Future Prospects. 425
Acknowledgments 426
References 427

Infrared fibers

Guangming Tao, Heike Ebendorff-Heidepriem,
Alexander M. Stolyarov, Sylvain Danto, John V. Badding,
Yoel Fink, John Ballato, and Ayman F. Abouraddy

1. Introduction

Infrared (IR) light is electromagnetic radiation that starts from the nominal edge of visible (VIS) light at a wavelength ~0.7 μm and extends up to ~1 mm [1–6]. Interestingly, there appears to be no consensus on either the nomenclature or the limits of the various IR spectral divisions, which usually vary according to the disciplines or applications that exploit the IR [1–6]. For the purposes of this review, we refer to the spectral window 0.7–2 μm as the near-IR (NIR), 2–15 μm as the mid-IR (MIR), and 15 μm–1 mm as the far-IR (FIR). The MIR, therefore, covers the important atmospheric windows of 3–5 μm and 8–12 μm [7], which comprise critical applications in remote sensing, biophotonics, homeland security, and minimally invasive medical surgery, to name just a few.

> "A precise border between 'visible' and 'infrared' cannot be defined, because visual sensation at wavelengths greater than 780 nm is noted for very bright sources at longer wavelengths. In some applications the infrared spectrum has also been divided into 'near,' 'middle,' and 'far' infrared; however, the borders necessarily vary with the application (e.g. in meteorology, photochemistry, optical design, thermal physics, etc.)."
>
> *The International Commission on Illumination (CIE) Standards* [1]

There is currently broad interest in extending optical technologies beyond the VIS and NIR into the less-explored realms of the MIR—driven by multiple opportunities in novel applications. There is also the general sense that the MIR is the next frontier for the optics and photonics community, where unexplored territory awaits to be claimed. The recent interest in the MIR is also partly fuelled by the current availability of MIR semiconductor sources such as quantum cascade lasers (QCLs) [8]. Nevertheless, to fully exploit the MIR, a complete swathe of optical technologies must be developed, including coherent narrowband and broadband sources, sensors, bulk and integrated photonic components, and—critically—IR optical fibers.

In this review, we define **IR optical fibers** as those that transmit radiation of wavelengths from ~2 up to ~25 μm, which extends across both the MIR and FIR. Fixing precise limits to these spectral windows is not germane to our task here, and thus they remain, by necessity, somewhat fuzzy. Such fibers have a rich and long history, dating back to the mid-1960s when the first chalcogenide

glass (ChG) fiber made of the IR glass arsenic trisulfide (As_2S_3) was reported [9]. This early success also highlighted two shortcomings that have been associated with IR fibers since—high optical losses (>10 dB/m in the wavelength range 2–8 μm [9]) and the lack of mechanical robustness. Dramatic improvements have been achieved on both these fronts for IR fibers, which bodes well for their potential widespread adoption in the near future.

In contrast to fibers used in the VIS and NIR where only a few materials dominate (particularly silica glass), a very broad spectrum of materials has been explored for producing IR fibers—ranging from chalcogenide, tellurite, germanate, and fluoride glasses, to crystalline materials such as yttrium aluminum garnet (YAG), and even—most recently—traditional semiconductors such as silicon, germanium, and zinc selenide. In addition to this surprisingly wide span of IR fiber materials investigated, new concepts are being exploited in engineering IR optical guidance. For example, the concept of photonic bandgaps (PBGs) underlies the design of different hollow-core microstructure IR fibers. Furthermore, recent breakthroughs in the compatibility of heterogeneous material families with the process of thermal fiber co-drawing have led to the emergence of a unique class of "multimaterial fibers" that may help address some of the perennial optical and mechanical shortcomings of IR fibers. Indeed, the implications of the multimaterial-fiber concept may even extend beyond IR fibers to lay the foundation for possible convergence of optics and electronics in a monolithic fiber form factor (see the review articles [10,11]).

As such, the field of IR fibers lies at the intersection of materials science, optical physics, and manufacturing engineering—and much recent excitement for such fibers has its origin in the synergy between these communities. The key feature of IR fibers is their ability to transmit wavelengths longer than those afforded by conventional silica glass fibers. Nevertheless, both the optical and mechanical properties of IR fibers remain, in general, inferior to conventional silica fibers. For example, most IR fibers have transmission losses in the ~dB/m range. Their usage, therefore, is limited primarily to short-haul applications requiring only meters rather than kilometers of fiber lengths, which is sufficient for applications in chemical sensing, thermometry, and IR laser power delivery. The repertoire of applications that exploit IR fibers is expanding rapidly, and is expected to continue to do so in the next few decades. In this review, we will focus on the recent progress in developing IR fibers—from the perspective of fabrication and novel materials and structures—against a background of previous achievements. We hope that this venerable but vital field will continue to attract increasing attention from both academia and industry to pave the way for the widespread adoption of IR fibers.

To provide a broad overview of the topics covered in this review, perhaps it is useful to start by giving some examples of the IR fibers we will explore. Figure 1 depicts a selection of 15 different IR fibers produced over the past decade or so, which highlight the broad range of materials and structures that are currently being investigated. Five distinct families of IR fibers are shown. The first family [Figs. 1(a)–1(c)] comprises step-index fibers where the core and cladding are selected from the *same* family of soft IR glass, whether fluoride [Fig. 1(a)] [22], tellurite [Fig. 1(b)] [23], or chalcogenide [Fig. 1(c)] glass [24,25]. These three families of glass have been extensively investigated, and fibers produced from these glasses have indeed been now commercialized.

Figure 1

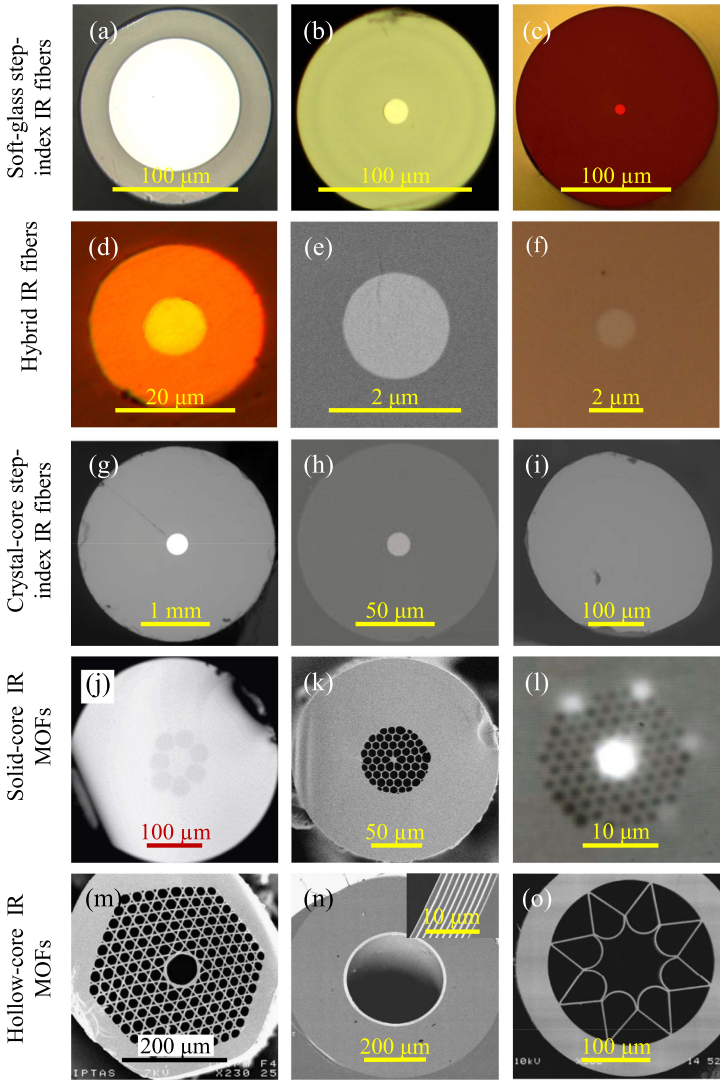

Examples of IR fibers. (a)–(c) Step-index IR fibers in which both the core and cladding belong to the same soft-glass family, in order of increasing long-wave cutoff wavelength: (a) fluoride glass fiber (courtesy of Dr. M. Saad); (b) tellurite glass fiber [12]; and (c) ChG fiber (courtesy of Dr. F. Chenard and IRflex Corporation). (d)–(f) Hybrid step-index fibers that combine heterogeneous materials: (d) step-index ChG fiber with a built-in polymer jacket [13]; (e) ChG core, silica cladding fiber [14]; (f) ChG core, tellurite cladding fiber [15]. (g)–(i) Crystalline-core step-index IR fibers: (g) InSb core, borosilicate glass cladding fiber [16]; (h) ZnSe core, silica cladding fiber [17]; (i) YAG fiber (courtesy of Dr. J. A. Harrington). (j)–(l) Solid-core microstructure IR fibers: (j) all-solid ChG PCF [18]; (k) fluoride PCF (courtesy of Dr. P. Russell); (l) ChG PCF (courtesy of Dr. J. S. Sanghera) [19]. (m)–(o) Hollow-core IR fibers: (m) hollow-core ChG PBG fiber [20]; (n) hollow-core fiber lined with a one-dimensional Bragg structure with an omnidirectional reflection [21]; (o) hollow-core IR silica fiber with negative curvature (courtesy Dr. J. C. Knight). (b) and (j): Reprinted with permission from Refs. [12] and [18], respectively. Copyright 2015 IEEE. (m): Reprinted with permission from [20]. Copyright 2015 Elsevier.

The second family in Fig. 1 [Figs. 1(d)–1(f)] comprises recently developed hybrid IR fibers where materials from heterogeneous families of materials are combined: chalcogenide glasses with a polymer [Fig. 1(d)], chalcogenide and silica glasses [Fig. 1(e)], and chalcogenide and tellurite glasses [Fig. 1(f)]. In each example, the juxtaposition and integration of two (or more) different materials in the fiber allows for a unique feature to be exploited for performance enhancement, whether mechanical strength or optical functionality.

The third family is that of IR crystalline-core fibers. One such example, YAG fibers [Fig. 1(i)], has been explored for decades, while others have only been recently investigated, such as InSb [Fig. 1(g)] and ZnSe [Fig. 1(h)] fibers. The latter examples may help usher in a new class of fibers where integration among optics, electronics, and optoelectronics could prove feasible [10,26,27].

More recently, a fourth family of solid-core IR photonic crystal fibers (PCFs) have been produced and studied. Examples include all-solid PCFs [Fig. 1(j)] and air-hole-clad PCFs [Figs. 1(k) and 1(l)] realized in either chalcogenide glass or fluoride glass. One may also add to this class so-called suspended-core fibers that have been realized using a wide range of soft glasses [28,29] and are lending themselves to dispersion engineering and nonlinearity enhancement, which are critical enablers for applications in nonlinear IR wavelength conversion [30,31].

Finally, a fifth family of hollow-core IR fibers is highlighted in Fig. 1, extending from PBG fibers [Fig. 1(m)] with air holes arranged in a two-dimensional lattice in the cladding to exploit a strategy that has proven successful in silica PBG fibers, to hollow-core fibers lined with a one-dimensional periodic photonic structure that provides optical guidance via omnidirectional reflection [32]. The latter fiber has been commercialized [33] for minimally invasive surgery and has helped save or improve thousands of lives to date. A recently emerging paradigm of distinct nature is shown in Fig. 1(o) where a hollow-core silica fiber with negative curvature exploits an interference effect to guide light in the core and minimize the overlap with the silica glass.

We are targeting multiple communities in optical and materials science and engineering with this review. First, for the sake of those readers whose work would be facilitated by the use of IR fibers, as silica fibers have done for the VIS and NIR, this review brings together the characteristics of various fiber material systems, which will hopefully then help inform the assessment of their choices. Second, for those engaged in IR fiber fabrication, this review brings together the vast repertoire of materials and processing approaches that have been developed in this area. The goal of this review is to provide a comprehensive survey that illuminates by virtue of the broad coverage and thus enables the cross-fertilization of ideas and concepts.

The paper is organized as follows. Section 2 presents the various classes of optical materials that are transparent in the IR. Although it was thought that some of these materials (such as crystalline semiconductors) are incompatible with the conventional process of thermal fiber drawing from a scaled-up preform, recent breakthroughs have proven this conventional wisdom lacking. Section 3 addresses the criteria for thermal fiber drawing and explains in the process how these recent unexpected achievements came about. Section 4 provides an outline of the various fabrication techniques that have been employed to date in producing IR fibers. The situation here is quite different from that in silica fibers, where one or two strategies [modified chemical vapor deposition (MCVD), and

stack-and-draw processes] have proven to be silver bullets that provide for almost all the needs of the silica fiber community. The broad range of heterogeneous materials of interest in the IR has led by necessity to the development of a variety of processing techniques. The choice of any such method is nevertheless constrained by the choice of material(s) to be incorporated in the fiber, and also by the fiber structure and feature dimension to be realized.

Next, we review the state-of-the-art of IR fibers made of particular glass systems, namely tellurite (Section 5), fluoride (Section 6), and chalcogenide (Section 7) glasses. In Section 7 we highlight the recent work on exploiting the concept of multimaterial fibers (here the combination of chalcogenide glasses and polymers) to address the lack of mechanical robustness of an IR fiber and to increase the flexibility in its optical characteristics. Section 8 describes recent additional work on multimaterial fibers aiming at IR applications, including hollow-core fibers for high-power IR beam delivery, to thermally drawn crystalline semiconductor-core fibers and even single-crystal fiber cores produced by MCVD in a pre-existing hollow fiber. In Section 9, we discuss briefly other types of IR fibers that do not fit into the above classification, some of which have been studied for decades, while others have emerged over only the past year or two. We then conclude the paper with an attempt to formulate a roadmap ahead for future developments.

A few words to the reader regarding what is *not* contained in this review. IR fiber nonlinear optics has developed rapidly over the past decade. The higher nonlinearity and concomitantly higher chromatic dispersion of most soft IR glasses with respect to silica provide vast opportunities and introduce new challenges in MIR nonlinear fiber optics. The recent growth spurt in this topic has made it impossible to incorporate those results here, and instead it awaits a review paper dedicated to that area. Second, we do not address in-depth research on rare-earth-ion doping [34], microstructured optical fibers (MOFs) [35,36], or lasing in IR fibers [37], each sub-topic of which is maturing into a thriving area in its own right.

There is no comprehensive and up-to-date review that covers the broad range of IR fibers provided here. However, the book by Harrington [38] has been a standard reference on IR fibers, especially for crystalline fibers, and we have benefited from it in preparing this review. We hope that the additional progress achieved in this field over the past decade since its publication is well-represented here.

2. Infrared Materials

Optical fibers are typically drawn from glassy materials such as inorganic glasses [39] and polymers [40]. In the NIR, high-purity silica glass has proven to be an ideal material for optical transmission [Fig. 2(a)] and is readily drawn into a fiber. In moving to longer wavelengths in the IR where silica is no longer a viable option, other materials—glassy or otherwise—need to be considered. Indeed, despite the fact that crystalline materials (such as Si and ZnSe) are not suitable for direct thermal fiber drawing [10], their favorable IR optical properties—in addition to their electronic and optoelectronic characteristics—have invited recent attempts at incorporating them into hybrid multimaterial fibers. Such fibers combine both crystalline and glassy components as the core and cladding, respectively, and offer multiple functionalities integrated monolithically in the fiber [10]. We will therefore discuss the IR optical transmission

Figure 2

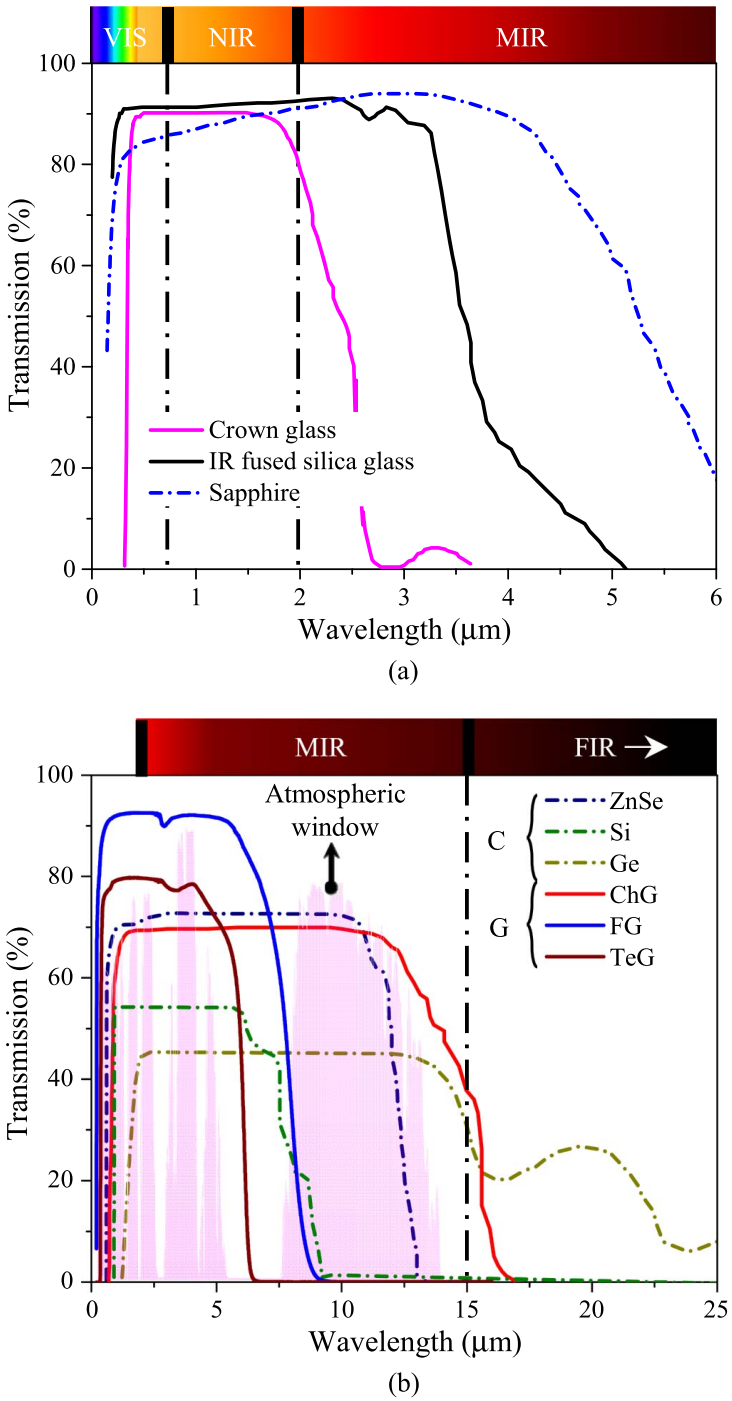

Optical transmission of various IR materials. (a) Materials that transmit from the VIS to the MIR (the sample thickness is in parentheses): crown glass (10 mm) [55], IR fused silica glass (1 mm) [55], and sapphire (3 mm) [55]. (b) Materials that transmit from the MIR to the FIR (the sample thickness is in parentheses): ZnSe (3 mm), Si (6 mm), Ge (1 mm), As_2S_3 (ChG; 10 mm) [55], ZBLAN fluoride glass (FG; 2 mm) [56], and tellurite glass (TeG; 2 mm) [57]. The atmospheric transmission window is shown in the background. Solid lines correspond to the transmission of glassy (G) materials and dashed–dotted lines to crystalline (C) materials.

Table 1. Typical Optical Parameters of Selected IR Glasses[a]

Glass	n 1.55 μm	n_2/n_2^{silica} 1.55 μm	β_2 (ps^2/km) 1.55 μm	ZDW (μm)	Transparency (μm) Bulk	Fiber
Silica	1.44	1.0	−26	1.26	0.2–3.5	0.3–2.1
ZBLAN FG	1.49	1.2	∼7.6	1.71	0.3–7.5	0.5–5.5
Tellurite glass	2.03	19	∼110	2.13	0.4–5.5	0.5–4.5
As_2S_3 ChG	2.5	200	∼500	4.81	0.6–12	1.0–6.0
As_2Se_3 ChG	2.9	600	∼1000	7.5	1.0–15	1.5–9.0
Te-based ChG	∼3.2 (2 μm)	∼1,000 (MIR)	—	>7.5	1.5–20	2.0–12

[a] n, linear refractive index; n_2, nonlinear refractive index; β_2, group velocity dispersion; ZDW, zero-dispersion wavelength.

of glassy and crystalline materials alike in anticipation of the subsequent sections of this review.

Figure 2 depicts the optical transmission spectra for a variety of glassy and crystalline IR materials. Note that, in general, the transmission spectrum of a millimeters-thick bulk differs from that of a meters-long fiber of the same material—the cut-off wavelength of the latter is significantly lower and the transparency window is narrower, as highlighted in Table 1 [7,13,41–49]. Additionally, differences between the measured transmission windows of bulk and fiber with the same length arise mainly from defective bonds introduced during the glass-melting and thermal-drawing processes [50]. Commonly used optical crown glass [51] transmits light only up to 2 μm even in thin samples [Fig. 2(a)]. Traditional single-mode silica fibers provide a low-loss transmission window that reaches only 2.1 μm, while 1-mm-thick bulk silica transmits light up to 3.5 μm [Fig. 2(a)]. Indeed, loss in silica fibers at 2.94 μm is estimated to be 800 dB/m, 4×10^6 times higher than that at 1.5 μm [38], which may nevertheless allow for very short lengths of silica fiber to be used in the 3–3.5 μm region [52]. Absorption in silica rises dramatically to thousands of dB/m beyond 3.5 μm [53]. Recently developed hollow-core microstructure fibers aim at eliminating the material absorption of silica beyond 2.1 μm using negative-curvature fiber structures [54]. The loss at 2.94 μm may be reduced to 0.06 dB/m (1.1 dB/m) for negative-curvature (positive-curvature) fiber structures. The limit set by absorption in silica remains insurmountable in the MIR and FIR.

Crystalline sapphire is used in optical windows since its transmission extends from the UV to the MIR [0.15–5.5 μm; see Fig. 2(a)] and is also extraordinarily scratch-resistant—more so than any other optical material [58]. Although sapphire is crystalline and thus cannot be thermally drawn directly, nevertheless approaches to produce sapphire fibers have been developed [38]. The main drawback of sapphire as a fiber material is the difficulty to identify a thermally compatible *glassy* cladding material [59–61]. It is conceivable that the approach used for crystalline YAG fibers—dipping the bare crystal fiber into a soft glass liquid to add a cladding [62]—may be applicable.

In Fig. 2(b) we examine materials that transmit light farther in the MIR. Generally speaking, IR glasses can be broadly classified into three groups: heavy-metal oxides, halides (fluorides and chlorides), and chalcogenides. The most popular IR heavy-metal oxide glasses are *tellurite* and (lead-) *germanate* glasses. Tellurite glasses are characterized by a wider transmission window than silicates that extends into the MIR, a lower phonon energy than silica, and higher linear and nonlinear refractive indices compared to other oxide glass systems [63], while remaining more stable than fluorides (see Section 5). These

promising features have led to the commercialization of IR tellurite fibers [23]. *Fluoride* glasses, including ZBLAN glasses, constitute a class of non-oxide optical glasses composed of fluorides of various metals. The first fluoride glass was discovered by Poulain *et al.* at Université de Rennes (France) in 1970s [41]. A typical fluoride glass has less thermal and chemical stability than other IR glasses, but has a wider transmission window compared to oxide glasses (though narrower than chalcogenide glasses). While a large number of multicomponent fluoride glass compositions have been synthesized, only a few have been drawn into fibers [64] (see Section 6). To date, *chloride* glasses have not proven to be sufficiently stable thermally for most applications [65].

Figure 2(b) shows the typical optical transmission of a *chalcogenide* glass (ChG). ChGs have found many applications in IR lens molding [66], nonlinear optics [67], phase-change memories [68,69], sensors [70], integrated photonics [71], and optical fibers [72]. Typically, sulfur (S)-based, selenium (Se)-based, and tellurium (Te)-based ChG bulk material transmit 0.6–12 μm, 1–15 μm, and 1.5–20 μm, respectively. The transparency window of ChGs makes them attractive for use in IR fibers (see Section 7) and as waveguides. Currently, there are commercially available IR ChG fibers produced by the double-crucible method [24,25] (see Section 4.2).

An intriguing class of IR materials—and one that has attracted attention only very recently to its potential as an IR fiber material—is *crystalline semiconductors*. In addition to the favorable IR optical properties of Si, Ge, and other compound semiconductors, they also display excellent electronic and optoelectronic functionalities that may potentially be integrated with the optical functionality of a fiber. Therefore, incorporating such materials in a fiber may allow for constructing new active fiber devices [26,73,74].

The attraction of Si as an IR material is that it offers wide transparency in the IR and strong nonlinear optical effects. Silicon not only has broad IR transmission of 1.2–10 μm [Fig. 1(b)], but it also transmits 48–100 μm radiation [75], which has led recently to increased interest in silicon-based MIR photonic devices [76] [77]. Crystalline Ge transmits across the whole atmospheric spectral window, and thus has been utilized in manufacturing lenses for IR-imaging systems since the 1990s (note, however, that the transparency of Ge is highly temperature-dependent, becoming opaque when heated). Both Si and Ge possess strong third-order nonlinear optical coefficients. Indeed, two-photon absorption, which is a limiting factor for nonlinear optical processes in the NIR, vanishes at longer wavelengths where the energy of two photons is not enough for a band-to-band transition [78]. Therefore, efficient nonlinear optical effects and devices at longer wavelengths are expected in the IR. There are current approaches to drawing Ge- and Si-core fibers with silica or borosilicate glass cladding [79–81]. We discuss in Section 8 the progress so far in utilizing Si and Ge (among other crystalline semiconductors) as IR fiber materials.

Finally, ZnSe—a critical IR II–VI optoelectronic crystal [82–84]—transmits light from the VIS to the FIR (up to ∼21.5 μm in 1-mm-thick samples [85] and up to ∼14 μm in 12-mm-thick samples). In addition to its usefulness in constructing bulk optical components (such as lenses) for IR systems [86], ZnSe is a useful IR laser host medium [87]. Thermal drawing of ZnSe into a fiber has not been demonstrated to date, but an alternate approach [17] has succeeded in producing single-crystal ZnSe inside a hollow silica fiber. Recent work on in-fiber

chemical synthesis has provided a new route to ZnSe fiber cores, where the crystalline ZnSe material is formed during the drawing process [88,89].

In conclusion, a wide range of amorphous and crystalline materials exist with broad IR transparency. Their suitability for thermal fiber drawing is the subject of the next section.

3. Criteria for Drawing an Infrared Fiber

The most common approach to producing an optical fiber is thermal drawing from a macroscopic scaled-up model—essentially bulk material—called a "preform." The preform is typically an axially symmetric cylindrical rod with diameter of the order of millimeters to a few centimeters and whose volume determines the fiber length produced. The internal transverse structure of the preform is designed to correspond to that of the desired fiber cross section. The preform is heated in a furnace until the material softens and plastically deforms under axial stress, thereby enabling thermal drawing into an extended fiber.

From the perspective of thermal drawing, the temperature (T) dependence of viscosity (η) is the most important physical characteristic of the materials combined in the preform. During drawing, whereupon the heated preform diameter is reduced to that of the fiber and the length concomitantly increases, the viscosity must be held relatively low—typically in the range from 10^4 to 10^7 Poise. Such an approach is *not* materials agnostic. Indeed, given the broad range of IR materials described in Section 2, which have quite diverse thermal and mechanical properties, thermal drawing is *not* suitable for all IR materials. Careful consideration of the materials' thermomechanical characteristics is necessary, particularly the temperatures at which the materials deform plastically, crystallize, and ultimately degrade. Consequently, alternative fiber fabrication approaches have been developed. We review these methodologies in Section 4 and focus here on thermal drawing only.

To appreciate the impact of viscosity on thermal drawing, let us first consider two limiting scenarios. On one hand, too high of a viscosity during drawing prevents the material's plastic flow and results in the fiber breaking. On the other hand, too low of a viscosity during drawing may potentially initiate capillary fluid instabilities, leading to a departure from the intended axial translational symmetry along the fiber [90,91]. This is particularly critical when submicrometer-scale highly curved surfaces are involved since surface energy may dominate over inertial viscous forces.

Figure 3(a) shows the viscosities of some materials highlighted in Section 2 for their IR transparency. Two distinct classes of materials emerge with respect to the thermal dependence of their viscosity. First, glassy materials, which lack long-range order, are characterized by a continuous and monotonic drop in viscosity with increasing temperature. Such materials are amenable to thermal drawing into a fiber; e.g., silica, As_2S_3, FG, TeG, and PEI polymer in Fig. 3(a). Second, crystalline materials undergo an abrupt phase change upon reaching their melting temperature—transforming from a solid directly to a low-viscosity liquid with little subsequent change in viscosity upon further increase in temperature; e.g., Si, Ge, and InSb in Fig. 3(a). Such materials—standing alone—are thus not amenable to thermal drawing into a fiber from bulk. Nevertheless,

Figure 3

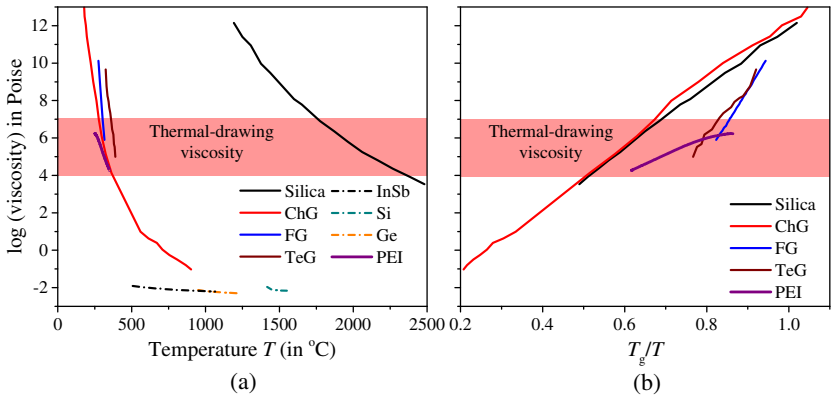

Viscosity curves of selected materials. (a) Viscosity of some common IR materials (see Fig. 2) versus temperature T in °C (data of PEI are measured at CREOL/UCF, the rest of the data are adapted from Fig. 2 in Ref. [10]). ChG, As_2S_3; FG, the fluoride glass ZBLAN; TeG, the tellurite glass $75TeO_2$–$20ZnO$–$5Na_2O$; PEI, the polymer polyetherimide. (b) Viscosity of some common glassy IR materials versus T_g/T selected from (a) silica ($T_g = 1215$°C), ChG ($T_g = 187$°C), FG ($T_g = 260$°C), TeG ($T_g = 299$°C), and PEI ($T_g = 216$°C). The thermal-drawing viscosity region is highlighted in the background. Solid lines correspond to glassy materials, and dashed–dotted lines to crystalline materials.

the emerging concept of multimaterial fibers has paved the way to thermally drawing crystalline materials into a fiber by relying on an amorphous scaffold that may be co-drawn along with the crystalline material to provide mechanical support (see Section 8 and Ref. [10]).

Glassy materials are particularly suitable for thermal drawing since they may be plastically deformed in a soft or supercooled state between the solid and liquid states that may be gradually reached by heating. This applies to almost all IR glasses and also to thermoplastic polymers. As a rule of thumb, the stable range of viscosity for thermally drawing a material into a fiber is 10^4–10^7 Poise. It is thus desirable for this viscosity range to be achieved at temperatures that are higher than the glass transition temperature T_g but lower than the crystallization temperature T_x. For example, if the viscosity of a glassy material at T_x is larger than 10^7 Poise, this material is not suitable for thermal drawing. Additionally, materials with small values of $\Delta T = T_x - T_g$, particularly $\Delta T < 100$°C, generally are less stably drawn into a fiber.

Thermal drawing of soft glass fibers is well known to be more challenging than drawing silica fibers, particularly with respect to their sensitivity to minute changes in the drawing temperature. Figure 3(a) provides a clue to the reason: the change of viscosity with T in the thermal-drawing region for silica is very gradual ($\frac{d\eta}{dT}$ is relatively small), while the viscosity–temperature slope is very sharp for most IR glasses ($\frac{d\eta}{dT}$ is relatively large). Consequently, a change in T of only a few degrees may lead to a significant change in viscosity and, hence, in the drawing conditions for IR glasses, while a similar change would have almost no impact on silica. For example, $\frac{d\eta}{dT}|_{\eta=10^6} \cong 1.5 \times 10^4$ Poise/°Cfor silica at 1925°C, while $\frac{d\eta}{dT}|_{\eta=10^6} \cong 8.2 \times 10^5$, 7.4×10^5, and 1.6×10^5 Poise/°C for

Table 2. Comparison for Silica, SF6 Glass, Fluoride Glass ZBLAN, Chalcogenide Glass As_2S_3, Polymer PMMA, Polymer PES, and Air[a]

Composition	SiO_2	SF6	ZBLAN	As_2S_3	PMMA	PES	Air
T_g (°C)	1120	423	265	187	105	225	—
Linear TEC (10^{-6}/K)	0.55	9.0	17.2	21.6	68	55	1490 (400°C)
σ (kJ kg^{-1} K^{-1})	0.75	0.39	0.63	0.46	1.26	1.1	1.068 (400°C)
C [W/(m ∗ K)]	1.38	0.67	0.63	0.17	0.19	∼0.15	0.052 (400°C)

[a] T_g, glass transition temperature; TEC, thermal expansion coefficient; σ, specific heat capacity; C, thermal conductivity.

tellurite glass at 378°C, fluoride glass at 314°C, and chalcogenide glass at 300°C in Fig. 3(a). This fact is further highlighted in Fig. 3(b) where we plot viscosity versus a normalized inverse temperature T_g/T of the same materials in Fig. 3(a). We note that the curves for silica and As_2S_3 are almost identical. Nevertheless, the lower T_g for As_2S_3 compared to silica (187°C–1215°C, respectively) results in the drawing process having a higher sensitivity with regards to temperature changes in a realistic setting. Assuming one has access to an ideal furnace, one in which the temperature is perfectly controlled without fluctuations, any material that has viscosity located in the thermal-drawing range may be, in principle, drawn into a fiber. For more details of studies on thermal drawing, see Refs. [92–101].

Table 2 [24,42,102–109] lists some of the critical thermomechanical characteristics that impact thermal fiber drawing for several optical materials, including silica, Schott SF6, the fluoride glass ZBLAN, the chalcogenide glass As_2S_3, polymethyl methacrylate (PMMA), and polyethersulfone (PES). We also list air in Table 2 for comparison. For better control over the preform-to-fiber transformation, it is preferable for the materials to have low thermal expansion to avoid structural deformation. The low thermal expansion of silica with respect to IR glasses is behind the more precise control over the structure of silica MOFs [35,36] compared to that achieved in IR MOFs [12,20,28,110,111]. A large specific heat necessitates a longer heating time to soften the material, but renders the material less sensitive to temperature fluctuations during drawing and the process thus more stable. A large thermal conductivity coefficient allows for the use of a narrower heating zone and thus faster drawing speed with a large reduction in diameter from the preform to fiber.

In addition to viscosity, there are multiple other parameters characterizing a material that impact the approach chosen for preform preparation, its thermal drawability into a fiber, and the handling of the drawn fiber. For example, the bulk mechanical characteristics may dictate the choice of nonthermal processing routes, such as drilling or stacking, to prepare the preform (see Section 4). Furthermore, convenient handling and storage of IR fibers necessitates the mechanical and chemical stability of the fiber materials. This is not always the case for IR materials; e.g., fluoride glass is prone to absorb moisture. Consequently, a polymer coating is essential for protection and increasing the mechanical robustness of IR fibers. Additional characteristics that impact the properties of the drawn fibers include the fatigue, strength, bending, hardness, and aging of the materials.

An important factor to consider when drawing an IR material into a fiber is that the preform is suspended in free space inside a furnace. The glass is heated up by absorption of radiation from the heat source and conduction from the

surrounding (gaseous) environment. In the case of IR-transmitting glasses, the absorption of radiation may potentially be low, which adds difficulties in heating up the material.

Not every IR material has been traditionally amenable to thermal fiber drawing. Nevertheless, recent advances in multimaterial fibers, micro- and nano-structured fibers, and fibers produced by nontraditional fabrication routes have dramatically increased the portfolio of materials that are currently used in IR fibers.

Finally, recent advances in fiber manufacturing have started to highlight the potential role of fluid instabilities in the fiber-drawing process itself [91,112–114]. The first intimation of this role was detected in an investigation of the origin of unexpectedly high optical transmission losses in hollow-core PBG fibers. A careful study of the free silica surface lining the hollow core revealed surface roughness compatible with frozen surface fluctuations having wavelengths predicted by the equipartition theorem. It is theorized that thermodynamically driven fluctuations arise at the free silica–air surface during drawing due to surface tension while the material viscosity is low. These fluctuations are frozen on the silica surface upon cooling, and the surface roughness results in unwanted optical scattering. This phenomenon does not occur in traditional silica step-index fibers since the surface energy at the core–cladding interface is negligible.

In multimaterial IR fibers, the surface energy at the heterogeneous interfaces may lead to new physical phenomena as a consequence of fluid instabilities. Two examples have been reported to date: breakup of a thin cylindrical film of an IR glass embedded in a thermoplastic polymer into an azimuthal array of axially intact filaments [115,116], and the axial breakup of a cylindrical IR glass core embedded in a polymer cladding into a necklace of spheres [112–114].

4. Infrared Fiber Fabrication Methodologies

With the above discussion of the thermomechanical properties of candidate materials for IR fibers in mind, we now proceed to a more detailed description of IR fiber fabrication. The situation here is quite distinct when compared to silica fibers where two standard approaches have emerged: MCVD for step-index fibers and the stack-and-draw approach for MOFs. The vast richness of available IR materials with a varied assortment of thermomechanical characteristics has resulted in the proliferation of a multiplicity of heterogeneous fabrication approaches that have yet to be standardized. We classify here the available IR fiber fabrication methodologies into two broad strategies: preform-to-fiber and non-preform-based approaches.

Preform-to-fiber approaches produce IR fibers from a macroscopic-scale bulk material, the preform, while non-preform-based approaches, as the name indicates, produce IR fibers without the preform intermediary. Instead, the fiber is produced directly from the melt as in the double-crucible method [117], from a billet or disk as in the hot-extrusion method [118,119], or by the cladded high-pressure microfluidic chemical deposition (HPMCD) method [74].

There is a multiplicity of general fabrication strategies that yield fibers starting from raw materials. For any given IR material, there could be multiple approaches that yield an IR fiber. The choice of any given process is governed by the characteristics of the material, the compatibility between the materials combined in the same fiber, and the target structure.

In general, there are two technological barriers that have plagued IR fibers: achieving low optical loss and achieving high mechanical strength or robustness. The optical loss in IR fibers stems from intrinsic absorption in the bulk materials (Section 2) and imperfections in the fiber structure that are introduced during preform fabrication and fiber drawing. The lack of mechanical robustness stems from the intrinsic mechanical properties of soft IR glasses and crystalline materials, which are typically brittle. Progress in materials purification has improved both IR fiber loss and strength by reducing glass-matrix defects in the fiber [120,121]. Furthermore, recent efforts in the area of multimaterial fibers (see Sections 7 and 8) have led to an altogether different approach for increasing IR fiber robustness. For example, an IR-transparent but mechanically brittle ChG step-index structure may be integrated with a thick robust built-in polymer jacket to offer superior mechanical support while not participating in the optical functionality [10]. Further research is needed to standardize these recent advances.

4.1. Preform-to-Fiber Approaches

The preform-to-fiber approach for IR fibers is similar overall to that employed in producing silica fibers: a macroscopic scaled-up preform is prepared from bulk materials, followed by continuous thermal drawing of the preform into an extended fiber (Section 3). Thermal drawing then reduces the transverse dimension while uniformly elongating it axially. The preform is fed into a furnace that softens the material, after which gravity or an external force pulls the molten gob at the preform tip until it stretches into a thin strand whose diameter is monitored with a gauge. This relatively simple fabrication process is behind the thousands of kilometers of silica optical fibers used in the communications networks that span the globe today [39]. Polymer coatings are typically applied to the fiber surface for protection. An alternative approach that is suitable for some IR materials is to incorporate a built-in polymer jacket that is co-drawn with the fiber, which requires that the polymer chosen be thermomechanically compatible with the IR fiber material, such as a ChG [10,122,123] or a ZBLAN fluoride glass [124].

4.1a. Step-Index Fibers

An archetypical fiber structure is the step-index (core–cladding) geometry. While producing a preform that draws into such a structure in silica is standardized via MCVD, producing an IR step-index preform is challenging and a host of processes have thus been developed, as outlined in Fig. 4. The most utilized strategy is called, for obvious reasons, the "rod-in-tube" approach, wherein a cylindrical rod of the higher-refractive-index core material is prepared separately from a hollow tube of the lower-refractive-index cladding material.

Figure 4

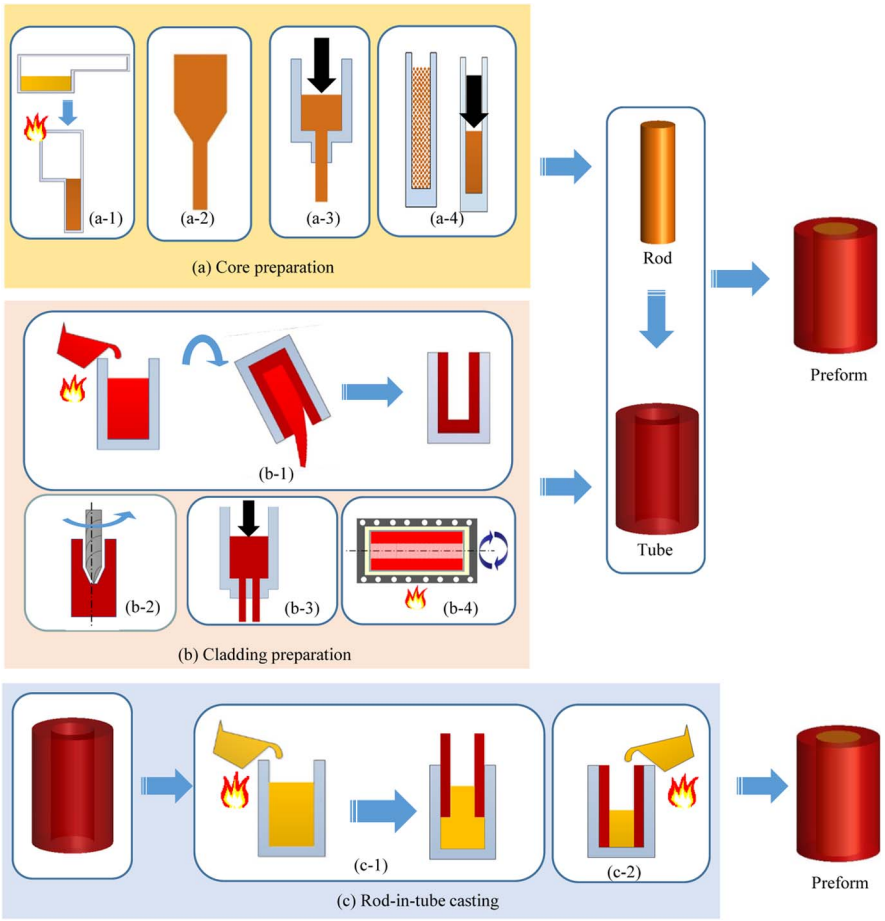

General methodologies for producing IR step-index preforms. (a) Core rod preparation via (a-1) casting, (a-2) thermal drawing, (a-3) extrusion, and (a-4) hot press. (b) Cladding tube preparation via (b-1) casting, (b-2) drilling, (b-3) extrusion, or (b-4) rotational casting. After preparing the rod and tube in the solid state, the rod is inserted into the tube to form a preform assembly. (c) Rod-in-tube casting.

Alternatively, the preform may be produced in a single step by extruding a structured billet.

I. Rod-in-tube approach for step-index fibers. Figure 4 depicts variations on the rod-in-tube method that have been used to produce step-index IR fiber preforms. The core rod [Fig. 4(a)] may be produced by melt casting, Fig. 4(a-1); thermally drawing a cane from a larger rod, Fig. 4(a-2) [35,36]; extrusion, Fig. 4(a-3) [110,125]; or hot-pressing from a powder, Fig. 4(a-4). The cladding tube [Fig. 4(b)], on the other hand, may be produced by casting, Fig. 4(b-1) [126]; drilling, Fig. 4(b-2) [122,127,128]; extrusion, Fig. 4(b-3) [125,129]; or rotational casting, Fig. 4(b-4) [130,131].

Theoretically, permutations of pairs of individual processes shown in Fig. 4 would lead to 24 possible methods to produce an IR step-index fiber preform. However, for any specific choice of core and cladding materials, only a limited subset of processes may be relevant. For example, casting- and drilling-based

methods are not appropriate for crystalline materials, and hot-pressing might be the only alternative in Fig. 4(a) that is appropriate if the crystalline material is not available in the form of a rod. Toxic materials or glasses with high vapor pressure in the liquid sate are ill-suited for use in casting methods. MCVD provides exquisite control over the refractive index of silica preforms. In comparison, melt-casting methods do not offer precise control over the refractive index, since the glass melts possess vapor pressures that may lead to loss of components through volatilization. This may cause changes in the glass composition, leading to deviations in the intended refractive index. Finally, the dimensional tolerances between the rod and tube result in an unavoidable gap at the core/cladding interface, which ultimately contributes to optical scattering due to bubble formation and glass soot deposition.

A. Rod preparation

Melt-casting. Raw materials are typically melted in a closed, evacuated container [Fig. 4(a-1)], but materials with low vapor pressure and that do not oxidize may be melt-cast in an open container. This process has been applied to most soft glasses, including tellurite, fluoride, and chalcogenide glasses.

Thermal-drawing. A small-diameter rod or "cane" may be thermally drawn from a pre-existing larger-diameter rod [Fig. 4(a-2)], as long as the thermal drawing process does not significantly decrease the purity of the material.

Extrusion. Extrusion is a well-established technique to produce axially symmetric rods with complex cross-sectional structure from bulk material, and has been used to produce rods from most IR glasses [132,133] and even crystalline materials [134]. As shown in Fig. 4(a-3), bulk material (usually called a "billet") is placed in a metal tube (sleeve) and is heated up to the material softening temperature. A force is then applied to push the softened material through a small-dimension die to produce a tube with the desired dimension and structure.

Hot-pressing. Starting from powderized raw material, as is the case for most semiconductor materials, hot-pressing is a viable option to condense powders into a solid rod under high pressure at a suitable temperature, as shown in Fig. 4(a-4).

B. Tube preparation

Melt-casting. Preparation of a hollow cladding tube via melt-casting [Fig. 4(b-1)] bears similarity to the process used to prepare a core rod [Fig. 4(a-1)] with one crucial difference. Hot glass liquid is first poured into an open container that is kept at a low temperature, and the inner hot glass that remains in a liquid state is poured out—leaving behind glass material taking the form of a bottle-like inner tank. Post-machining and polishing then yield the desired glass tube. This process has been used for some IR glasses with low vapor pressure in the liquid state, such as tellurite and fluoride glasses, but *not* for most of chalcogenide glasses.

Drilling. Either mechanical or ultrasonic drilling [Fig. 4(b-2)] may be applied to most IR glasses to produce a tube, including tellurite, fluoride, and chalcogenide glasses. Further machining and polishing processes are typically necessary to obtain an optical-quality inner surface. Indeed, beyond simple tubes, drilling has also been used to prepare MOF preforms [135].

Extrusion. By modifying the die structure, a tube can be extruded from a solid billet [Fig. 4(b-3)] instead of a rod. In general, extrusion is quite versatile with regards to the materials that may be exploited or structures produced, the latter of which may be engineered through judicious design of the die or the billet. Extrusion may thus be used to produce MOF preforms [136] and even multimaterial fiber preforms [10].

Rotational casting. Rotational casting has been exploited in producing tubes of tellurite, fluoride, and chalcogenide glasses. In this approach, raw glass material is sealed in a silica or metal cylindrical container mounted in a horizontal lathe. The sealed container is rotated at a high speed (~ several thousand rpm) while maintained above the material melting temperature. Centrifugal force shapes the glass liquid into a tube, followed by a careful cooling process [130].

C. Rod-in-tube assembly

With the preparation of the desired rod and tube, a rod-in-tube assembly is formed by simply inserting the rod into the tube. The result is a step-index fiber preform en route to thermal drawing.

II. Rod-in-tube casting. An alternative approach to preparing the rod-in-tube assembly that starts from a pre-existing tube relies on directly casting the rod into the tube. Figure 4(c) shows two examples, where the tube is inserted into the core liquid or the core liquid is poured into the tube to form a rod-in-tube assembly upon cooling. This strategy particularly helps to obtain an intermediate preform with a small core-to-cladding ratio [126] for single-mode fiber, in addition to improving the quality of the core–cladding interface. For glasses having a high vapor pressure in the liquid state, such as chalcogenides, complex setups have been designed to produce step-index fiber preforms [126,130].

III. Multimaterial coextrusion for step-index fibers. Structured fiber preforms may be obtained via extrusion in one step by structuring the billet itself. For example, using a vertically stacked billet consisting of multiple discs, the horizontal interfaces are converted into a vertically nested structure [Fig. 5(a)] [13,137–144]. This strategy can therefore yield step-index structures from a billet consisting of two disks [137,139] or 1D multilayer structured preforms from a billet comprising more than two disks [140–142,144]. This strategy can be traced back to efforts by Itoh *et al.*, reported in 1994 [139], to extrude a step-index preform made of fluorozirco-aluminate glass from two stacked disks. Subsequently, research groups at Nottingham University [144], Rutgers University [141], and Southampton University [142,143] reported similar approaches to produce step-index and 1D MOF preforms. An alternative approach reported by the Université de Rennes 1 relies on a custom system involving a series of *in situ* vacuum distillations followed by casting of the preform through sequential rotation [145].

Alternatively, a rod-in-tube assembly may be used as the billet [122]; Fig. 5(b). This method was exploited recently to produce robust step-index Te-based chalcogenide fibers for long-wave IR transmission using a multimaterial billet. The compression of the structure occurring during extrusion helps eliminate any potential gaps at the core–cladding interface in this approach.

Figure 5

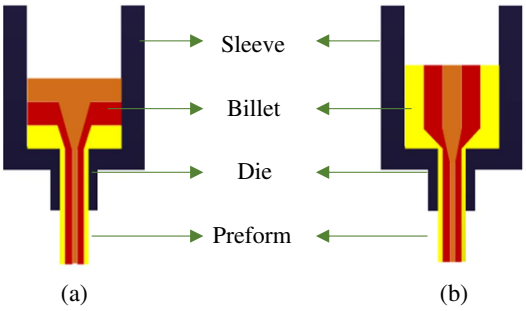

Multimaterial coextrusion strategies for IR fiber preforms. (a) Multimaterial stacked coextrusion and (b) multimaterial rod-in-tube coextrusion.

4.1b. IR Microstructure Fibers

MOFs provide a large degree of controllability over the fiber performance through structural design while constructing the fiber from a single material by the incorporation of air holes in the cladding. This approach has proven particularly valuable in silica in the VIS and NIR [35,36]. A unique aspect in the IR is the large span of refractive indices of IR materials (Table 1). This feature offers the potential for constructing all-solid MOFs while maintaining a large refractive index contrast. Several methods have been utilized to date in fabricating IR MOF preforms, including the stack-and-draw method [35,36], thin-film rolling [11], extrusion [136], MCVD [146], drilling [135,147], and casting [148].

Stack-and-draw. The stack-and-draw approach has been used extensively in preparing silica MOFs, both PCFs and PBG fibers [35,36,149]. The first demonstration of the stack-and-draw method to produce an optical fiber may be traced back to Bell Labs in 1974 [150], where a fiber containing a hanging core surrounded by air was produced. Rods, tubes, or plates from a single material or multiple materials may be assembled into a preform [Fig. 6(a)]. Multiple stack-and-draw steps may be applied recursively to reach the required dimensions and attain complex transverse structures. However, stacking raises challenges for reproducibility and is less suited to fragile glasses. Nevertheless, the stack-and-draw method has been used to produce the first hollow-core chalcogenide PBG fiber [20], but low-loss IR transmission has not yet been confirmed. The stack-and-draw method has also been used to produce all-solid MOFs [18,151].

Thin-film rolling. Polymers may be incorporated into an IR fiber—typically to impart mechanical robustness—using any of the above three approaches. A unique process involves rolling a thin polymer film around a rod followed by thermal consolidation under vacuum above the glass transition temperature of the constituent materials to allow the individual films to fuse [Fig. 6(b)]. The polymer film can be replaced by a bilayer film (polymer film with deposited material), resulting in a 1D multilayer structure. This process is the basis for fabricating hollow-core multimaterial PBG fibers with an all-solid photonic structure lining the core that provides an omnidirectional bandgap (see Section 8) [21].

Extrusion. Extrusion can be used to produce MOF fiber preforms from soft glasses with complex structures [141,142]. Figure 6(c) depicts the extrusion

Figure 6

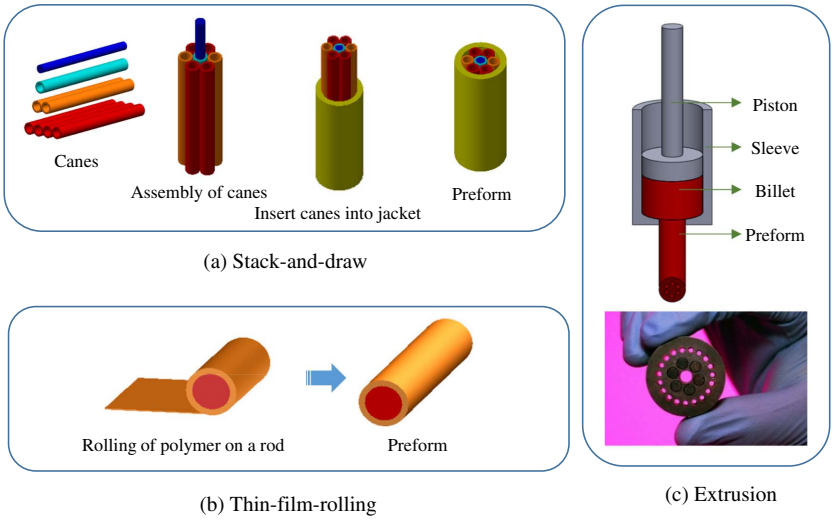

(a) Stack-and-draw

(b) Thin-film-rolling

(c) Extrusion

Three main strategies to produce IR MOF preforms: (a) stack-and-draw, (b) thin-film rolling, and (c) extrusion methodologies. The photograph in (c) is of an extrusion die that produces a six-holed preform.

of a MOF preform schematically. Compared with the stack-and-draw, drilling, and casting approaches, extrusion involves a single step to produce the preform despite the complexity of the transverse structure. Kiang *et al.* [152] reported the first MOF preform fabricated by extrusion. Ebendorff-Heidepriem and Monro have reported significant advances in preform extrusion and die design for the fabrication of complex-structured preforms using soft glasses [136].

Other approaches. Drilling produces tubes that might be used either as cladding [Fig. 4(b-2)] or canes for the stack-and-draw method [Fig. 6(a)], and may even be used to produce IR MOF preforms directly [135,148,153]. However, drilling is limited to short preform lengths and necessitates polishing to reduce surface roughness and contamination. Casting techniques may be used to produce rods, tubes, and rod-in-tube assemblies for step-index fiber preforms [Fig. 4], and may additionally be used to produce MOF preforms from soft glass [148]. To date, casting of preforms with a large number of transverse features has been achieved only by using sol-gel and *in situ* polymerization techniques. In the context of IR fibers, an exception has been the demonstration of chalcogenide MOF preforms produced from a complex sealed silica casting setup [148].

4.2. Non-Preform-Based Approaches

A particularly important process that has proven useful for producing high-quality IR fibers—initially from fluoride glasses in the early 1980s [117] and subsequently chalcogenide glasses—is the double-crucible fiber drawing approach, the principle of which is shown in Fig. 7(a) [154]. A system of two crucibles is assembled: an inner quartz crucible concentrically positioned within an outer quartz crucible, with each connected individually to an inert gas source. The core and cladding glasses are placed in the inner and outer crucibles, respectively. The glasses are melted and the temperature is then lowered quickly to the drawing temperature whereupon fiber fabrication commences.

Figure 7

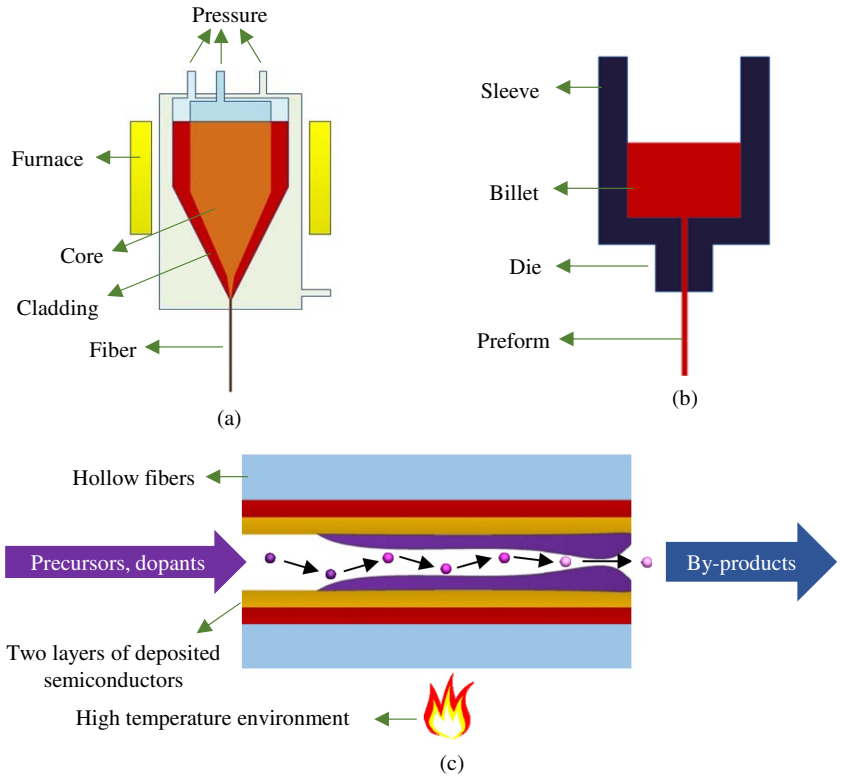

Non-preform-based approaches to produce IR fibers: (a) the double crucible method, (b) hot extrusion, and (c) HPMCD.

The fiber outer diameter and the core–cladding ratio are controlled by adjusting the gas pressures in the inner and outer tubes independently, by altering the drawing rate or by adjusting the temperature [155–158]. As such, both multimode and single-mode fibers can be drawn using this process. Since the fiber is drawn directly from the melt, the two glasses are required to have closer viscosities than tolerable when drawing from a preform. This constraint usually excludes the possibility of achieving a large-refractive-index contrast. The double crucible method typically provides higher-quality fibers compared to those drawn from a rod-in-tube preform, but the latter offers a higher level of control over the fiber structure and dimensions.

IR fibers may also be fabricated by the hot-extrusion technique, which enables "drawing" polycrystalline halides [118,119,124,159] into fibers with diameters in the range 500–900 μm with no buffer jacket. In this method, a single-crystal billet is placed in a heated chamber and a piston forces it through a die. Step-index fibers have been co-extruded into fiber in this fashion [118,159], but they usually have a highly irregular core region and poor core–cladding interface quality, resulting in higher losses than unclad fibers. There has been much progress in reducing the loss in clad polycrystalline IR fibers through careful adjustment of the core and cladding compositions and the extrusion parameters. To date, Ag-halides produce the best polycrystalline IR fibers [124].

Crystalline materials are not amenable to thermal fiber drawing without support from a glassy backbone or scaffold material forming an outer cladding

(Sections 3 and 8). Nevertheless, crystalline sapphire fibers have been produced via modified crystal-growth techniques in which the fiber is pulled from the melt using edge-defined, film-fed growth or laser-heated pedestal growth techniques [160,161].

More recently, HPMCD [74] has emerged as a microscale variant of chemical vapor deposition (CVD) to produce fibers from materials not amenable to thermal drawing, particularly single-crystal semiconductors including ZnSe [17] (Section 8). The main drawback of this technique is the limited lengths of fiber produced compared to thermal drawing.

5. Heavy Metal Oxide Glass Infrared Fibers

Heavy metal oxide glasses (HMOGs), such as germanate, lead-silicate, and tellurite glasses, have—in general—spectral transmission windows that extend over the VIS and MIR (Section 2). Furthermore, these glasses are endowed with better mechanical and thermal characteristics and possess, in addition, higher optical nonlinear coefficients than fluoride glasses (Section 6). Nevertheless, they have lower nonlinearities and shorter transmission cut-off wavelengths compared to chalcogenide glasses (Section 7) [Fig. 8(c)]. Fibers made of these glasses have been commercialized [23] and are finding increasing applications for laser gain material.

The most common oxide glass is based on silicates, which are not useful in fibers transmitting IR light. Replacing silicon with heavy metals (e.g., lead and tungsten) results in oxide glasses with their transparency window extending further into the IR, albeit not as far as fluoride and chalcogenide glasses.

5.1. Tellurite Glass Infrared Fibers

The tellurite glass family was discovered by Stanworth in 1952 [162], and the first significant characterization of their optical properties in fiber form was reported in 1994 [63]. Tellurite glasses offer a transmission window that extends from the VIS to the MIR [Fig. 8(c)]. In the 1990s, rare-earth-ion-doped tellurite glass fibers attracted attention as potential NIR broadband amplifiers for telecommunications applications [163–165] and recently for white-light generation through nonlinear upconversion [166]. Over the past decade, the high optical nonlinearity of tellurite glasses [63,167,168] has attracted interest for applications in IR nonlinear optical processing [169–172]. Critically, from the perspective of fiber drawing, the glasses exhibit high crystallization stability relative to fluoride glasses, so they may be readily shaped into a large variety of preform structures using casting [164,173,174], drilling [175], and extrusion techniques [176]; see Fig. 9.

The key to capitalizing on the intrinsic MIR transmission of tellurite glass is the reduction of OH groups, which cause strong absorption at 3–4 μm. Several methods, including melting in a dry atmosphere, raw-material dehydration,

Figure 8

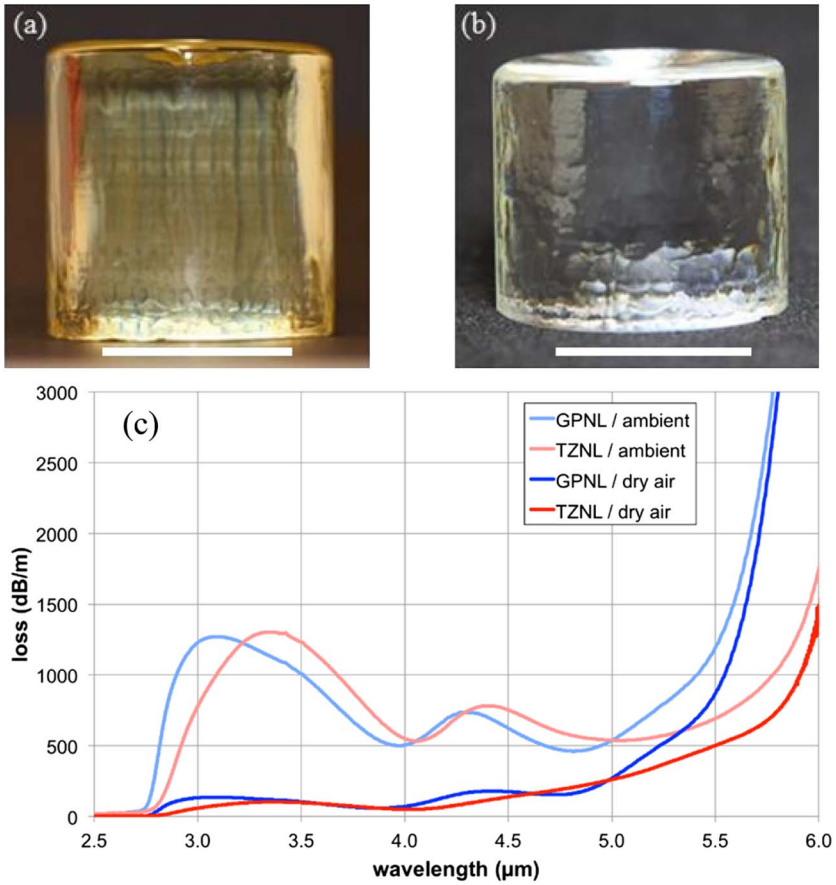

Photographs of typical (a) sodium-zinc-tellurite (b) and lead-germanate glass billets. Scale bars are 20 mm. (c) Absorption spectra of sodium-zinc-tellurite (TZNL) and lead-germanate (GPLN) glasses melted in ambient and dry atmospheres. Reprinted with permission from [111]. Copyright 2013 Optical Society of America.

and the use of fluoride or chloride raw materials and combinations thereof, have been investigated to reduce the OH content in tellurite glasses, and recent results are listed in Table 3 [164,173–184]. The OH content in tellurite glasses is caused by water impurities in the raw materials. There is an equilibrium between the water vapor in the atmosphere above the glass melt and the water in the glass melt (in the form of OH groups). Use of a dry atmosphere releases the water from the melt to the atmosphere. Churbanov *et al.* [177] found that the OH content in glass is proportional to the square root of water vapor pressure over the melt. The release of water from the melt increases with longer melting time and higher melting temperatures [176,177]. However, melting time and temperature are limited to prevent significant evaporation of the glass melt itself.

In addition to the use of a dry atmosphere, partial replacement of oxide raw materials by fluoride raw materials has been demonstrated to be an effective method to reduce the OH content [174,175,178,179,181,183–185]. Unfortunately, fluorotellurite glasses exhibit reduced crystallization stability

Figure 9

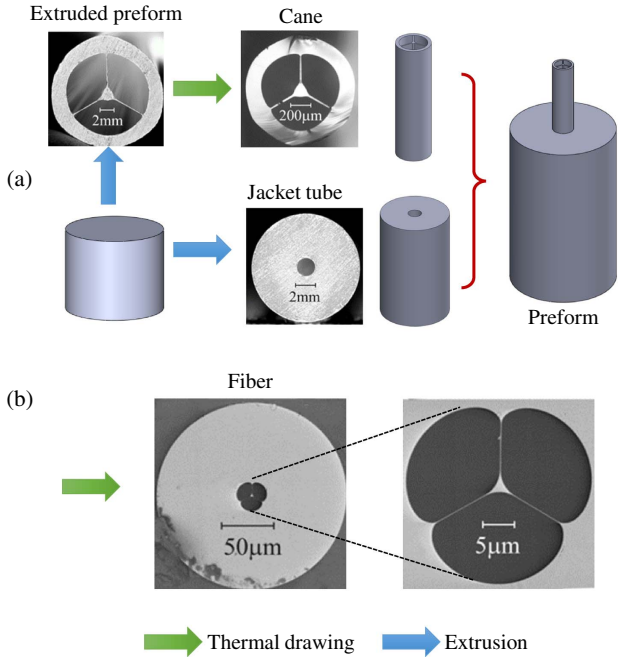

Steps to fabricate a small-core extruded tellurite preform. (a) Preform preparation; (b) resulting tellurite MOF [186].

and have lower linear and nonlinear refractive indices, which is undesirable for target nonlinear applications such as supercontinuum generation. Furthermore, fluoride incorporation reduces the glass transition temperature, which leads to reduced thermal and mechanical stability. As an alternative to fluoride, the use of chloride raw material has been shown to be an effective dehydration agent [164].

Apart from OH groups, metal impurities such as 3d and 4f elements cause absorption and thus enhanced loss. This effect is particularly prominent in the NIR, where absorption due to OH groups is significantly lower compared with the MIR. Table 3 lists the results of fiber loss measurements in the NIR (1.5–2.1 μm). The use of commercially available, high-purity raw materials (99.999% and higher for TeO_2, 99.99% and higher for other raw materials) led to losses of 0.1–0.2 dB/m at 1.55 μm [175,176]. The use of ultrapure raw materials made in-house has been demonstrated to result in bulk glass losses of 0.04–0.08 dB/m at 1.56 μm and 0.05–0.10 dB/m at 1.97 μm [174,179]. Single-index fibers made from such ultrapure glasses exhibited higher losses of 0.5 and 0.3 dB/m at 1.56 and 1.97 μm, respectively [174]. However, step-index multimode fibers made from such ultrapure glasses demonstrated losses that were similar to the bulk glass loss: 0.05 dB/m at 1.6 and 2.1 μm [179]. The lowest NIR loss was reported for a tellurite fiber made from in-house prepared TeO_2 is 0.02 dB/m at 1.55 μm [187]. Recently, multimode tellurite fibers produced by NP Photonics, Inc. have shown no measurable OH absorption at 3–4 μm, and a minimum loss of 0.2 dB/m at 3.5 μm [23].

For tellurite glass fibers with low OH content, it becomes apparent that the multiphonon edge is composed of two components with different slopes [111]. The short wavelength tail of the multiphonon edge in the range of approximately

Table 3. Example of Recently Synthesized Tellurite Glasses and Fibers with Low OH Content

Composition[a] (mol. %)							
Main Components	Na-Content	F-Content	H_2O Content (ppm)	OH-Induced Loss[b] (dB/m)	Dehydration Method	IR Fiber Loss (dB/m) at λ (μm)	Ref.
TeO_2–ZnX–Na_2O	10% Na_2O	10% ZnF_2	<1	8	dry O_2 + ZnF_2	13 at 3.3	[175]
TeO_2–ZnO–Na_2X	5% Na_2X	2% NaCl	<0.2	45	dry O_2 + NaCl	—	[164]
TeO_2–PbX	none	20% $PbCl_2$	<0.2	10	dry O_2 + N_2 + $PbCl_2$	—	[164]
TeO_2–ZnO–La_2O_3–Na_2O	5% Na_2O	none	10	50	dry N_2 + O_2	0.8 at 2.0 1.7 at 2.3–2.4	[176]
TeO_2–ZnX–Na_2O	10% Na_2O	20% ZnF_2	<3	10	dry O_2 + ZnF_2	—	[183]
TeO_2–ZnO–Na_2O–Bi_2O_3	5% Na_2O	none with	0.5	5 0.5		0.9–1.2 at 1.4–2.2	[174]
TeO_2–WO_3–La_2O_3	none	none with	0.5	3 0.8	dry O_2+ fluoride	0.2–0.4 at 1.4–2.2	[174]
TeO_2–WO_3–La_2O_3	none	with	0.5	0.6	dry O_2+ fluoride	0.05 at 2.1–2.160.1 at 1.4–2.25	[179]
TeO_2–ZnO–Bi_2O_3–$(Li, Na)_2O$	with	—[c]	—	—	—	—	[173]
TeO_2–WO_3	none	none	0.5	0.5	dry O_2	—	[177]
Tellurite	—[c]	—[c]	—[c]	—[c]	—[c]	0.2 at 3.5	[23]

[a] $X = O, F_2, Cl_2$.
[b] For bulk glass or fiber at ~3.3–3.4 μm.
[c] Not available.

4.0–5.7 μm has a smaller slope, whereas for wavelengths >5.8 μm a steep edge is observed. The short wavelength tail causes losses of ~10–500 dB/m in the range of 4.0–5.7 μm, which presents a severe limitation for MIR fiber applications. For bulk glass samples with usually a few millimeter to ~1 cm thickness, the short wavelength tail has a negligible or small impact on the transmission, and thus the steep multiphonon edge >5.8 μm limits the transmission of bulk glass samples.

In conclusion, the combination of high nonlinearity, IR transmission up to 4 μm, high rare-earth solubility, high crystallization stability, and relatively good chemical durability make tellurite glasses attractive candidates for fiber lasers and nonlinear optical applications in the IR. However, the relatively high loss due to OH groups at 3–4 μm and minimum loss of >0.1 dB/m in most fibers demonstrated to date has hampered commercial applications of tellurite glass IR fibers.

5.2. (Lead)–Germanate and Tungsten–Tellurite-Glass Infrared Fiber

Germanate glass fibers generally do not contain fluoride compounds. They also do not contain silica (SiO_2); rather they contain heavy metal oxides to shift the IR absorption edge to longer wavelengths. The advantage of germanate fibers over fluoride fibers is that germanate glass has a higher T_g and, therefore, a higher laser-damage threshold, but the loss for the fluoride fibers is lower.

Within the tellurite glass family, Na, Li-Zn-tellurite glasses have been most widely investigated for supercontinuum generation [169,175,194,195] and IR

Table 4. Example of Typical Tellurite and Germanate Glasses Used for High-Nonlinearity and High-Power Applications in the Infrared[a]

Glass Composition	T_g °C	TEC 10^{-7}/°C	n	E_{ph} (cm^{-1})	Ref.
$75TeO_2$–$15ZnO$–$10Na_2O$	290	190	2.0	750	[188]
$73TeO_2$–$20ZnO$–$5Na_2O$–$2La_2O_3$	315	170	2.0	750	[111]
$60TeO_2$–$30WO_3$–$10La_2O_3$	455	120	2.1	920	[189,190]
$60GeO_2$–$30PbO$–$5Na_2O$–$5La_2O_3$	455		1.9	800	[111]
$56GeO_2$–$31PbO$–$9Na_2O$–$4Ga_2O_3$	390	110	1.8	800	[187,191]
$65GeO_2$–$20BaO$–$10Ga_2O_3$–$5La_2O_3$	610	90	1.7	850	[192,193]

[a] T_g, glass transition temperature; TEC, thermal expansion coefficient; n, refractive index at 1–1.5 μm; E_{ph}, phonon energy.

laser applications at wavelengths above 2 μm [196–198]. However, the low $T_g \sim 300$°C combined with high thermal expansion coefficient (TEC) of $\sim(190–200) \times 10^{-7}$/°C for these glasses (Table 4) limits their thermal and mechanical stability, resulting in low laser damage threshold, in particular for small-core tellurite fibers [194]. Therefore, recently, lead–germanate glasses [111,187,191,197] and tungsten–tellurite glasses [189,199] have been investigated as viable alternatives to Zn-tellurite glasses. Both glass types exhibit comparatively high T_g of ≥400°C and low TEC of $(110–120) \times 10^{-7}$/°C, while having high refractive indices of 1.9–2.1 similar to Zn-tellurite glasses (Table 4). Lead–germanate glasses have the advantage of lower phonon energies compared with tungsten–tellurite glasses (Table 4), which is of importance for applications in the MIR. For applications that do not require high refractive indices, e.g., high-power fiber lasers at ∼2 μm, Ba-Ga-germanate glasses have been demonstrated to be an attractive alternative [192,200]. This type exhibits high T_g of >600°C, which is accompanied with lower refractive index, while the phonon energy is between those of lead–germanate and tungsten–tellurite glasses (Table 4).

Summary. (Lead–)germanate and tungsten–tellurite glasses offer IR transmission up to ∼4 μm, relatively high nonlinearity, and rare-earth solubility combined with higher thermomechanical stability compared to zinc–tellurite and fluoride glass fibers. This makes such glasses particularly well suited for applications requiring high optical nonlinearity and gain combined with high laser-damage threshold. To date, these characteristics have been exploited in fiber lasers at ∼2 μm.

6. Fluoride Glass Infrared Fibers

Fluoride glasses exhibit the lowest refractive index among IR glasses, hence, the lowest optical nonlinearity [64,167,201], which makes them particularly well suited for high-power delivery and lasing applications where nonlinear effects are undesirable. Another unique property of fluoride glasses is their extremely broad transmission window from the UV (∼300 nm) to the MIR (4–6 μm for ∼1-m-long fiber) [64,167,201,202]; see Fig. 10.

Fluoride glasses can be divided into four types: fluoroaluminate glasses based on AlF_3, fluorozirconate glasses based on ZrF_4, fluoroindate glasses based on InF_3,

Figure 10

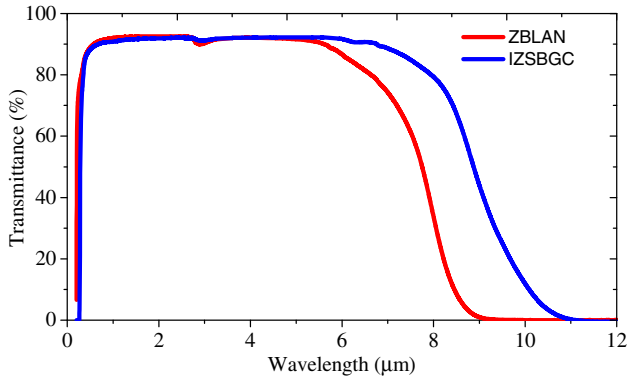

FTIR spectra of typical ZrF_4-based fluoride (ZBLAN) and InF_3-based fluoride (IZSBGC) glass bulk samples of 2 mm thickness.

and fluoride glasses based on divalent fluorides. As the energy of the stretching vibration between the metal and fluorine ions decreases in the order AlF_3 > ZrF_4 > InF_3 > MF_2, the MIR transmission edge is shifted to longer wavelengths in the same order [64,202,203].

The most-established and widely used fluoride glasses are the fluorozirconate glasses. The first ZrF_4-based glass was discovered in the 1970s [41]. Within this glass family, the so-called "ZBLAN" glass with composition (in mol. %) $53ZrF_4$–$20BaF_2$–$4LaF_3$–$3AlF_3$–$20NaF$ has been the most widely used. Indeed, ZBLAN exhibits high crystallization stability, enabling low-loss fiber fabrication [64,204]. By contrast, no fibers have been reported for divalent-fluoride-based glasses, which is attributed to their low crystallization stability. Recently, fluoroindate glasses have gained increased interest due to their extended transmission compared with ZBLAN [22,202], while fluoroaluminates have not gained comparable interest for MIR applications due to their limited transmission up to ~4 μm.

To date, fluoride glasses—compared to other IR glasses—have met with the most commercial success in fibers produced for IR power delivery and active fiber applications, such as fiber lasers. Nevertheless, the transparency window of fluoride glasses does not extend beyond 5.5 μm.

6.1. ZBLAN Glass Fibers

For fluorozirconate glasses, it was found that the theoretical loss limit of <0.01 dB/km at 2–3 μm is 1 order of magnitude lower than that of silica [205]. This discovery stimulated a large amount of research in the 1980s and 1990s to develop ultralow-loss fluorozirconate fibers. Although a low loss of 0.7 dB/km at 2.7 μm was demonstrated [206,207], the intrinsic loss limit was not achieved due to extrinsic losses caused by metal impurities and scattering

defects (mainly small crystals) in the glass [64,207]. The use of high-purity raw materials (both metals and fluorides) is essential to reduce both extrinsic absorption (through a reduction in their water and oxide content) and scattering losses (by preventing the formation of crystals in the glass). Unfortunately, ultrahigh-purity, ultradry fluoride raw materials are not commercially available and thus in-house purification is required to fabricate ultralow-loss fluoride glass [204,208]. In addition to raw-material purity, glass processing conditions play a significant role. Numerical simulations demonstrated that extreme fiber drawing conditions of high draw speed and high tension can reduce fiber loss to levels close to the theoretical intrinsic loss [209]. However, these extreme drawing conditions are not practical.

Building on the large effort in developing low-loss fibers, fluorozirconate step-index fibers with 5–50 dB/m at 2–3 μm are commercially available [64]. Recently, it was demonstrated that MOFs can also be produced from ZBLAN glass using extrusion or the stack-and-draw technique [210,211].

ZBLAN glass fibers have found widespread interest in fiber lasers [37,212–214] and supercontinuum generation applications [215–218]. The combination of low nonlinearity, MIR transmission up to 5 μm, and low optical loss make ZBLAN particularly well suited for high-power lasing and beam delivery applications. A range of rare-earth-doped ZBLAN fiber lasers operating in the MIR at 3–4 μm have been demonstrated [37,213]. High-power delivery requires large fiber cores combined with good beam quality, which cannot be provided by traditional multimode fibers. However, the MOF technology was demonstrated to enable both large mode area and high beam quality [210]. Although ZBLAN glass exhibits low nonlinearity, its interest for supercontinuum generation (a nonlinear process) stems from its low loss in the MIR at 3–6 μm [219–221] and zero dispersion wavelength at ∼1.6 μm, which is close to the wavelengths of available high-power erbium-doped fiber lasers at 1.5 μm and thulium fiber lasers at ∼2 μm [216]. Kubat *et al.* proposed an approach for generating MIR supercontinuum by using concatenated fluoride and ChG fibers pumped with a pulsed thulium fiber laser [222]. To date, investigation of supercontinuum generation has been limited to step-index ZBLAN fibers [218]. A ZBLAN MOF with tailored dispersion has been recently demonstrated [211].

Figure 11(a) shows a photograph of multiple pathways toward producing fluoride glass fiber preforms. One example is a cast rod that be drawn directly, while another example includes cast disks that are then extruded 20°C above the glass transition temperature ($T_g = 310$°C) using graphite dies into rods for fiber drawing. One preform (Preform 1) was cleaned by isopropyl alcohol in an ultrasonic bath prior to fiber drawing, while the other preform (Preform 2) was etched in a 15 wt. % HCl solution to remove a ∼0.5-mm-thick outer layer. Both cast rod and extruded rods were then pulled into unclad fibers with diameters of ∼130–180 μm. Furthermore, the extrusion method has also been used to produce ZBLAN MOFs [Fig. 11(b)] [210].

6.2. Fluoroindate Glass Fibers

As noted above, fluoroindate glasses offer extended IR transmission due to their lower phonon energies. Moreover, they offer higher T_g of ∼300°C [64,202] compared to ZBLAN glass, whose $T_g \sim 260$°C [203,204], thereby promising higher thermal stability.

Figure 11

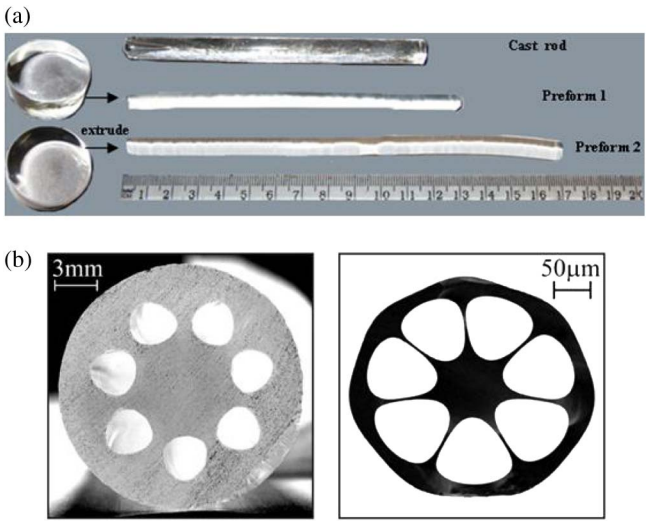

(a) Fluoroindate glass in the form of (left) cast billets, (top) cast rod, (center) preforms extruded from cast billets. Reprinted with permission from [110] Copyright 2013 Optical Society of America. (b) Extruded preform and scanning electron microscope image of a ZBLAN MOF Reprinted with permission from [210] Copyright 2008 Optical Society of America.

The potential for extended IR transmission stimulated research on the development of fluoroindate fibers in the past decade [64,223,224]. Step-index fluoroindate fiber with low loss of 0.6 dB/m at 5 μm is now commercially available [22]. At this wavelength, the theoretical loss of ZBLAN is 6 dB/m (calculated using the equations and parameters given in [167]). Recently, extruded fluoroindate fibers with 2 dB/m at 5 μm, made from commercially available raw materials, have been reported [202].

Summary. Fluoride glass fibers offer IR transmission up to 5–6 μm combined with low optical nonlinearity. They are particularly well suited for applications requiring high-power handling and low optical loss. Therefore, fluoride glasses are the material of choice for fiber lasers in the range 3–5 μm. Recently, fluoride glass fibers have also attracted increasing interest for supercontinuum generation applications. The drawbacks of fluoride glasses are their relatively poor chemical stability, requiring the fibers to be well packaged or used in a dry environment. In addition, fluoride glasses exhibit low crystallization stability compared with oxide and chalcogenide glasses, which hinders their processing into fibers with complex structures. ZBLAN glass is the most widely used fluoride glass for IR fiber applications. Although fluoroindate glass offers extended IR transmission, its higher crystallization tendency during fiber drawing hampers development of low-loss fibers.

7. Chalcogenide Glass Infrared Fibers

Chalcogens are the chemical elements in group VIA of the periodic table—specifically the elements sulfur (S), selenium (Se), and tellurium (Te). Chalcogenide glasses (ChGs) are endowed with a unique set of physical characteristics that have made them attract considerable recent interest despite their long history [66]. From the perspective of their utility in IR fibers, ChGs are well known for their broad IR transparency—extending to the FIR—and amenability to thermal drawing. Typical commercially available ChG compositions are based on As-S(Se), Ge-As-Se(Te), As-Se-Te, Ga-La-S, and Ge-Sb-Se systems [42,108,225].

Bulk samples that are millimeter-thick of S-, Se-, and Te-based ChG transmit light in the 0.5–12 μm, 1–16 μm, and 1.5–20 μm spectral windows, respectively, as shown in Fig. 12. In addition to their IR transparency, ChGs have the highest third-order nonlinear refractive indices among all optical glasses. These characteristics make ChGs ideal candidates for MIR nonlinear fiber optics where short fiber lengths or ultralow optical power levels are sufficient to elicit nonlinear optical behavior. The typical optical loss in ChG fibers in the MIR is of the order of 0.1–10 dB/m [120,157,226–228]. These values are much higher than theoretical predictions that indicate a minimum attenuation of 11 dB/m at 4.5 μm for GeS_3 [205] and ~0.01 dB/m loss at 5.0 μm from As_2S_3 ChG fibers [229]. Therefore, despite substantial efforts over the past several decades, the full potential of ChGs has not yet been achieved.

Although the concentration and mobility of free charge carriers in ChGs are lower than in crystalline semiconductors and the Fermi level is apparently pinned, the combination of these optical and electronic characteristics in an IR glass bodes well for the development of novel functionalities in ChG fibers. Indeed, ChGs—despite their amorphous structure that lacks long-range order—are p-type semiconductors, unlike all IR glasses described in the previous

Figure 12

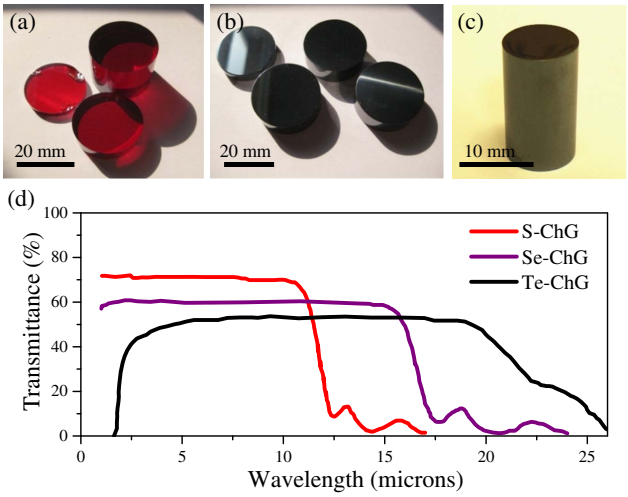

(a)–(c) Photographs of three typical S, Se, and Te ChGs [342]: (a) As_2S_3, (b) As_2Se_3, and (c) $Ge_{20}As_{20}Te_{45}Se_{15}$. (d) Typical IR transmission spectra (starting at 1 μm) of S, Se, and Te ChG millimeter-thick bulk samples.

sections that are electrical insulators [230]. Furthermore, ChGs exhibit threshold and memory-switching phenomena [231] not known to exist in other glass systems. Consequently, besides their utility in IR fibers, ChGs have been exploited recently in fabricating waveguide devices for MIR sensing [70,232,233], nonlinear optics [234,235], integrated photonics [71,236], laser amplifiers [237,238], and ultrahigh-bandwidth optical signal processing [239,240]. Furthermore, CVD techniques or thermal evaporation are used to fabricate ChG-based waveguides [241,242] or even 1D MOFs [243].

Efforts on multiple fronts have been aimed at developing active MIR sources based on ChG fibers. One strategy relies on the IR nonlinear properties of ChG fibers [43,44,169244–256], and there has been success in demonstrating ChG Raman fiber lasers [257–263]. Another approach has been to use ChGs as hosts for rare-earth ions (REIs) [218,256,264–299], or nanoscale doped crystal [300–302]. Despite the extensive research on REI-doped ChGs since the 1990s, there has been only limited success to date [34,37]. Further efforts have been carried out on identifying ChG compositions that enable high doping concentrations [272,273,303] while maintaining low phonon energy for IR emission, rare-earth co-doping schemes [266,304], in addition to reducing the fiber loss by increasing the ChG purity and uniformity [305]. Crystalline Cr^{2+}: ZnS/Se nanoparticles have also been introduced into AsS-Se glass systems and fibers for active applications [300–302]. More details on the major applications of ChG fibers are provided in Refs. [228,256,306].

ChG IR fiber sensors have proven to be excellent candidates for real-time remote quantitative detection and quantification of gas, organic, and biological species [307–317]. Low-phonon Te-based ChGs show great potential for analyzing the atmosphere of extra-solar Earth-like planets in search of life as their wide optical transmission spectrum encompasses the spectral signatures of H_2O (~6 μm), O_3 (~9 μm), and CO_2 molecules (~16 μm). To further cover the FIR region, new Te-based ChGs have been developed with transparency windows extending up to 25 μm [226,318–320].

Uniquely, ChGs cover the broadest IR spectrum of all IR glasses, have the highest optical linear and nonlinear refractive indices, and offer the widest tuning range of optical parameters achieved through compositional engineering. ChG fibers may potentially cover the entire span of QCL wavelengths.

The systematic study of ChGs as IR materials started in the mid-20th century, dating back to the investigation by Frerichs of As_2S_3 glass [321]. Subsequently, As-S step-index ChG fibers were reported in 1965 by Kapany and Simms [322], who demonstrated a relatively high transmission loss of 20 dB/m at 5.5 μm.

Considerable efforts by several Japanese corporations and agencies laid the groundwork for future developments in ChG fibers, including the Nippon Telegraph and Telephone Public Corporation (NTT) [157,323,324], Hitachi, Ltd. [325–329], Horiba, Ltd. [330], Non-oxide Glass R&D Co., Ltd. [331], the Kyota Semiconductor Corporation [332], the HOYA Corporation [333],

and the Communications Research Laboratory (now The National Institute of Information and Communications Technology, NICT) [334,335]. These efforts led to drawing fibers from several ChG systems (Ge-P-S, As-S, As-Ge-Se, Ge-S, Ge-As-Se-Te-(Tl),), having either unclad or step-index [157,331,336] structures, in addition to fiber bundles [329,334,337], where each strand in the bundle consists of a ChG core and a Teflon cladding. The mechanical robustness of ChG fibers was fortified by developing UV-curable polymer coatings or incorporation of a Teflon FEP polymer cladding at the preform level—thereby presciently initiating the field of multimaterial fibers [10]. Furthermore, the study of optical nonlinearity [338–341] and REI doping in ChG fibers [333] were initiated. These extensive efforts established the framework for future developments and highlighted the need for efficient methodologies to produce low-cost, low-loss, robust ChG fibers.

In the USA, Amorphous Materials, Inc., started the manufacturing of bulk ChGs in 1977, and subsequently reported the fabrication of ChG fibers and fiber bundles using several compositions from the GeAsSe, AsSe, AsS, and AsSeTe systems—the most successful being As-Se-Te (2–11 μm) and As_2S_3 (VIS–8 μm) glasses. Despite the lack of mechanical robustness that plagues these fibers, they were used to transmit watt-level (<5 W) of CO and CO_2 CW laser light through fibers with cores of hundreds of micrometers. The IR imaging fiber bundles were based on As_2S_3 fibers with a plastic epoxy serving as cladding, which limits the IR transmission spectra. See the interesting book [72] that recounts the detailed history of these efforts.

Research and development efforts in the area of ChG fibers have now proliferated around the world. Examples of such teams include The Institute of Chemistry of High-Purity Substances of the Russian Academy of Sciences (1980s–), Université de Rennes 1 (1990s–), the US Naval Research Laboratory (NRL) (1990s–), University of Southampton (1990s–), and the University of Nottingham (1990s–), which have collectively led to the current maturation of the ChG fiber field.

7.1. Current Status of Optical Losses in Chalcogenide Glass Fiber

Bulk ChGs are normally prepared by melt quenching from high-purity (99.999%–99.9999%) elements and compounds that may have incongruent melting points, exhibit high partial vapor pressure during melting, and are potentially susceptible to oxidation and hydrolysis. Therefore, synthesis must be carried out in sealed evacuated quartz ampules in the absence of oxygen or water. ChGs need to be agitated to promote mixing and homogeneity during the melt-based processing as the elemental constituents react to form a glass liquid. The primary contaminants ([O], [H], [C], and dissolved compounds)—which have a noticeable impact on the properties of the drawn optical fibers—may largely be attributed to trace-level constituents in the starting raw materials [343]. Consequently, attempts to obtain ChGs via alternate routes, such as the use of nonvolatile compounds, have been made [225]. The expected advantage of such an approach is a lower rate of impurity inclusion, if synthesis is possible at a lower temperature over a shorter period of time. In addition to the melt-quenching technique, several other approaches have been developed to produce glassy ChGs, such as the utilization of microwave radiation

[344–346] or CVD [347]. Despite the wide range of bulk ChGs available, only a subset of thermally stable glasses has been found useful for thermal fiber drawing.

The lowest optical attenuation to date in ChG fibers [120] remains approximately ×1000 higher than the intrinsic losses (estimated to be 0.08 dB/km at 5.0 and 6.1 μm for As-S and As-Se glass fibers, respectively [348]). Extensive investigations by Russian researchers over the past few decades into the nature and origin of impurities in ChGs [343,349–355] have led to a reduction in optical loss <1 dB/m in fibers from the As-S, As-Se, and As-S-Se systems (except for several IR absorption bands caused by stubborn impurities [356]). Using the double-crucible method, step-index As-S fibers were fabricated in the early 1990s [158], followed by step-index As-Se-Te and As-S-Se glass fibers with minimal optical losses of 0.15 dB/m at 6.6 μm and 0.06 dB/m at 4.8 μm, respectively [357]. To date, the lowest loss for ChG-based optical fibers has been achieved in multimode As_2S_3 optical fibers, with losses of 0.012 and 0.014 dB/m at 3.0 and 4.8 μm, respectively [120].

Since the late 1980s, scientists at Université de Rennes 1 have developed Te-based ChGs (Te-ChG) fibers, especially from the Te-halide (TeX, X = Cl, Br, I) systems [358,359]. Both unclad and step-index fibers have been produced (by the rod-in-tube and double-crucible methods) that offer wider transmission windows than S- and Se-ChGs, typically up to 9–9.5 μm [360–363]. Indeed, 2.6 W output at 9.3 μm power was obtained from 7 W input power out of a 1-m-long, 600-μm-diameter unclad TeX fiber provided with an antireflection coating [363]. The long-wavelength transmission Te-ChG fibers has enabled their use for remote chemical analysis/detection and temperature sensing [364–366]. The minimum optical loss of unclad Te-ChG fibers (TeAsSe system) is less than 0.1 dB/m in the 6.7–7.3 μm window [307], while step-index single-mode TeAsSe fibers have a minimum loss of typically ∼0.33 dB/m at 7.5 μm [367]. Broadband step-index Te-ChG fibers that possess higher loss (7–40 dB/m in the 4.0–15.0 μm region) have been produced by the rod-in-tube approach for the Darwin mission [368].

The U.S. Naval Research Laboratory started in the 1990s to report their efforts in developing IR ChG fibers from the As-S, As-Se-S, As-Se-Te, and Ge-As-Se-Te systems [156,228,229,256,369–373] in a variety of structures, including unclad and step-index fiber and MOFs. The core and cladding diameters of a typical single-mode ChG fiber fabricated by the double-crucible technique are 12 and 125 μm, respectively, with the addition of a 62.5-μm-thick acrylate coating and typical loss ∼0.9 dB/m at 2.7 μm for As-S(Se)-based fiber [374]. The step-index ChG IR fibers that have emerged from these efforts are currently commercialized [24,25].

7.2. Enhancement of Mechanical Robustness

Polymer/plastic/resin coatings (typically UV acrylate) have been used to offer mechanical protection to fragile ChG fibers for several decades [39]. Such protection is critical for ChG fibers, which possess only 1/10 the tensile strength of silica glass fibers [375]. To overcome this drawback, several approaches have been explored, including coating the fiber with a combination of multiple polymer layers [376], providing a jacket by heat-shrink that reduces the inevitable interfacial gap usually remaining when the rod-in-tube approach is used

[373], and more recently including a thick built-in thermomechanically compatible jacket at the preform level [13,122,123] surrounding a step-index ChG structure through multimaterial coextrusion—all of which result in better mechanical support when compared to the traditional single-layer polymer coating.

The general idea of combining glasses with polymers in an optical fiber has been investigated since the 1980s (typically via the rod-in-tube approach) to appropriate the favorable mechanical properties of polymers and compensate for the less-favorable mechanical properties of soft glasses. Thermal co-drawing of glasses with a polymer jacket, such as Teflon, results in fibers with greatly improved mechanical properties—whether step-index fluoride [377] or ChG [157] fibers, or IR fiber bundles [329,334,337]. However, there are inherent limitations imposed on the dimensions of the internal glass structure and the outer diameter that stem from reliance on a single fiber-drawing step. Furthermore, lack of independent control over the dimensions of the glass and polymer portions of the fiber leads to thermal effects, limiting the power handling capability of the fiber. These dimensional limitations are lifted using the multimaterial coextrusion fabrication approach.

7.3. Multimaterial Infrared Chalcogenide Glass Fibers

The brittleness of ChGs sets limits on the machining of such glasses for preform preparation and also on the strength of drawn ChG fibers. Indeed, the fragility and difficulty of handling and processing of ChG IR fibers have limited their widespread use [379]. Despite impressive progress, there has been no definitive answer to the lack of robustness of ChG fibers. Recent efforts have culminated in the development of a low-cost process that yields robust multimaterial ChG fibers with broad dimensional control over both the ChG and the polymer sections of the multimaterial fiber [13,122,123,380]. Additionally, the diversity of applications of ChG fibers—stemming from the very distinct optical, electronic, and optoelectronic characteristics of these materials—requires a fabrication approach flexible enough to harness material combinations with precise dimensional control not usually attainable through the rod-in-tube or double-crucible approaches.

A recent addition to the IR fiber fabrication portfolio has been that of multimaterial coextrusion combined with thin-film-rolling processes, as shown in Fig. 13. A first generation of this process utilized a vertically stacked billet of ChG and polymer disks that is extruded through a small die, leading to the transformation of the vertical disks into a cylindrically nested structure [Fig. 13(a)].

A variation (or "second-generation") on this theme [123] exploits a structured extrusion billet that minimizes the amount of glass needed to produce an IR fiber, as shown in Fig. 13(b)—leading to high-efficiency "disc-to-fiber" coextrusion. As alluded to above, large-scale synthesis of high-purity ChG—necessary for the usual pathways to producing ChG fibers—remains a materials-processing challenge, especially in an academic environment, and thus presents an obstacle to the transfer of research results from academia to industry. The modified billet structure shown in Fig. 13(b) allows for the drawing of ~50 m of robust IR ChG fiber starting from only ~2 g of glass! This approach will hopefully enable rapid prototyping of ChG fibers from the wide range of

Figure 13

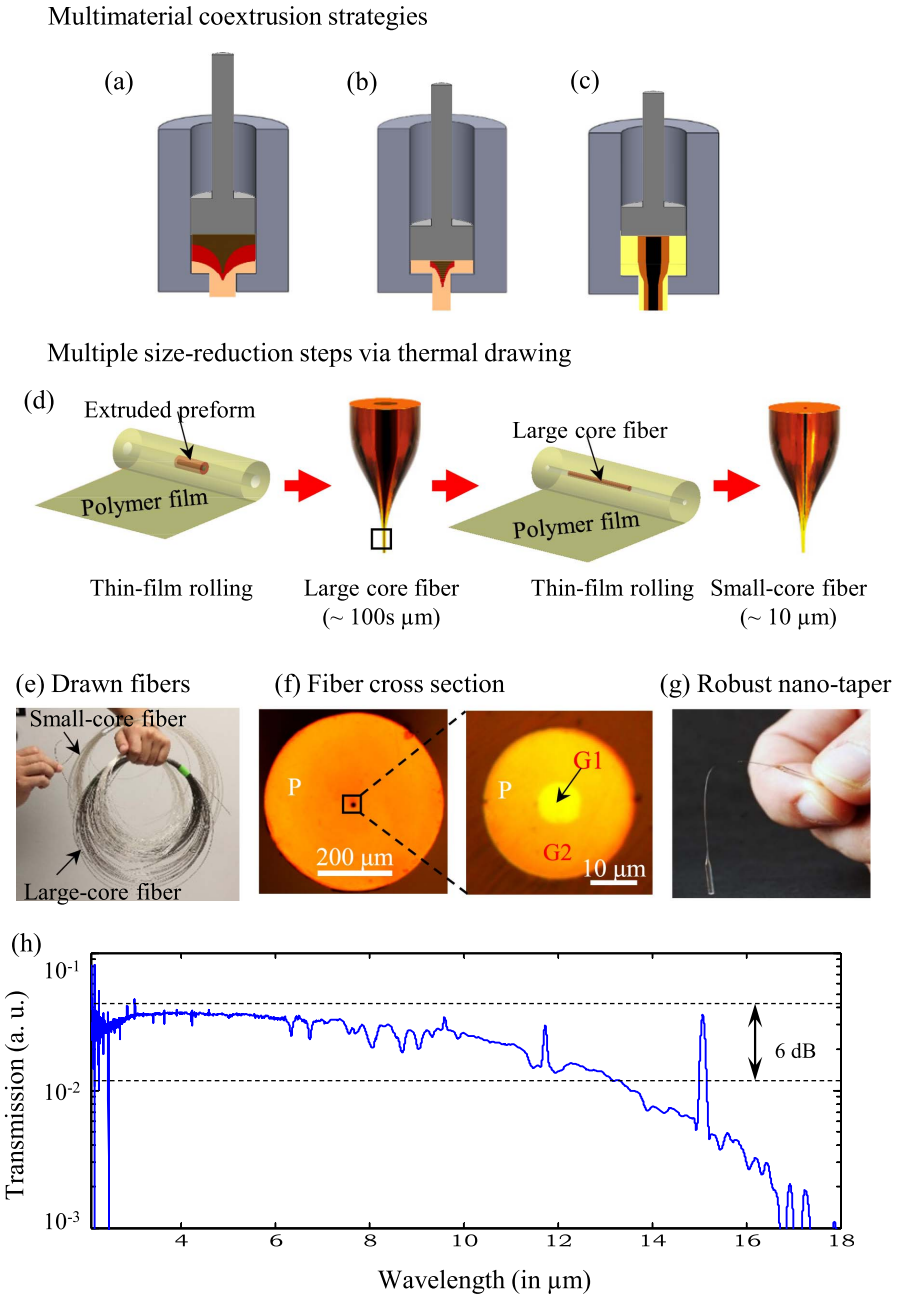

(a)–(c) Three multimaterial coextrusion strategies that differ in the billet structure. (d) Producing a preform using the thin-film rolling technique [13,122,123]. (e) Photograph of extended lengths of drawn multimaterial ChG fibers [378]. (f) Reflection optical micrographs of the fiber cross section. G_1, As_2Se_3; G_2, As_2S_3; P, polyethersulfone (PES) [13]. (g) Photograph of a robust ChG multimaterial nanotaper. (h) Transmission spectrum of a robust Te-ChG multimaterial fiber [122].

available compositions tailored with specific applications in mind without the stringent requirements of large-scale, high-purity ChG synthesis. Finally, this multimaterial coextrusion approach is sufficiently flexible to extend to a wide span of ChG compositions, including Te-ChGs coextruded from a multimaterial

rod-in-tube billet [Fig. 13(c)] [122]. Figure 13(h) is the transmission spectrum of a 3-cm-long Te-ChG fiber sample [122].

When using any of the three coextrusion variations in Figs. 13(a)–13(c), the extruded rod is then moved to a thin-film-rolling step followed by thermal consolidation under vacuum to produce a preform [10]. This extra step provides flexibility over the relative dimension of the ChG and polymer sections without adding further constraints on the coextrusion process. Robust IR fibers are then thermally drawn in an ambient atmosphere into continuous lengths of fiber with desired diameters. Furthermore, multiple draws or additional stack-and-draw steps may be used to control the ultimate size of the fiber core [381].

The multimaterial ChG fibers resulting from this procedure have multiple salutary features that may be exploited in a variety of settings: (1) dramatic increase the mechanical robustness of the fiber [13], (2) enabling one to take advantage of the wide IR transmission window of ChGs, (3) increasing the potential refractive index contrast between fiber core and cladding (controllable from 0.02 to >1), which is useful in dispersion and nonlinearity engineering [43,44,244], (4) enabling control over the core-to-cladding diameter ratio [13], (5) control over the dimension of the core from millimeters down to a few nanometers [381], and (6) reduction of the volume of costly IR material [13]. Several of the advantages of these multimaterial ChG fibers combine to deliver novel nonlinear fiber devices. Since the polymer and the ChG are thermally compatible, the fibers may be tapered without first removing the polymer, leading to robust tapers even with submicrometer core diameters [43,44,244]. The large index contrast afforded between the core and cladding allows for both dispersion control [244] and strong field confinement in the core [13], which allows one to overcome the high material group velocity dispersion (GVD) of ChGs and at the same time harness their high nonlinearities (Table 1).

By adapting the new concept of multimaterial fibers to bear upon the stubborn problem of lack of mechanical robustness in IR fibers, IR-transparent ChGs may be exploited despite their inferior mechanical characteristics by combining them with thermoplastic polymers to produce robust multimaterial IR fibers. This overall strategy, developed mainly at CREOL, The College of Optics & Photonics (University of Central Florida), may pave the way to a new generation of robust ChG IR fibers.

Recent innovations in multimaterial fiber fabrication technology in which thermoplastic polymers are combined with ChGs yield robust, continuously drawn, extended lengths of fiber, with wide tunability of the geometric and physical parameters. This approach may render ChG fibers commercially viable and useful for QCL light transmission across the entire IR.

7.4. Chalcogenide Glass Infrared Microstructure Fibers

Silica-based MOF technology typically relies on arranging a lattice of air holes in an otherwise solid cladding. ChGs of various compositions uniquely offer a large range of refractive indices ranging from 2.1 to 3.5 in the MIR, thereby

offering the opportunity for all-solid MOFs that nevertheless maintain large index contrasts that are not accessible in silica. In addition, ChG MOFs with air holes in the cladding have also been demonstrated. Several fabrication approaches have been exploited to produce ChG MOFs, including stack-and-draw [18,275,382,383], mechanical drilling [135], rod-in-tube [384], and casting methods [148]. Initial theoretical [385] and experimental [20] studies of hollow-core ChG bandgap MOFs have been realized, but more work is required before conclusive PBG guidance is demonstrated. Furthermore, suspended-core ChG fibers have been demonstrated, with applications in supercontinuum generation [250,386,387].

8. Multimaterial Infrared Fibers

The past decade or so has witnessed a proliferation of innovative approaches for producing fibers from materials or material combinations that are not typically associated with optical fibers. For example, while both polymers and glasses have each individually been utilized to draw fibers, combining polymers and glasses in the same fiber has only been recently explored [7,10,11,21,32,122,123,388]. As another example, while crystalline semiconductors are the mainstay of the electronics and optoelectronics industries, their use in optical fibers has not been considered except very recently. In both these examples, issues related to the thermomechanical compatibility of the materials systems with traditional fiber drawing have been conceived as a hindrance to success, and conventional wisdom has thus proven here to be an unwelcome roadblock.

In Section 3, we have seen that careful design of the fiber preform can help alleviate some traditional constraints in material choices with regards to fiber drawing. Several successful multimaterial fibers now bear witness to the fruitfulness of this general approach to producing IR fibers [10]. An early example is that of hollow-core fibers where IR light is guided via a PBG effect—a 1D periodic photonic structure endowed with high index contrast lines the core and confines the light via an omnidirectional reflection effect [388]. The high index contrast needed for successful hollow-core guidance is achieved by a unique combination of optical polymer (low index) and soft glass (high index) that are, nevertheless, thermomechanically compatible at the drawing temperature. These fibers have laid the foundation for a new generation of IR fiber delivery devices for minimally invasive medical surgery, and have to date helped save or improve thousands of lives [33].

On a different front, the IR transparency of crystalline semiconductors (Section 2) have invited efforts to draw semiconductor-core, glass-cladding fibers [389–391] with the amorphous cladding facilitating the drawing procedure (Section 3). Several semiconductors have been drawn continuously in this fashion, ranging from elemental semiconductors such as Si [391] and Ge [79] to compounds such as InSb [16]. These early achievements now require concerted efforts to tackle the challenges that face this paradigm: identifying thermomechanically compatible amorphous cladding materials that are IR-transparent, elimination of unwanted thermochemical reactions, and reduction of irregularities along the fiber stemming from the mismatch of thermal expansion coefficients of the crystalline core and the glassy cladding. Success in this effort may

usher in a new synthesis of optics and electronics—the two main information-processing technologies of our time.

Finally, recent efforts have been directed at the use of hollow silica fibers as a "substrate" or scaffold for deposition of single-crystal semiconductors from a vapor phase [74]. Although this approach may not produce the fiber lengths typically resulting from thermally drawing a preform, useful active fiber devices may be produced. For example, IR-transparent ZnSe [17], a wide-gap II–VI semiconductor [392] that finds many optical and optoelectronic applications, has been deposited via CVD in the hollow core of a silica fiber while maintaining high-quality polycrystallinity. It is conceivable that such fibers may lead to novel IR fiber lasers at wavelengths extending beyond 2 μm [393].

In this section, we elaborate on these three families of multimaterial fibers. In addition to the other examples described in the previous sections (such as the hybrid robust ChG-polymer fibers in Section 7), it is clear that the field of multimaterial fibers is in a healthy growth phase that promises many surprises in the years to come [10].

8.1. Hollow-Core Multimaterial Photonic Bandgap Infrared Fibers

Silica optical fibers—the mainstay of the telecommunications and other industries—rely on index guiding of light through a solid core and, thus, have fundamental limitations in their attenuation and nonlinearities that stem from the interaction of light with a dense, solid core. Since the MIR is particularly challenging for fiber transmission owing to the high absorption losses in most glasses and polymers used in fiber optics, hollow-core fibers offer the opportunity to greatly reduce these limitations. One of the earliest efforts on such fibers for the MIR relied on thermal drawing of hollow-core fibers lined with an all-dielectric omnidirectional reflecting mirror [32,388,394]. Light is confined to the fiber core by a large PBG established by a high-refractive-index-contrast multilayer stack comprised of a high-index chalcogenide glass and a low-index polymer [21,395–402]. The layer dimensions determine the transmission bandgap, which can be tuned from the VIS to the IR. Light propagation through air in a hollow fiber greatly reduces problems associated with material absorption, nonlinearities, thermal lensing, and end reflections, and facilitates high-power laser guidance and other applications that may be impossible using conventional solid-core fibers.

Early notions of hollow-core fibers lined by a multilayered reflective surface have existed since the 1970s [403], but there are multiple challenges associated in realizing such structures. First, a pair of materials must be identified that—on the one hand—have compatible thermomechanical properties to enable them to be co-drawn at the same temperature and—on the other hand—have a high refractive-index contrast. Second, in order to prevent scattering and obtain low-loss fibers, the drawing process must preserve the interfaces of the multilayer structure down to the microscale. Figure 14(a) depicts the fabrication procedure used to produce such fibers. To date, several pairs of materials have been identified that yield low-loss, hollow-core, multimaterial PBG fibers under appropriate fabrication conditions. A typical pair consists of a low-refractive-index polymer and a high-refractive-index ChG, glassy materials that are thermomechanically compatible for fiber drawing [21,395,396] (Section 3).

Figure 14

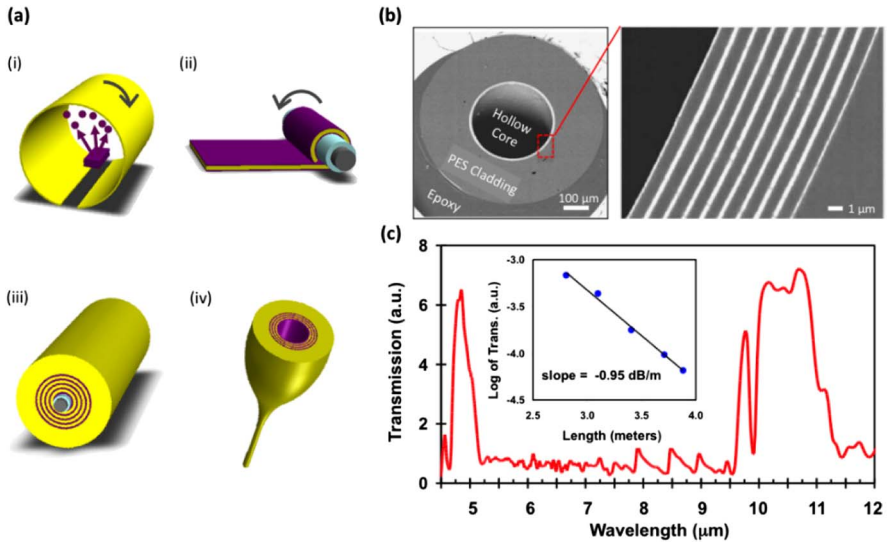

Multimaterial PBG fibers. (a) Schematic of the multimaterial PBG fiber fabrication process. (i) The high refractive-index-contrast in the layered structure lining the core is achieved by thermal evaporation of a ChG (As_2Se_3, refractive index of 2.8) onto a thermoplastic polymer (PES, refractive index of 1.55). (ii) This bilayer film is subsequently rolled onto a mandrel to form the multilayer structure and additional polymer cladding films are added for mechanical stability. (iii) The entire structure is thermally consolidated under vacuum until the materials fuse together into a solid preform. (iv) After removing the mandrel, the cross-sectional dimensions of the preform are reduced by drawing the preform into a fiber. The ratio of the preform down-feed speed and fiber draw speed dictates the final layer thicknesses. (b) Cross-sectional SEM micrograph of a hollow cylindrical multilayer fiber mounted in epoxy. The hollow core appears black, the PES layers and cladding are gray, and the As_2Se_3 layers are bright white. The PES layers are 900 nm thick and the As_2Se_3 layers are 270 nm. This fiber has a fundamental PBG centered at 3.55 μm. (c) Typical transmission spectrum of hollow-core fibers designed to transmit CO_2 laser light. The fundamental PBG is centered near a wavelength of 10.6 μm, and the second-order PBG is at 5 μm. Inset: plot of the logarithm of the transmitted power versus the fiber length reveals a loss of 0.95 dB/m.

Figure 14(b) shows a typical hollow-core fiber structure and layer uniformity resulting from the fiber draw. The desired transmission PBG can be achieved by controlling the fiber draw speed, which, in turn, directly scales the layer thicknesses. Figure 14(c) shows the transmission spectrum of a fiber drawn to transmit in a wavelength range centered at the CO_2 laser wavelength of 10.6 μm, with losses below 1 dB/m. This is 1 order of magnitude less than the intrinsic losses of the chalcogenide glass (As_2Se_3) and 5 orders of magnitude less than the polymer (PES) that make up the multilayer reflector. These relatively low losses are made possible by the fact that most of the energy is carried in the hollow core and by the very short penetration depth of the core-guided fiber modes in the PBG structure [398], allowing these materials to be used at wavelengths that would be considered impractical in the index-guiding regime.

Hollow-core multimaterial PBG fibers have already gained a solid footing in the medical device industry, where they are used for the delivery of high-power CO_2 laser light in minimally invasive surgical procedures [33]. Future research in this area is expected to focus both on new materials and process development for further reducing transmission losses, as well as exploration of new applications, such as chemical vapor sensing, where hollow core fibers can be employed as a medium that can simultaneously transmit light and various chemical species for detection and analysis [404–410].

8.2. Thermally Drawn Crystalline Semiconductor Infrared Fibers

Optical fibers comprising cores of semiconductor materials have gained considerable attention [411] given their potential to unify two fields central to modern information and computing technologies: silicon photonics [412] and fiber optics. Given the rapid growth of interest in this topic, this section will summarize the state of the art. For completeness, the reader is referred to several thorough reviews of semiconductor optical fibers for greater detail [80,413].

Semiconductor materials as core phases in optical fibers pose a unique opportunity for optical device, component, and system designers. Unlike conventional silica glass or less-conventional soft-glass IR materials, semiconductors possess a range of optical and optoelectronic functionality [411] that could be of great value as growing demands continue to be placed on photonic systems. For example, cubic semiconductors can possess very large Kerr optical nonlinearities that are useful for efficient wavelength conversion and optical signal processing [413]. To date, only cubic semiconductor phases have been realized in optical fiber form and losses have generally been too high to make practical devices, with the exception of recent work employing microspheres generated using a semiconductor optical fiber [414]. Indeed, if the technologies can be matured such that crystalline $\chi^{(2)}$ semiconductor-based fibers can be fabricated, then the field of nonlinear fiber optics could be redefined.

To date, two principal fabrication approaches have emerged—each possessing relative advantages and disadvantages. The first employs CVD of unary and selected binary semiconductors inside of silica microstructured optical fibers [73]. The main advantages of this approach are that both amorphous and crystalline semiconductors cores can be realized, as can optoelectronic junctions between differently doped semiconductors [26,415], realized, however, at slow growth rates in short fiber lengths that these produced by thermal drawing (see below).

The second main approach is the molten-core method, which has been employed to make glass-clad optical fibers with crystalline cores of Si [391], Ge [79], and InSb [16] (see Fig. 15). In the molten-core method, the core phase is selected such that it is molten at the temperature where the cladding glass draws into fiber; see Ref. [416] for a recent review of this process. For example, Si ($T_{melt} \sim$ 1414°C) is sleeved inside a pure silica ($T_{draw} \sim 1950$°C) tube and drawn directly into fiber. The advantages of this method are long lengths (>100 s meters to kilometers) and compatibility with existing commercial optical fiber fabrication infrastructure. Disadvantages include the necessary high draw temperatures to fabricate fibers with silica cladding, which promotes thermochemical reactions

Figure 15

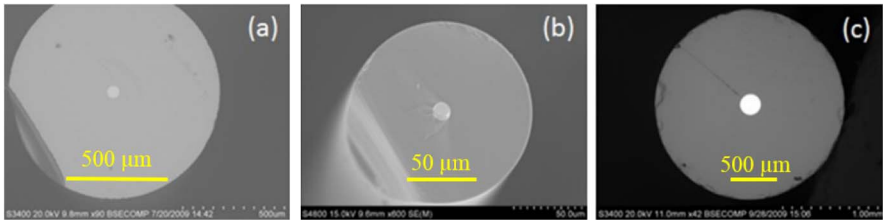

Crystalline-semiconductor-core fibers. (a) Silicon core, silica cladding fiber. (b) Germanium core, borosilicate glass cladding fiber. (c) InSb core, borosilicate glass cladding fiber.

that can dissolve silica (from the cladding glass) into the semiconductor core, leading to scattering from precipitated oxide phases.

From a practical perspective much optimization remains with respect to both fabrication methodologies. Optical losses at present are high (~dB/cm) and the attainment of closer-to-theoretical values (10s of dB/km [80]) requires continued effort. That said, the dominant sources of fairly high propagation loss are understood and are being addressed systematically [417].

From a materials perspective, only oxide-based cladding glasses have been employed to date for all of the semiconductor optical fiber efforts. In the IR, where such fibers hold their greatest potential for applications, the oxide cladding will limit performance by absorbing the evanescent field of the propagating mode. This is especially the case for single-mode and small-diameter (e.g., tapered [418]) semiconductor-core fibers. IR-transparent claddings have been identified [419] and are presently under development. Furthermore, and for completeness, purity and scattering issues associated with oxide contamination from the cladding glass are being addressed through creative use of diffusion barriers and *in situ* melt-phase chemistry. While there likely is no "one size fits all" solution to the optimization of future semiconductor optical fibers, a combination of designer cladding glasses with diffusion/buffer layers and precursor purification measures could rapidly reduce the present attenuation values (dB/cm) to the levels (dB/m) where practical devices become possible.

8.3. Chemically Deposited Crystalline Semiconductor Infrared Fibers

MIR optical fibers are typically not as robust as silica optical fibers [124]. The constraints on viscosity placed by the fiber drawing process limit the palette of materials suitable for these fibers primarily to those that have relatively low optical damage thresholds and strength [124]. MIR optical materials such as crystalline compound semiconductors (e.g., zinc chalcogenides) can have much higher optical damage thresholds but, in general, cannot be drawn into fibers alone because they have sharp melting points. Many of them also melt incongruently or have high melt vapor pressures that make drawing impossible [17]. Oxidation, deviations in stoichiometry, and the incorporation of impurities are additional issues that must be addressed when drawing such fibers.

Sparks *et al.* fabricated ZnSe and ZnS optical fibers by high pressure CVD over centimeters of length into silica capillaries [Fig. 16] and silica MOF [Fig. 17(a)]

Figure 16

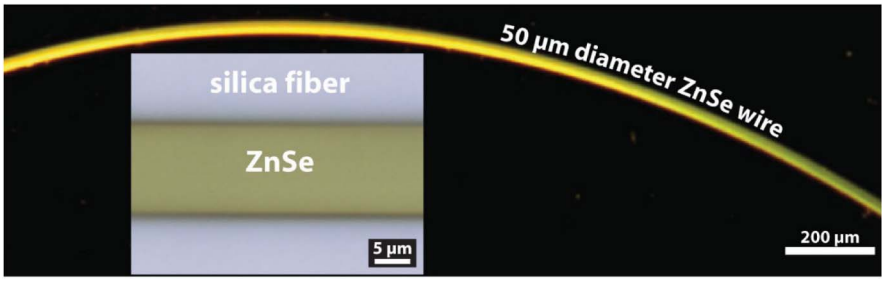

ZnSe optical fiber. A centimeters-long, 50 μm diameter, cylindrical ZnSe optical fiber core, embedded in a silica cladding, which is not visible, is illuminated with VIS light. Inset: optical micrograph of a smaller-diameter ZnSe optical fiber.

[17,73,392]. High pressures facilitate mass transport into the silica fiber pores [74]. The silica cladding into which the ZnSe fiber cores are deposited allows these fibers to have high strength and be handled much as conventional silica fibers. Losses thus far for ZnSe fibers with single cores 10s of micrometers in diameter range from 0.5 to 1 dB/cm. The wavelength dependence of the optical loss varies as $\lambda^{-3.9}$, suggesting that grain boundary or other bulk inhomogeneity scattering may be dominant. Chalcogenide fibers can be much longer than crystalline ZnSe fibers and can exhibit much lower optical losses of the order of 1 dB/m, but are limited to continuous wave optical power densities of 10 to 20 kW/cm^2 [124], much lower than that of silica.

Compound semiconductor fibers are anticipated to have much higher optical damage thresholds than soft-glass fibers in view of their refractory nature, high thermal conductivity, and wide optical bandgaps [73]. The ability of crystalline compound chalcogenide semiconductors such as ZnSe to host transition metal ions, e.g., Cr^{2+}, that have excellent optical gain properties in the MIR suggests that one of the first applications of ZnSe fibers may be for high-power tunable MIR fiber lasers. ZnSe fiber lasers should have less thermal lensing and improved thermal management in comparison with bulk ZnSe lasers. Fibers fabricated from ZnSe may also be useful for nonlinear frequency conversion in view of its substantial second-order nonlinear optical coefficient.

Figure 17

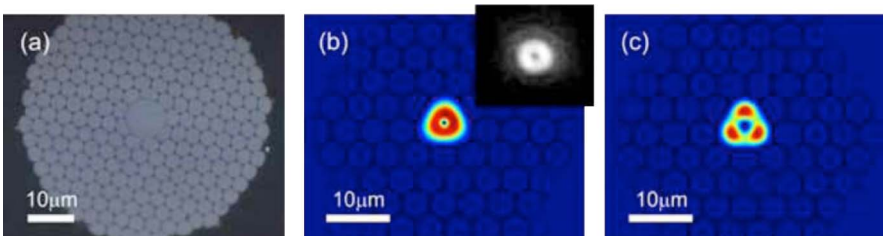

(a) Optical micrograph of core–cladding ZnSe microstructured fiber fabricated from a silica fiber template. (b) Finite element simulation of the fundamental mode for this fiber at 1550 nm. (c) Finite element simulation of the second-order mode at 1550 nm. Inset in (b) shows the measured near-field intensity of the guided mode at 1550 nm.

Lower optical losses, greater control over mode structure, and longer length fibers can be anticipated in the future for chemically deposited semiconductor fibers. Microstructured ZnSe optical fibers allow for control over mode geometry [Figs. 17(b) and 17(c)]; these modes overlap with only a small amount of silica, decreasing losses due to silica absorption. Deposition of a Zn-S/Se cladding layer followed by a ZnSe core can allow for complete elimination of the mode overlap with silica present in silica clad ZnSe fibers (Fig. 10) [392]. Appropriate modification of the grain/microstructure may allow for considerably lower optical losses, as the intrinsic optical loss of ZnSe is very low [73]. Finally, the deposition of Si layers up to 10 m long [415] inside silica fiber pores suggests that longer chemically deposited optical fiber cores may be possible in the future.

Summary. Combining multiple materials with disparate optical, electronic, and mechanical characteristics in the same fiber—so-called multimaterial fibers—is a research endeavor that has flourished over the past decade and is currently having a significant impact on IR fibers. This methodology is particularly useful in producing fibers from IR materials that cannot be drawn into a fiber directly, such as crystalline semiconductors.

9. Other Infrared Fibers

In view of the difficulty of identifying IR-transparent materials that produce low-loss and robust IR fibers, a long-exploited approach has been to rely on hollow-core fibers, the earliest realization being hollow metal fibers [420] (see Section 8 for hollow-core multimaterial PBG fibers as an alternative avenue). Such fibers offer various advantages; for example, they may transmit wavelengths well beyond 20 μm, in addition to having low insertion loss, minimal end reflection, and small beam divergence. In contrast to solid-core IR fibers, their hollow-core counterparts have high damage thresholds for high-peak-power and high-average-power lasers (over a kilowatt of CW laser power in Ref. [421], for instance). Indeed, it has been noted that front-end clipping in a CO_2 laser beam delivered through a hollow-core metal fiber is the main cause of thermal loading [422].

9.1. Hollow-Core Silica Infrared Fibers

While silica is of itself quite opaque in the MIR, the robustness of silica and the well-established technology of silica fiber fabrication have motivated the search for photonic structures that nevertheless allow for low-loss MIR propagation utilizing silica. The key feature of this approach is to create structures that minimize the fraction of light guided in the material to take advantage of the IR transparency of air or other gases in the core. Indeed, a hollow-core silica PBG fiber demonstrated MIR transmission in 2005 [423] with a loss of 2.6 dB/m at a wavelength of 3.14 μm, which is 2 orders of magnitude lower than the material loss in silica at this wavelength. With a 40-μm-diameter core, this fiber exhibited quasi-single-mode guidance and low bend losses.

Recent efforts have further reduced the fraction of light overlapping with the silica glass by exploiting a hollow-core design with *negative curvature* along the circumference of the hollow core. While hollow-core PBG fibers rely on PBG guidance from a periodic cladding structure, negative curvature (NC) fibers or antiresonant (AR) fibers rely for guidance on a combination of inhibited coupling to low density of states cladding modes and antiresonance [424,425]. The typical advantages of AR fibers over PBG fibers are expanding new transmission regions in the UV and IR spectral regions, while also offering wider bandwidths than PBG fibers. This concept originates from the early studies on antiresonant reflecting optical waveguides (ARROWs) in SiO_2-Si multilayer structures in the 1980s [426]. More studies were carried out on the guiding conditions, single-mode operation, and analysis of leakage properties of various ARROWs where the core is either a low-refractive-index material or air (hollow core) [427–433]. The major motivation behind these studies is the applications of these waveguides in integrated photonics, sensing, and quantum communications. Similar simple design strategies were applied to cylindrical waveguides (fibers) consisting of high-index inclusions that surround a low-index core, either to integrate them with existing fiber infrastructures or to extend the transmission to longer wavelengths into the MIR and THz region both theoretically and experimentally [434–443]. The demonstration of high-average-power picosecond and nanosecond pulse delivery at the NIR (1030 and 1064 nm, respectively) region [444] and MIR (2.94 μm) [54] through hollow-core AR fibers proves the potential for applications in micromachining and surgical devices. Furthermore, deep-ultraviolet (UV) light is also guided by a double AR hollow-core fiber in the single-mode regime by modified tunneling of leaky modes [445]. This design led to fibers with losses of 0.034 dB/m at 3.05 μm wavelength for a 9.4 μm core diameter [446] and 50 dB/m at 7.7 μm for a 119 μm core [434]. These fiber losses are 3–4 orders of magnitude lower than those of bulk silica at these wavelengths. See Table 5 for a comparison of the state of the art. These fiber examples demonstrate the potential of the hollow-core fiber approach to achieve MIR guidance at wavelengths where the fiber material has significantly high loss.

The limitation of this approach is that larger core diameters (>10 μm) are required to reduce the fraction of guided light in the material surrounding the hollow core. Furthermore, hollow-core fibers, in general, suffer from some drawbacks, ranging from the need for more complicated fabrication methodologies to difficulties in splicing to other fibers. Additionally, surface modes appear in these structures, limiting significantly the fiber properties. Recent efforts to experimentally reduce the bending loss of hollow AR fibers [447] and theoretically explore new design strategies for ultralow loss at the MIR region [448] further prove the feasibility of utilizing AR fibers with multiple applications and positive aspects for future commercialization. Interestingly, the hollow-core AR fiber approach has been successfully extended to IR glasses, such as ChGs, that are inherently IR transparent. A recent report demonstrated a fiber with 11 dB/m loss at 10.6 μm for a 380-μm-diameter core [449].

9.2. Hollow Metallic Infrared Fibers

Fabrication of such fibers typically involves the use of a glass, polymer, or metallic tubing in which metal and dielectric layers are deposited to enhance the IR reflectivity from the inner surface [450–452]. Miyagi *et al.* pioneered the

Table 5. Examples of Hollow-Core Fiber with Low Loss in the MIR

Fiber Type	D_{core} (μm)	Material	λ (μm)	Material Loss (dB/m)	Fiber Loss (dB/m)	Ref.
PBG via omnidirectional dielectric mirror	700	ChG polymer	10.6	10^1 for glass 10^5 for polymer	0.95	[21]
PBG via periodic air/glass structure	40	silica	3.14	6×10^1	2.6	[423]
ARG via negative-curvature hollow core	94	silica	3.05	6×10^1	0.034	[446]
ARG via negative-curvature hollow core	119	silica	3.4 7.7	6×10^1 10^5	0.05 50	[434]
ARG via negative-curvature hollow core	380	silica	10.6	5×10^1	11	[449]

development of metallic waveguides based on a hollow nickel substrate [451], and further developed dielectric coatings (ZnS) over silver with losses as low as 0.25 dB/m at 10.6 μm [453], in addition to hollow-core structures having a square cross section with 0.1 dB/m loss at 10.6 μm [454]. A critical disadvantage of hollow metallic fibers is the high bending losses (which depends largely on the quality of the inner surface).

To date, hollow metallic fibers have found numerous applications in transmitting broadband IR light for dental and medical laser treatment and industrial laser materials processing. Moreover, metallic IR fibers are an ideal platform for thermal radiometry (the peak of blackbody radiation near room temperature is around 10 μm) and have been used to transmit radiation produced in the nondestructive measurements of jet engine blade temperatures (corresponding to blackbody radiation above 1000°C). More recently, hollow metallic fibers have been used to transmit incoherent light for broadband spectroscopic and radiometric applications [455–457]. In addition they may be used as delivery systems in chemical remote sensing applications, either as a passive fiber or as an active platform filled with the medium to be probed [458]. Nevertheless, these fibers have not been fully accepted as flexible delivery systems for industrial lasers, due partially to the relatively high loss when compared to other technologies (e.g., articulated arms) and to the potential distortions of beam profiles in large-diameter multimode hollow-core metal fibers.

9.3. Crystalline Infrared Fibers by Hot Extrusion

Step-index polycrystalline alkali halide fibers have been fabricated using a hot-extrusion technique [119,459]. An example is KBr/KCl fibers, which have demonstrated a minimum loss of ~0.1 dB/m at 10.6 μm [119]. There are run-to-run variations in fabricating such fibers, leading to an average loss 0.69 dB/m with a standard deviation of 0.32 dB/m over different runs (varying typically in the range between 0.3 and 1.0 dB/m) for freshly extruded step-index fibers with core/cladding diameters of 800/1000 μm. The maximum output power from such a fiber is 67 W of CW CO_2 laser power, corresponding to a power density of 13.3kW/cm^2. Bending the fiber with a diameter of curvature of 12 cm was found to reduce the transmission through such 1000 μm salt fibers by ≈5%. These fibers are typically coated with Teflon to minimize surface fracture from microcleavage cracks and to protect the fiber from contamination.

Recently, multiple hot extrusion of flexible 1-mm-diameter, 1-m-long silver halide polycrystalline fibers has been reported [460]. These fibers are highly

transparent in the MIR. The core was AgBr while the cladding consisted or AgCl fiber optic elements arranged in two concentric hexagonal rings around the core. These (effectively step-index) fibers are potentially useful for IR laser power transmission, IR radiometry, and IR spectroscopy [435,461–463].

9.4. Hybrid Infrared Fibers by Pressure-Assisted Melt Filling

ChG–silica hybrid fibers of limited length (a few centimeters) may be fabricated using a pressure-assisted melt-filling technique, as illustrated in Fig. 18. First, a ChG fiber is inserted into a silica capillary with inner diameter 150 μm and outer diameter 200 μm [Fig. 18(a)]. This capillary is then spliced to a second capillary having inner and outer diameters of 1 and 200 μm, respectively. The inner diameter of the second capillary determines the resultant ChG core diameter. Second, both capillaries are placed in an oven at a high temperature (~600°C for As_2S_3 glass) while applying argon gas to force the melted ChG from the first capillary into the channel of the second [Fig. 18(b)]. A filling time of typically 1 h is needed for ChG to fill in a few-centimeter length. Small bubbles that nucleate and grow during the filling process may be removed using a heat source scanned along the capillary. Finally, a continuous part is sectioned and cleaved to form the target short fiber.

This technique has been successfully adapted to S- and Se-ChG and tellurite glasses to fabricate hybrid fiber with core diameters ranging from 200 nm to 6 μm [14,464], with the aim of broadband MIR supercontinuum generation. Most recently, this technique was modified to integrate nanotapers at the input and output ends of the fiber to increase the incoupling and outcoupling efficiency [465]. In addition to step-index fibers, it is also possible to fabricate hybrid MOFs using this technique to realize all-solid bandgap guidance [466,467].

Figure 18

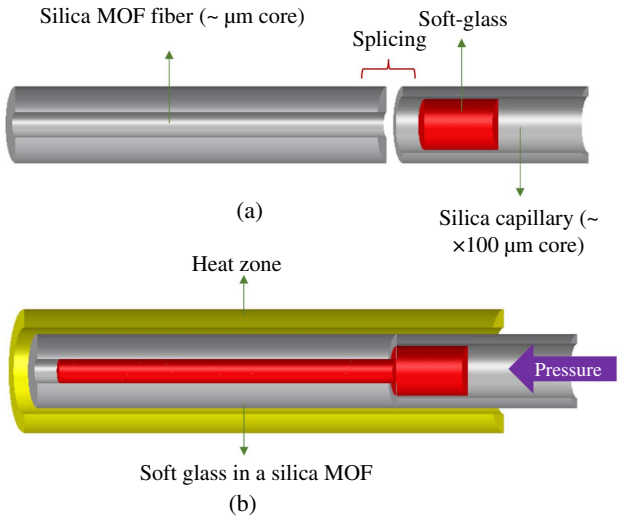

Pressure-assisted melt-filling technique for ChG-core, silica-cladding IR fiber. (a) A soft glass fiber is inserted into a silica capillary, which is spliced with another silica capillary. (b) High temperature and pressure are applied to force soft glass into the channel of the left silica capillary.

10. Future Prospects

As mentioned in the introduction, considerable recent research in optics has been mobilized by the prospect of extending well-known concepts and technologies from the VIS and NIR to the MIR. This less-explored spectral vista offers unique capabilities, particularly in metrology, sensing, and biomedicine. Consequently, the field of IR fibers—as an essential technology for facilitating the utilization of the IR spectrum—is currently witnessing sustained and dramatic growth. Perhaps a measure of one aspect of this growth, at least from the perspective of academic research, is the number of published journal articles and citations, as shown in Fig. 19. Steady growth is readily observed, especially with regards to tellurite and chalcogenide fibers. Figure 19 obviously relates to only a segment of the field of IR fibers; therefore, these figures represent a lower estimate, but are nevertheless indicative of the field in general. The concomitant growth in the IR fiber industry, as evinced by recent commercialization of IR fibers for QCL light delivery, also bodes well for future growth.

Figure 19

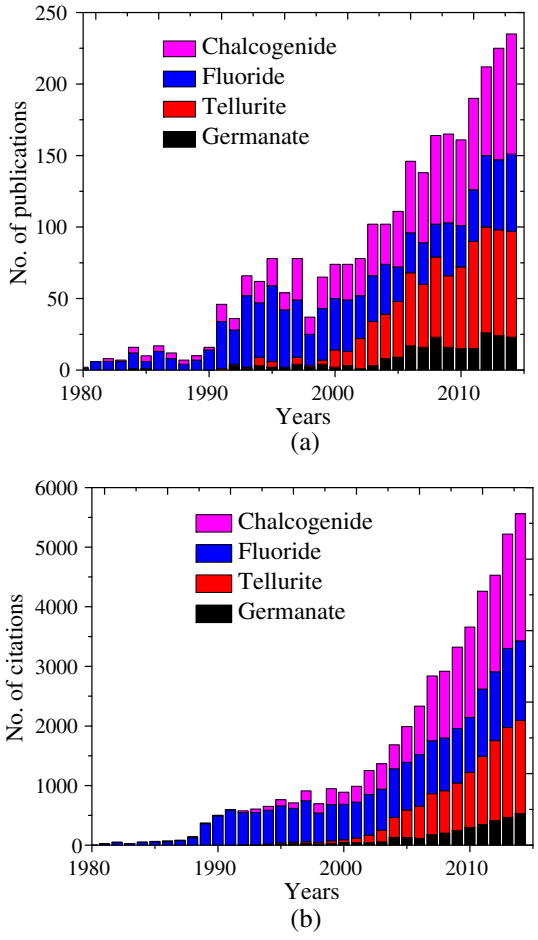

Number of publications and citations to these publications at Web of Science from 1980 to 2014. The search was carried out using the following keywords in the title: "X AND glass AND fiber," where X corresponds to "Chalcogenide," "Fluoride," "Tellurite," or "Germanate," as shown in the figure legend.

Several critical tasks lie ahead for the IR fiber community. There is acute need for standardization: in fabrication processes (especially of bulk IR glasses) and in characterization techniques—and even in nomenclature—to facilitate the exchange of knowledge across the various research communities involved in optical physics and engineering and materials science. Since there appears to be no one-size-fits-all material or fabrication approach that will dominate this field in the foreseeable future, it will be crucial to develop more applications that benefit from IR light to continue to motivate research.

This review may also help lay out a roadmap for future developments in IR-fiber-based technologies that will be critical for exploiting the IR spectrum. The first milestones, which have already been partially addressed, lie in the optimization of IR fibers for the delivery of QCL light and also high-power IR lasers. Both of these optical sources are undergoing rapid development and the availability of convenient IR delivery fibers will have profound impact on applications in biosensing, pollution monitoring, and defense. Furthermore, novel fiber-based IR sources are a potential growth area. There has been tremendous progress in IR supercontinuum generation from IR fibers [14,43,44,169,216,220,246,248,250,468–473], but other nonlinear wavelength conversion schemes need also to be developed, such as Raman shifting and four-wave mixing. The high optical nonlinearity of IR glasses and the potential for dispersion engineering in high-index-contrast fibers may be exploited in producing IR laser combs [474–476]. Moreover, postprocessing of IR fibers, via tapering, for example, can allow for tailoring the fiber device characteristics to a target function [254,477–480]. Finally, while research on REI doping of IR fibers has occupied the community for decades, there has not yet been a decisive breakthrough that may lead to high-power lasing using the approaches followed in shorter-wavelength (VIS and NIR) fiber lasers [37].

In achieving the milestones along this roadmap, the technical hurdles facing IR fibers—such as high optical losses and mechanical fragility—need to be at the fore of the community's attention. Hurdles to the standardization of procedures for fiber facet polishing, fiber splicing, and connectorization need to be tackled. Additionally, recent progress in spatial mode control and modal analysis will be of utility in both linear and nonlinear applications of IR fibers [481]. Such advances will particularly facilitate extending the capabilities of fiber sensing technology to the IR.

We anticipate a bright future for IR fibers and hope that this article serves as an entry point to the vast literature that has already accumulated in this field.

Acknowledgments

G. Tao acknowledges Dr. Rongping Wang and Dr. Shangran Xie, for illuminating discussions; Dr. Shangran Xie, Prof. Philip St. J. Russell, Dr. Fei Yu, and Prof. Jonathan Knight, Dr. Jas Sanghera, Dr. Mohammed Saad, Prof. James A. Harrington, Dr. Tomer Lewi for offering images of their results; and He Ren, Dr. Kunlun Yan, Ruilin Zheng, Dr. Yinsheng Xu, and Dr. Xinghua Yang for assistance with preparing this manuscript. H. Ebendorff-Heidepriem acknowledges Jiafang Bei for glass transmission measurements. S. Danto acknowledges Prof. Thierry Cardinal for his support. Work at the University of Adelaide was supported by the Defence Science and Technology Organisation (DSTO), the Asian Office of Aerospace R&D (AOARD), the South Australian Government, and the

Australian Research Council (ARC). Work at the University of Adelaide was performed in part at the OptoFab node of the Australian National Fabrication Facility utilizing Commonwealth and SA State Government funding. Work at Pennsylvania State University was supported by the U.S. National Science Foundation (DMR-0806860, DMR-1107894, and NSF MRSEC DMR-0820404). Work at MIT was supported by the Materials Research Science and Engineering Program of the U.S. National Science Foundation (DMR-0819762) and also in part by the U.S. Army Research Office through the Institute for Soldier Nanotechnologies (W911NF-07-D-0004). Work at Clemson University was supported by Northrop Grumman Corporation and the Raytheon Company. Work at the University of Central Florida was supported by the U.S. National Science Foundation (ECCS-1002295) and in part by the U.S. Air Force Office of Scientific Research (FA-9550-12-1-0148).

References

1. http://eilv.cie.co.at/term/580, retrieved April 1, 2015.
2. "Optics and photonics—spectral bands," ISO 20472:2007 (2010).
3. J. S. Byrnes, *Unexploded Ordnance Detection and Mitigation* (Springer, 2009).
4. W. M. Haynes, *CRC Handbook of Chemistry and Physics* (CRC Press, 2015).
5. http://www.ipac.caltech.edu/outreach/Edu/Regions/irregions.html, retrieved April 1, 2015.
6. J. L. Miller, E. Friedman, and E. Friedman, *Photonics Rules of Thumb* (McGraw-Hill, 2003).
7. G. Tao, S. Shabahang, H. Ren, Z. Yang, X. Wang, and A. F. Abouraddy, "Multimaterial rod-in-tube coextrusion for robust mid-infrared chalcogenide fibers," Proc. SPIE **8982**, 898223 (2014).
8. F. Capasso, "High-performance midinfrared quantum cascade lasers," Opt. Eng. **49**, 111102 (2010).
9. N. S. Kapany and R. J. Simms, "Recent developments in infrared fiber optics," Infrared Phys. **5**, 69–80 (1965).
10. G. Tao, A. M. Stolyarov, and A. F. Abouraddy, "Multimaterial fibers," Int. J. Appl. Glass Sci. **3**, 349–368 (2012).
11. A. F. Abouraddy, M. Bayindir, G. Benoit, S. D. Hart, K. Kuriki, N. Orf, O. Shapira, F. Sorin, B. Temelkuran, and Y. Fink, "Towards multimaterial multifunctional fibres that see, hear, sense and communicate," Nat. Mater. **6**, 336–347 (2007).
12. J. Toulouse, A. Lin, A. Ryaznyanskiy, A. Belwalkar, C. Guintrand, C. Lafontaine, W. Misiolek, and I. Biaggio, "Development of new tellurite fibers for mid-IR applications," in *Winter Topicals (WTM)* (IEEE, 2011), pp. 185–186.
13. G. Tao, S. Shabahang, E.-H. Banaei, J. J. Kaufman, and A. F. Abouraddy, "Multimaterial preform coextrusion for robust chalcogenide optical fibers and tapers," Opt. Lett. **37**, 2751–2753 (2012).
14. N. Granzow, S. P. Stark, M. A. Schmidt, A. S. Tverjanovich, L. Wondraczek, and P. S. J. Russell, "Supercontinuum generation in chalcogenide-silica step-index fibers," Opt. Express **19**, 21003–21010 (2011).
15. T. Cheng, W. Gao, H. Kawashima, D. Deng, M. Liao, M. Matsumoto, T. Misumi, T. Suzuki, and Y. Ohishi, "Widely tunable second-harmonic

generation in a chalcogenide-tellurite hybrid optical fiber," Opt. Lett. **39**, 2145–2147 (2014).
16. J. Ballato, T. Hawkins, P. Foy, C. McMillen, L. Burka, J. Reppert, R. Podila, A. M. Rao, and R. R. Rice, "Binary III–V semiconductor core optical fiber," Opt. Express **18**, 4972–4979 (2010).
17. J. R. Sparks, R. He, N. Healy, M. Krishnamurthi, A. C. Peacock, P. J. A. Sazio, V. Gopalan, and J. V. Badding, "Zinc selenide optical fibers," Adv. Mater. **23**, 1647–1651 (2011).
18. Z. Lian, Q. Li, D. Furniss, T. M. Benson, and A. B. Seddon, "Solid microstructured chalcogenide glass optical fibers for the near- and mid-infrared spectral regions," IEEE Photon. Technol. Lett. **21**, 1804–1806 (2009).
19. J. S. Sanghera, B. Shaw, R. Gattass, L. Busse, W. Kim, S. Bayya, D. Gibson, V. Nguyen, F. Kung, G. Chin, C. Baker, K. Ewing, and I. Aggarwal, "Infrared optical fibers for sensors," in *International Conference on Fibre Optics and Photonics*, OSA Technical Digest (online) (Optical Society of America, 2012), paper T2A.3.
20. F. Désévédavy, G. Renversez, J. Troles, P. Houizot, L. Brilland, I. Vasilief, Q. Coulombier, N. Traynor, F. Smektala, and J.-L. Adam, "Chalcogenide glass hollow core photonic crystal fibers," Opt. Mater. **32**, 1532–1539 (2010).
21. B. Temelkuran, S. D. Hart, G. Benoit, J. D. Joannopoulos, and Y. Fink, "Wavelength-scalable hollow optical fibres with large photonic bandgaps for CO_2 laser transmission," Nature **420**, 650–653 (2002).
22. www.thorlabs.com, retrieved April 1, 2015.
23. www.npphotonics.com, retrieved April 1, 2015.
24. www.irflex.com, retrieved April 1, 2015.
25. www.coractive.com, retrieved April 1, 2015.
26. R. He, P. J. A. Sazio, A. C. Peacock, N. Healy, J. R. Sparks, M. Krishnamurthi, V. Gopalan, and J. V. Badding, "Integration of gigahertz-bandwidth semiconductor devices inside microstructured optical fibres," Nat. Photonics **6**, 174–179 (2012).
27. P. Dragic, T. Hawkins, P. Foy, S. Morris, and J. Ballato, "Sapphire-derived all-glass optical fibres," Nat. Photonics **6**, 629–635 (2012).
28. H. Ebendorff-Heidepriem, S. C. Warren-Smith, and T. M. Monro, "Suspended nanowires: fabrication, design and characterization of fibers with nanoscale cores," Opt. Express **17**, 2646–2657 (2009).
29. M. Duhant, W. Renard, G. Canat, T. N. Nguyen, F. Smektala, J. Troles, Q. Coulombier, P. Toupin, L. Brilland, P. Bourdon, and G. Renversez, "Fourth-order cascaded Raman shift in AsSe chalcogenide suspended-core fiber pumped at 2 μm," Opt. Lett. **36**, 2859–2861 (2011).
30. M. El-Amraoui, J. Fatome, J. C. Jules, B. Kibler, G. Gadret, C. Fortier, F. Smektala, I. Skripatchev, C. F. Polacchini, Y. Messaddeq, J. Troles, L. Brilland, M. Szpulak, and G. Renversez, "Strong infrared spectral broadening in low-loss As-S chalcogenide suspended core microstructured optical fibers," Opt. Express **18**, 4547–4556 (2010).
31. I. Savelii, O. Mouawad, J. Fatome, B. Kibler, F. Désévédavy, G. Gadret, J. C. Jules, P. Y. Bony, H. Kawashima, W. Gao, T. Kohoutek, T. Suzuki, Y. Ohishi, and F. Smektala, "Mid-infrared 2000-nm bandwidth supercontinuum generation in suspended-core microstructured sulfide and tellurite optical fibers," Opt. Express **20**, 27083–27093 (2012).

32. Y. Fink, J. N. Winn, S. Fan, C. Chen, J. Michel, J. D. Joannopoulos, and E. L. Thomas, "A dielectric omnidirectional reflector," Science **282**, 1679–1682 (1998).
33. www.omni-guide.com, retrieved April 1, 2015.
34. A. B. Seddon, Z. Tang, D. Furniss, S. Sujecki, and T. M. Benson, "Progress in rare-earth-doped mid-infrared fiber lasers," Opt. Express **18**, 26704–26719 (2010).
35. J. C. Knight, "Photonic crystal fibres," Nature **424**, 847–851 (2003).
36. P. Russell, "Photonic crystal fibers," Science **299**, 358–362 (2003).
37. S. D. Jackson, "Towards high-power mid-infrared emission from a fibre laser," Nat. Photonics **6**, 423–431 (2012).
38. J. A. Harrington, *Infrared Fibers and Their Applications* (SPIE, 2004).
39. T. Li, *Optical Fiber Communications: Fiber Fabrication* (Academic, 1985).
40. C. Emslie, "Polymer optical fibres," J. Mater. Sci. **23**, 2281–2293 (1988).
41. M. Poulain, M. Poulain, and J. Lucas, "Verres fluores au tetrafluorure de zirconium proprietes optiques d'un verre dope au Nd^{3+}," Mater. Res. Bull. **10**, 243–246 (1975).
42. http://www.amorphousmaterials.com/, retrieved April 1, 2015.
43. S. Shabahang, G. Tao, M. P. Marquez, H. Hu, T. R. Ensley, P. J. Delfyett, and A. F. Abouraddy, "Nonlinear characterization of robust multimaterial chalcogenide nanotapers for infrared supercontinuum generation," J. Opt. Soc. Am. B **31**, 450–457 (2014).
44. S. Shabahang, M. P. Marquez, G. Tao, M. U. Piracha, D. Nguyen, P. J. Delfyett, and A. F. Abouraddy, "Octave-spanning infrared supercontinuum generation in robust chalcogenide nanotapers using picosecond pulses," Opt. Lett. **37**, 4639–4641 (2012).
45. S. Cherukulappurath, M. Guignard, C. Marchand, F. Smektala, and G. Boudebs, "Linear and nonlinear optical characterization of tellurium based chalcogenide glasses," Opt. Commun. **242**, 313–319 (2004).
46. E. D. Palik, *Handbook of Optical Constants of Solids* (Academic, 1998).
47. F. Gan, "Optical properties of fluoride glasses: a review," J. Non-Cryst. Solids **184**, 9–20 (1995).
48. S. Fujino and K. Morinaga, "Material dispersion and its compositional parameter of oxide glasses," J. Non-Cryst. Solids **222**, 316–320 (1997).
49. P. France, S. Carter, M. Moore, and C. Day, "Progress in fluoride fibres for optical communications," British Telecommun. Technol. J. **5**, 28–44 (1987).
50. R. Wang, Laser Physics Centre, Research School of Physics and Engineering, The Australian National University, Canberra ACT 2600, Australia (personal communication, 2015).
51. H. Bach and N. Neuroth, *The Properties of Optical Glass* (Springer, 1998).
52. J. Lægsgaard and H. Tu, "How long wavelengths can one extract from silica-core fibers?" Opt. Lett. **38**, 4518–4521 (2013).
53. R. Kitamura, L. Pilon, and M. Jonasz, "Optical constants of silica glass from extreme ultraviolet to far infrared at near room temperature," Appl. Opt. **46**, 8118–8133 (2007).
54. A. Urich, R. R. J. Maier, F. Yu, J. C. Knight, D. P. Hand, and J. D. Shephard, "Silica hollow core microstructured fibres for mid-infrared surgical applications," J. Non-Cryst. Solids **377**, 236–239 (2013).
55. http://www.newport.com/Optical-Materials/144943/1033/content.aspx, retrieved April 1, 2015.

56. D. G. Lancaster, S. Gross, H. Ebendorff-Heidepriem, M. J. Withford, T. M. Monro, and S. D. Jackson, "Efficient 2.9 μm fluorozirconate glass waveguide chip laser," Opt. Lett. **38**, 2588–2591 (2013).
57. M. R. Oermann, H. Ebendorff-Heidepriem, Y. Li, T.-C. Foo, and T. M. Monro, "Index matching between passive and active tellurite glasses for use in microstructured fiber lasers: erbium doped lanthanum-tellurite glass," Opt. Express **17**, 15578–15584 (2009).
58. E. R. Dobrovinskaya, L. A. Lytvynov, and V. Pishchik, *Sapphire: Material, Manufacturing, Applications* (Springer, 2009).
59. Y. Shen, L. Tong, and S. Chen, "Performance stability of the sapphire fiber and cladding under high temperature," Proc. SPIE **3852**, 134 (1999).
60. H. Jiang, Z. Cao, R. Yang, L. Yuan, H. Xiao, and J. Dong, "Synthesis and characterization of spinel $MgAl_2O_4$ thin film as sapphire optical fiber cladding for high temperature applications," Thin Solid Films **539**, 81–87 (2013).
61. R. K. Nubling, R. L. Kozodoy, and J. A. Harrington, "Optical properties of clad and unclad sapphire fiber," Proc. SPIE **2131**, 56–61 (1994).
62. H. J. Kim, G. E. Fair, S. A. Potticary, M. J. O'Malley, and N. G. Usechak, "Processing and characterization of polycrystalline YAG (yttrium aluminum garnet) core-clad fibers," Proc. SPIE **9081**, 908103 (2014).
63. J. Wang, E. Vogel, and E. Snitzer, "Tellurite glass: a new candidate for fiber devices," Opt. Mater. **3**, 187–203 (1994).
64. M. Saad, "Fluoride glass fiber: state of the art," Proc. SPIE **7316**, 73160N (2009).
65. M. Poulain, M. Matecki, J.-L. Mouric, and M. Poulain, "Cadmium halide glasses. II. Chloride glasses," Mater. Res. Bull. **18**, 631–636 (1983).
66. J.-L. Adam and X. Zhang, *Chalcogenide Glasses: Preparation, Properties and Applications* (Woodhead, 2014).
67. A. Zakery and S. R. Elliott, *Optical Nonlinearities in Chalcogenide Glasses and Their Applications* (Springer, 2007).
68. M. Wuttig and N. Yamada, "Phase-change materials for rewriteable data storage," Nat. Mater. **6**, 824–832 (2007).
69. J. Orava, A. Greer, B. Gholipour, D. Hewak, and C. Smith, "Characterization of supercooled liquid $Ge_2Sb_2Te_5$ and its crystallization by ultrafast-heating calorimetry," Nat. Mater. **11**, 279–283 (2012).
70. J. Charrier, M.-L. Brandily, H. Lhermite, K. Michel, B. Bureau, F. Verger, and V. Nazabal, "Evanescent wave optical micro-sensor based on chalcogenide glass," Sens. Actuators B **173**, 468–476 (2012).
71. L. Li, H. Lin, S. Qiao, Y. Zou, S. Danto, K. Richardson, J. D. Musgraves, N. Lu, and J. Hu, "Integrated flexible chalcogenide glass photonic devices," Nat. Photonics **8**, 643–649 (2014).
72. A. R. Hilton, *Chalcogenide Glasses for Infrared Optics* (McGraw-Hill, 2009).
73. J. R. Sparks, P. J. Sazio, V. Gopalan, and J. V. Badding, "Templated chemically deposited semiconductor optical fiber materials," Annu. Rev. Mater. Res. **43**, 527–557 (2013).
74. P. J. Sazio, A. Amezcua-Correa, C. E. Finlayson, J. R. Hayes, T. J. Scheidemantel, N. F. Baril, B. R. Jackson, D.-J. Won, F. Zhang, and E. R. Margine, "Microstructured optical fibers as high-pressure microfluidic reactors," Science **311**, 1583–1586 (2006).
75. www.rmico.com, retrieved April 1, 2015.

76. G. T. Reed, G. Mashanovich, F. Gardes, and D. Thomson, "Silicon optical modulators," Nat. Photonics **4**, 518–526 (2010).
77. J. Leuthold, C. Koos, and W. Freude, "Nonlinear silicon photonics," Nat. Photonics **4**, 535–544 (2010).
78. V. Raghunathan, R. Shori, O. M. Stafsudd, and B. Jalali, "Nonlinear absorption in silicon and the prospects of mid-infrared silicon Raman lasers," Phys. Status Solidi A **203**, R38–R40 (2006).
79. J. Ballato, T. Hawkins, P. Foy, B. Yazgan-Kokuoz, R. Stolen, C. McMillen, N. Hon, B. Jalali, and R. Rice, "Glass-clad single-crystal germanium optical fiber," Opt. Express **17**, 8029–8035 (2009).
80. J. Ballato, T. Hawkins, P. Foy, B. Yazgan-Kokuoz, C. McMillen, L. Burka, S. Morris, R. Stolen, and R. Rice, "Advancements in semiconductor core optical fiber," Opt. Fiber Technol. **16**, 399–408 (2010).
81. S. Morris, T. Hawkins, P. Foy, C. McMillen, J. Fan, L. Zhu, R. Stolen, J. Ballato, and R. Rice, "Reactive in-situ processing of silicon optical fiber," in *Advanced Photonics Congress*, OSA Technical Digest (online) (Optical Society of America, 2012), paper STu3F.4.
82. K. Shahzad, D. J. Olego, and D. A. Cammack, "Optical transitions in ultra-high-purity zinc selenide," Phys. Rev. B **39**, 13016 (1989).
83. M. A. Haase, J. Qiu, J. M. DePuydt, and H. Cheng, "Blue-green laser diodes," Appl. Phys. Lett. **59**, 1272–1274 (1991).
84. J. Ren, K. A. Bowers, B. Sneed, F. E. Reed, J. W. Cook, Jr., and J. F. Schetzina, "Blue (ZnSe) and green ($ZnSe_{0.9}Te_{0.1}$) light emitting diodes," J. Cryst. Growth **111**, 829–832 (1991).
85. http://www.kayelaby.npl.co.uk/general_physics/2_5/2_5_8.html, retrieved April 1, 2015.
86. E. Gavrushchuk, "Polycrystalline zinc selenide for IR optical applications," Inorg. Mater. **39**, 883–899 (2003).
87. A. Gallian, V. V. Fedorov, J. Kernal, S. B. Mirov, and V. V. Badikov, "Laser oscillation at 2.4 μm from Cr^{2+} in ZnSe optically pumped over Cr ionization transitions," in *Advanced Solid-State Photonics (TOPS)*, C. Denman and I. Sorokina, eds., Vol. **98** of OSA Trends in Optics and Photonics (Optical Society of America, 2005), paper 241.
88. N. D. Orf, O. Shapira, F. Sorin, S. Danto, M. A. Baldo, J. D. Joannopoulos, and Y. Fink, "Fiber draw synthesis," Proc. Natl. Acad. Sci. USA **108**, 4743–4747 (2011).
89. C. Hou, X. Jia, L. Wei, A. M. Stolyarov, O. Shapira, J. D. Joannopoulos, and Y. Fink, "Direct atomic-level observation and chemical analysis of ZnSe synthesized by in situ high-throughput reactive fiber drawing," Nano Lett. **13**, 975–979 (2013).
90. G. Zhai and L. Tong, "Roughness-induced radiation losses in optical micro or nanofibers," Opt. Express **15**, 13805–13816 (2007).
91. P. Roberts, F. Couny, H. Sabert, B. Mangan, T. Birks, J. Knight, and P. Russell, "Loss in solid-core photonic crystal fibers due to interface roughness scattering," Opt. Express **13**, 7779–7793 (2005).
92. R. Kostecki, H. Ebendorff-Heidepriem, S. C. Warren-Smith, and T. M. Monro, "Predicting the drawing conditions for microstructured optical fiber fabrication," Opt. Mater. Express **4**, 29–40 (2014).
93. S. Rosenberg, H. Papamichael, and I. Miaoulis, "A two-dimensional analysis of the viscous problem of a glass preform during the optical fibre drawing process," Glass Technol. **35**, 260–264 (1994).

94. A. Fitt, K. Furusawa, T. Monro, C. Please, and D. Richardson, "The mathematical modelling of capillary drawing for holey fibre manufacture," J. Eng. Math. **43**, 201–227 (2002).
95. A. Mawardi and R. Pitchumani, "Optical fiber drawing process model using an analytical neck-down profile," IEEE Photon. Technol. Lett. **2**, 620–629 (2010).
96. G. Luzi, P. Epple, M. Scharrer, K. Fujimoto, C. Rauh, and A. Delgado, "Influence of surface tension and inner pressure on the process of fibre drawing," J. Lightwave Technol. **28**, 1882–1888 (2010).
97. S. Lee and Y. Jaluria, "Simulation of the transport processes in the neck-down region of a furnace drawn optical fiber," Int. J. Heat Mass Transfer **40**, 843–856 (1997).
98. U. Paek and R. Runk, "Physical behavior of the neck-down region during furnace drawing of silica fibers," J. Appl. Phys. **49**, 4417–4422 (1978).
99. E. Pone, C. Dubois, N. Guo, S. Lacroix, and M. Skorobogatiy, "Newtonian and non-Newtonian models of the hollow all-polymer Bragg fiber drawing," J. Lightwave Technol. **24**, 4991–4999 (2006).
100. R. M. Wynne, "A fabrication process for microstructured optical fibers," J. Lightwave Technol. **24**, 4304–4313 (2006).
101. R. M. Wynne, "Manufacturing conditions for microstructured and nanostructured optical fibers," J. Lightwave Technol. **29**, 104–108 (2011).
102. http://www.matweb.com/, retrieved April 1, 2015.
103. http://www.goodfellowusa.com/A/Polyethersulfone-Polymer.html, retrieved April 1, 2015.
104. http://www.plasticoptics.com/optical-plastic-materials.html, retrieved April 1, 2015.
105. http://en.wikipedia.org/wiki/Poly(methyl_methacrylate), retrieved April 1, 2015.
106. http://www.makeitfrom.com/compare/Polymethylmethacrylate-PMMA-Acrylic/Soda-Lime-Float-Glass/, retrieved April 1, 2015.
107. http://hyperphysics.phy-astr.gsu.edu/hbase/tables/thrcn.html, retrieved April 1, 2015.
108. http://www.schott.com/advanced_optics/us/abbe_datasheets/schott_datasheet_all_us.pdf, retrieved April 1, 2015.
109. Y. Wang, D. Richardson, G. Brambilla, X. Feng, M. Petrovich, M. Ding, and Z. Song, "Bend sensors based on periodically tapered soft glass fibers," Proc. SPIE **7753**, 77534J (2011).
110. J. Bei, T. M. Monro, A. Hemming, and H. Ebendorff-Heidepriem, "Fabrication of extruded fluoroindate optical fibers," Opt. Mater. Express **3**, 318–328 (2013).
111. H. T. Munasinghe, A. Winterstein-Beckmann, C. Schiele, D. Manzani, L. Wondraczek, S. Afshar V., T. M. Monro, and H. Ebendorff-Heidepriem, "Lead-germanate glasses and fibers: a practical alternative to tellurite for nonlinear fiber applications," Opt. Mater. Express **3**, 1488–1503 (2013).
112. J. J. Kaufman, G. Tao, S. Shabahang, E.-H. Banaei, D. S. Deng, X. Liang, S. G. Johnson, Y. Fink, and A. F. Abouraddy, "Structured spheres generated by an in-fibre fluid instability," Nature **487**, 463–467 (2012).
113. J. J. Kaufman, R. Ottman, G. Tao, S. Shabahang, E.-H. Banaei, X. Liang, S. G. Johnson, Y. Fink, R. Chakrabarti, and A. F. Abouraddy, "In-fiber

production of polymeric particles for biosensing and encapsulation," Proc. Natl. Acad. Sci. USA **110**, 15549–15554 (2013).
114. S. Shabahang, J. Kaufman, D. Deng, and A. Abouraddy, "Observation of the Plateau-Rayleigh capillary instability in multi-material optical fibers," Appl. Phys. Lett. **99**, 161909 (2011).
115. D. Deng, N. Orf, A. Abouraddy, A. Stolyarov, J. Joannopoulos, H. Stone, and Y. Fink, "In-fiber semiconductor filament arrays," Nano Lett. **8**, 4265–4269 (2008).
116. D. Deng, N. Orf, S. Danto, A. Abouraddy, J. Joannopoulos, and Y. Fink, "Processing and properties of centimeter-long, in-fiber, crystalline-selenium filaments," Appl. Phys. Lett. **96**, 023102 (2010).
117. H. Tokiwa, Y. Mimura, T. Nakai, and O. Shinbori, "Fabrication of long single-mode and multimode fluoride glass fibres by the double-crucible technique," Electron. Lett. **21**, 1131–1132 (1985).
118. M. Kimura, S. Kachi, and K. Shiroyama, "Characteristics of KRS-5 fiber with crystalline cladding," Proc. SPIE **0618**, 85–88 (1986).
119. J. A. Harrington, "Infrared alkali halide fibers," Appl. Opt. **27**, 3097–3101 (1988).
120. M. Churbanov, G. Snopatin, V. Shiryaev, V. Plotnichenko, and E. Dianov, "Recent advances in preparation of high-purity glasses based on arsenic chalcogenides for fiber optics," J. Non-Cryst. Solids **357**, 2352–2357 (2011).
121. S. Danto, M. Dubernet, B. Giroire, J. D. Musgraves, P. Wachtel, T. Hawkins, J. Ballato, and K. Richardson, "Correlation between native As_2Se_3 preform purity and glass optical fiber mechanical strength," Mater. Res. Bull. **49**, 250–258 (2014).
122. G. Tao, S. Shabahang, H. Ren, F. Khalilzadeh-Rezaie, R. E. Peale, Z. Yang, X. Wang, and A. F. Abouraddy, "Robust multimaterial tellurium-based chalcogenide glass fibers for mid-wave and long-wave infrared transmission," Opt. Lett. **39**, 4009–4012 (2014).
123. G. Tao, S. Shabahang, S. Dai, and A. F. Abouraddy, "Multimaterial disc-to-fiber approach to efficiently produce robust infrared fibers," Opt. Mater. Express **4**, 2143–2149 (2014).
124. A. Méndez and T. F. Morse, *Specialty Optical Fibers Handbook* (Academic, 2011).
125. D. Furniss and A. B. Seddon, "Towards monomode proportioned fibreoptic preforms by extrusion," J. Non-Cryst. Solids **256**, 232–236 (1999).
126. Y. Ohishi, S. Mitachi, and S. Takahashi, "Fabrication of fluoride glass single-mode fibers," J. Lightwave Technol. **2**, 593–596 (1984).
127. I. Savelii, J. Jules, G. Gadret, B. Kibler, J. Fatome, M. El-Amraoui, N. Manikandan, X. Zheng, F. Désévédavy, and J. Dudley, "Suspended core tellurite glass optical fibers for infrared supercontinuum generation," Opt. Mater. **33**, 1661–1666 (2011).
128. G. Barton, M. A. van Eijkelenborg, G. Henry, M. C. Large, and J. Zagari, "Fabrication of microstructured polymer optical fibres," Opt. Fiber Technol. **10**, 325–335 (2004).
129. A. Belwalkar, H. Xiao, W. Z. Misiolek, and J. Toulouse, "Extruded tellurite glass optical fiber preforms," J. Mater. Process. Technol. **210**, 2016–2022 (2010).
130. D. C. Tran, C. F. Fisher, and G. H. Sigel, "Fluoride glass preforms prepared by a rotational casting process," Electron. Lett. **18**, 657–658 (1982).

131. J. Massera, A. Haldeman, D. Milanese, H. Gebavi, M. Ferraris, P. Foy, W. Hawkins, J. Ballato, R. Stolen, and L. Petit, "Processing and characterization of core–clad tellurite glass preforms and fibers fabricated by rotational casting," Opt. Mater. **32**, 582–588 (2010).
132. E. Roeder, "Extrusion of glass," J. Non-Cryst. Solids **5**, 377–388 (1971).
133. E. Roeder, "Flow behaviour of glass during extrusion," J. Non-Cryst. Solids **7**, 203–220 (1972).
134. L. Butvina, A. Butvina, E. Dianov, N. Lichkova, and V. Zagorodnev, "New mid-infrared extruded single and multi component metal halides crystalline fibers," in *Lasers, Sources, and Related Photonic Devices*, OSA Technical Digest (CD) (Optical Society of America, 2012), paper ITh1B.4.
135. M. El-Amraoui, G. Gadret, J. C. Jules, J. Fatome, C. Fortier, F. Désévédavy, I. Skripatchev, Y. Messaddeq, J. Troles, L. Brilland, W. Gao, T. Suzuki, Y. Ohishi, and F. Smektala, "Microstructured chalcogenide optical fibers from As_2S_3 glass: towards new IR broadband sources," Opt. Express **18**, 26655–26665 (2010).
136. H. Ebendorff-Heidepriem and T. M. Monro, "Extrusion of complex preforms for microstructured optical fibers," Opt. Express **15**, 15086–15092 (2007).
137. G. Tao, S. Shabahang, X. Wang, and A. F. Abouraddy, "Efficient disc-to-fiber multimaterial stacked coextrusion for robust infrared optical fibers," in *Frontiers in Optics* 2013, I. Kang, D. Reitze, N. Alic, and D. Hagan, eds., OSA Technical Digest (online) (Optical Society of America, 2013), paper FTu4B.3.
138. D. Furniss and A. B. Seddon, "Extrusion of gallium lanthanum sulfide glasses for fiber-optic preforms," J. Mater. Sci. Lett. **17**, 1541–1542 (1998).
139. K. Itoh, K. Miura, I. Masuda, M. Iwakura, and T. Yamashita, "Low-loss fluorozirco-aluminate glass fiber," J. Non-Cryst. Solids **167**, 112–116 (1994).
140. M. Zhu, X. Wang, Z. Pan, C. Cheng, Q. Zhu, C. Jiang, Q. Nie, P. Zhang, Y. Wu, and S. Dai, "Fabrication of an IR hollow-core Bragg fiber based on chalcogenide glass extrusion," Appl. Phys. A, doi: 10.1007/s00339-015-9017-3 (to be published).
141. D. J. Gibson and J. A. Harrington, "Extrusion of hollow waveguide preforms with a one-dimensional photonic bandgap structure," J. Appl. Phys. **95**, 3895–3900 (2004).
142. X. Feng, T. M. Monro, P. Petropoulos, V. Finazzi, and D. J. Richardson, "Extruded single-mode high-index-core one-dimensional microstructured optical fiber with high index-contrast for highly nonlinear optical devices," Appl. Phys. Lett. **87**, 081110 (2005).
143. Y. West, T. Schweizer, D. Brady, and D. Hewak, "Gallium lanthanum sulphide fibers for infrared transmission," Fiber Integr. Opt. **19**, 229–250 (2000).
144. S. D. Savage, C. A. Miller, D. Furniss, and A. B. Seddon, "Extrusion of chalcogenide glass preforms and drawing to multimode optical fibers," J. Non-Cryst. Solids **354**, 3418–3427 (2008).
145. D. Le Coq, C. Boussard-Plédel, G. Fonteneau, T. Pain, B. Bureau, and J. Adam, "Chalcogenide double index fibers: fabrication, design, and application as a chemical sensor," Mater. Res. Bull. **38**, 1745–1754 (2003).

146. H. T. Bookey, S. Dasgupta, N. Bezawada, B. P. Pal, A. Sysoliatin, J. E. McCarthy, M. Salganskii, V. Khopin, and A. K. Kar, "Experimental demonstration of spectral broadening in an all-silica Bragg fiber," Opt. Express **17**, 17130–17135 (2009).
147. M. Feng, A. K. Mairaj, D. W. Hewak, and T. M. Monro, "Nonsilica glasses for holey fibers," J. Lightwave Technol. **23**, 2046–2054 (2005).
148. Q. Coulombier, L. Brilland, P. Houizot, T. Chartier, T. N. N'Guyen, F. Smektala, G. Renversez, A. Monteville, D. Mechin, T. Pain, H. Orain, J.-C. Sangleboeuf, and J. Troles, "Casting method for producing low-loss chalcogenide microstructured optical fibers," Opt. Express **18**, 9107–9112 (2010).
149. C. M. Smith, N. Venkataraman, M. T. Gallagher, D. Muller, J. A. West, N. F. Borrelli, D. C. Allan, and K. W. Koch, "Low-loss hollow-core silica/air photonic bandgap fibre," Nature **424**, 657–659 (2003).
150. P. Kaiser, E. Marcatili, and S. Miller, "A new optical fiber," Bell Syst. Tech. J. **52**, 265–269 (1973).
151. F. Luan, A. K. George, T. D. Hedley, G. J. Pearce, D. M. Bird, J. C. Knight, and P. St. J. Russell, "All-solid photonic bandgap fiber," Opt. Lett. **29**, 2369–2371 (2004).
152. K. M. Kiang, K. Frampton, T. M. Monro, R. Moore, J. Tucknott, D. W. Hewak, D. J. Richardson, and H. N. Rutt, "Extruded singlemode non-silica glass holey optical fibres," Electron. Lett. **38**, 546–547 (2002).
153. M. Large, L. Poladian, G. Barton, and M. A. van Eijkelenborg, *Microstructured Polymer Optical Fibres* (Springer, 2007).
154. J. Sanghera, L. Shaw, L. Busse, V. Nguyen, P. Pureza, B. Cole, B. Harrison, I. Aggarwal, R. Mossadegh, and F. Kung, "Development and infrared applications of chalcogenide glass optical fibers," Fiber Integr. Opt. **19**, 251–274 (2000).
155. J. Kobelke, J. Kirchhof, M. Scheffler, and A. Schwuchow, "Chalcogenide glass single mode fibres—preparation and properties," J. Non-Cryst. Solids **256–257**, 226–231 (1999).
156. J. S. Sanghera, I. D. Aggarwal, L. E. Busse, P. C. Pureza, V. Q. Nguyen, R. E. Miklos, F. H. Kung, and R. Mossadegh, "Development of low-loss IR transmitting chalcogenide glass fibers," Proc. SPIE **2396**, 71–77 (1995).
157. T. Kanamori, Y. Terunuma, S. Takahashi, and T. Miyashita, "Chalcogenide glass-fibers for mid-infrared transmission," J. Lightwave Technol. **2**, 607–613 (1984).
158. A. Vasilyev, G. G. Devyatykh, E. M. Dianov, A. N. Gur'yanov, A. Y. Laptev, V. G. e. Plotnichenko, Y. N. Pyrkov, G. E. Snopatin, I. V. Skripachev, and M. F. Churbanov, "Two-layer chalcogenide-glass optical fibers with optical losses below 30 dB/km," Quantum Electron. **23**, 89–90 (1993).
159. F. Moser, N. Barkay, A. Levite, E. Margalit, I. Paiss, A. Sa'ar, I. Schnitzer, A. Zur, and A. Katzir, "Research and development on silver halide fibers at Tel Aviv University," Proc. SPIE **1228**, 128–139 (1990).
160. G. N. Merberg and J. A. Harrington, "Optical and mechanical properties of single-crystal sapphire optical fibers," Appl. Opt. **32**, 3201–3209 (1993).
161. G. Dhanaraj, K. Byrappa, V. Prasad, and M. Dudley, *Springer Handbook of Crystal Growth* (Springer, 2010).

162. J. E. Stanworth, "Tellurite glasses," Nature **169**, 581–582 (1952).
163. A. Jha, B. D. O. Richards, G. Jose, T. T. Fernandez, C. J. Hill, J. Lousteau, and P. Joshi, "Review on structural, thermal, optical and spectroscopic properties of tellurium oxide based glasses for fibre optic and waveguide applications," Int. Mater. Rev. **57**, 357–382 (2012).
164. X. Feng, J. Shi, M. Segura, N. M. White, P. Kannan, W. H. Loh, L. Calvez, X. Zhang, and L. Brilland, "Halo-tellurite glass fiber with low OH content for 2–5 μm mid-infrared nonlinear applications," Opt. Express **21**, 18949–18954 (2013).
165. C. Wang, P. Wang, R. Zheng, S. Xu, W. Wei, and B. Peng, "Spectroscopic properties of new Yb^{3+}-doped TeO_2–ZnO–Nb_2O_5 based tellurite glasses with high emission cross-section," Opt. Mater. **34**, 1549–1552 (2012).
166. D. Manzani, Y. Ledemi, I. Skripachev, Y. Messaddeq, S. J. L. Ribeiro, R. E. P. de Oliveira, and C. J. S. de Matos, "Yb^{3+}, Tm^{3+} and Ho^{3+} triply-doped tellurite core-cladding optical fiber for white light generation," Opt. Mater. Express **1**, 1515–1526 (2011).
167. T. M. Monro and H. Ebendorff-Heidepriem, "Progress in microstructured optical fibers," Annu. Rev. Mater. Res. **36**, 467–495 (2006).
168. K. Richardson, D. Krol, and K. Hirao, "Glasses for photonic applications," Int. J. Appl. Glass Sci. **1**, 74–86 (2010).
169. P. Domachuk, N. A. Wolchover, M. Cronin-Golomb, A. Wang, A. K. George, C. M. B. Cordeiro, J. C. Knight, and F. G. Omenetto, "Over 4000 nm bandwidth of mid-IR supercontinuum generation in sub-centimeter segments of highly nonlinear tellurite PCFs," Opt. Express **16**, 7161–7168 (2008).
170. M. Liao, X. Yan, G. Qin, C. Chaudhari, T. Suzuki, and Y. Ohishi, "A highly non-linear tellurite microstructure fiber with multi-ring holes for supercontinuum generation," Opt. Express **17**, 15481–15490 (2009).
171. R. Thapa, D. Rhonehouse, D. Nguyen, K. Wiersma, C. Smith, J. Zong, and A. Chavez-Pirson, "Mid-IR supercontinuum generation in ultra-low loss, dispersion-zero shifted tellurite glass fiber with extended coverage beyond 4.5 μm," Proc. SPIE **8898**, 889808 (2013).
172. C. Wei, X. Zhu, R. A. Norwood, F. Song, and N. Peyghambarian, "Numerical investigation on high power mid-infrared supercontinuum fiber lasers pumped at 3 μm," Opt. Express **21**, 29488–29504 (2013).
173. A. Mori, "Tellurite-based fibers and their applications to optical communication networks," J. Ceram. Soc. Jpn. **116**, 1040–1051 (2008).
174. A. N. Moiseev, V. V. Dorofeev, A. V. Chilyasov, I. A. Kraev, M. F. Churbanov, T. V. Kotereva, V. G. Pimenov, G. E. Snopatin, A. A. Pushkin, V. V. Gerasimenko, A. F. Kosolapov, V. G. Plotnichenko, and E. M. Dianov, "Production and properties of high purity TeO_2-ZnO-Na_2O-Bi_2O_3 and TeO_2-WO_3-La_2O_3-MoO_3 glasses," Opt. Mater. **33**, 1858–1861 (2011).
175. I. Savelii, F. Desevedavy, J.-C. Jules, G. Gadret, J. Fatome, B. Kibler, H. Kawashima, Y. Ohishi, and F. Smektala, "Management of OH absorption in tellurite optical fibers and related supercontinuum generation," Opt. Mater. **35**, 1595–1599 (2013).
176. H. Ebendorff-Heidepriem, K. Kuan, M. R. Oermann, K. Knight, and T. M. Monro, "Extruded tellurite glass and fibers with low OH content for mid-infrared applications," Opt. Mater. Express **2**, 432–442 (2012).

177. M. Churbanov, A. Moiseev, A. Chilyasov, V. Dorofeev, I. Kraev, M. Lipatova, T. Kotereva, E. Dianov, V. Plotnichenko, and E. Kryukova, "Production of high-purity TeO_2-ZnO and TeO_2-WO_3 glasses with the reduced content of OH-groups," J. Optoelectron. Adv. Mater. **9**, 3229–3234 (2007).
178. M. D. O'Donnell, C. A. Miller, D. Furniss, V. K. Tikhomirov, and A. B. Seddon, "Fluorotellurite glasses with improved mid-infrared transmission," J. Non-Cryst. Solids **331**, 48–57 (2003).
179. V. V. Dorofeev, A. N. Moiseev, M. F. Churbanov, T. V. Kotereva, A. V. Chilyasov, I. A. Kraev, V. G. Pimenov, L. A. Ketkova, E. M. Dianov, V. G. Plotnichenko, A. F. Kosolapov, and V. V. Koltashev, "Production and properties of high purity TeO_2–WO_3–(La_2O_3, Bi_2O_3) and TeO_2–ZnO–Na_2O–Bi_2O_3 glasses," J. Non-Cryst. Solids **357**, 2366–2370 (2011).
180. X. Feng, S. Tanabe, and T. Hanada, "Hydroxyl groups in erbium-doped germanotellurite glasses," J. Non-Cryst. Solids **281**, 48–54 (2001).
181. G. Liao, Q. Chen, J. Xing, H. Gebavi, D. Milanese, M. Fokine, and M. Ferraris, "Preparation and characterization of new fluorotellurite glasses for photonics application," J. Non-Cryst. Solids **355**, 447–452 (2009).
182. A. Lin, A. Zhang, E. J. Bushong, and J. Toulouse, "Solid-core tellurite glass fiber for infrared and nonlinear applications," Opt. Express **17**, 16716–16721 (2009).
183. A. Lin, A. Ryasnyanskiy, and J. Toulouse, "Fabrication and characterization of a water-free mid-infrared fluorotellurite glass," Opt. Lett. **36**, 740–742 (2011).
184. J. Massera, A. Haldeman, J. Jackson, C. Rivero-Baleine, L. Petit, and K. Richardson, "Processing of tellurite-based glass with low OH content," J. Am. Ceram. Soc. **94**, 130–136 (2011).
185. S. N. Xu, P. F. Wang, R. L. Zheng, W. Wei, and B. Peng, "Effects of alkaline-earth fluorides and OH- on spectroscopic properties of Yb^{3+} doped TeO_2-ZnO-B_2O_3 based glasses," J. Lumin. **140**, 26–29 (2013).
186. M. R. Oermann, H. Ebendorff-Heidepriem, D. J. Ottaway, D. G. Lancaster, P. J. Veitch, and T. M. Monro, "Extruded microstructured fiber lasers," IEEE Photon. Technol. Lett. **24**, 578–580 (2012).
187. X. Jiang, J. Lousteau, and A. Jha, "The structural, thermal, and optical analyses of multicomponent germanium oxide glasses for engineering mid-infrared fiber chemical sensing," J. Am. Ceram. Soc. **93**, 3259–3266 (2010).
188. S. Manning, H. Ebendorff-Heidepriem, and T. M. Monro, "Ternary tellurite glasses for the fabrication of nonlinear optical fibres," Opt. Mater. Express **2**, 140–152 (2012).
189. K. Li, G. Zhang, and L. Hu, "Watt-level ~2 μm laser output in Tm^{3+}-doped tungsten tellurite glass double-cladding fiber," Opt. Lett. **35**, 4136–4138 (2010).
190. L. Ke-Feng, W. Guo-Nian, H. Li-Li, Z. Jun-Jie, and H. Jun-Jiang, "Effects of WO_3 contents on the thermal and spectroscopic properties of Tm^{3+}-doped TeO_2-WO_3-La_2O_3 glasses," J. Inorg. Mater. **25**, 429–434 (2010).
191. X. Jiang, J. Lousteau, B. Richards, and A. Jha, "Investigation on germanium oxide-based glasses for infrared optical fibre development," Opt. Mater. **31**, 1701–1706 (2009).

192. R. Xu, Y. Tian, L. Hu, and J. Zhang, "Efficient ~2 μm emission and energy transfer mechanism of Ho^{3+} doped barium gallium germanate glass sensitized by Tm^{3+} ions," Appl. Phys. B **108**, 597–602 (2012).
193. S. S. Bayya, G. D. Chin, J. S. Sanghera, and I. D. Aggarwal, "Germanate glass as a window for high energy laser systems," Opt. Express **14**, 11687–11693 (2006).
194. M. Liao, W. Gao, Z. Duan, X. Yan, T. Suzuki, and Y. Ohishi, "Directly draw highly nonlinear tellurite microstructured fiber with diameter varying sharply in a short fiber length," Opt. Express **20**, 1141–1150 (2012).
195. G. Qin, M. Liao, C. Chaudhari, X. Yan, C. Kito, T. Suzuki, and Y. Ohishi, "Second and third harmonics and flattened supercontinuum generation in tellurite microstructured fibers," Opt. Lett. **35**, 58–60 (2010).
196. F. Fusari, S. Vetter, A. Lagatsky, B. Richards, S. Calvez, A. Jha, M. Dawson, W. Sibbett, and C. Brown, "Tunable laser operation of a Tm^{3+}-doped tellurite glass laser near 2 μm pumped by a 1211 nm semiconductor disk laser," Opt. Mater. **32**, 1007–1010 (2010).
197. F. Fusari, A. A. Lagatsky, G. Jose, S. Calvez, A. Jha, M. D. Dawson, J. A. Gupta, W. Sibbett, and C. T. A. Brown, "Femtosecond mode-locked Tm^{3+} and Tm^{3+}-Ho^{3+} doped 2 μm glass lasers," Opt. Express **18**, 22090–22098 (2010).
198. B. Richards, A. Jha, Y. Tsang, D. Binks, J. Lousteau, F. Fusari, A. Lagatsky, C. Brown, and W. Sibbett, "Tellurite glass lasers operating close to 2 μm," Laser Phys. Lett. **7**, 177 (2010).
199. K. Li, G. Zhang, X. Wang, L. Hu, P. Kuan, D. Chen, and M. Wang, "Tm^{3+} and Tm^{3+}-Ho^{3+} co-doped tungsten tellurite glass single mode fiber laser," Opt. Express **20**, 10115–10121 (2012).
200. J. Wu, Z. Yao, J. Zong, and S. Jiang, "Highly efficient high-power thulium-doped germanate glass fiber laser," Opt. Lett. **32**, 638–640 (2007).
201. D. Tran, G. Sigel, and B. Bendow, "Heavy metal fluoride glasses and fibers: a review," J. Lightwave Technol. **2**, 566–586 (1984).
202. J. Bei, T. M. Monro, A. Hemming, and H. Ebendorff-Heidepriem, "Reduction of scattering loss in fluoroindate glass fibers," Opt. Mater. Express **3**, 1285–1301 (2013).
203. J.-L. Adam, "Fluoride glass research in France: fundamentals and applications," J. Fluorine Chem. **107**, 265–270 (2001).
204. P. W. France, *Fluoride Glass Optical Fibres* (Blackie, 1990).
205. S. Shibata, M. Horiguchi, K. Jinguji, S. Mitachi, T. Kanamori, and T. Manabe, "Prediction of loss minima in infra-red optical fibres," Electron. Lett. **17**, 775–777 (1981).
206. T. Kanamori and S. Sakaguchi, "Preparation of elevated NA fluoride optical fibers," Jpn. J. Appl. Phys. **25**, L468 (1986).
207. S. F. Carter, J. R. Williams, M. W. Moore, D. Szebesta, and S. T. Davey, "Prospects for ultra-low-loss fluoride fibres at BTRL," J. Non-Cryst. Solids **140**, 153–158 (1992).
208. W. M. Patterson, P. C. Stark, T. M. Yoshida, M. Sheik-Bahae, and M. P. Hehlen, "Preparation and characterization of high-purity metal fluorides for photonic applications," J. Am. Ceram. Soc. **94**, 2896–2901 (2011).
209. G. F. West and W. Höfle, "Spectral attenuation of fluoride glass fibers," J. Non-Cryst. Solids **213–214**, 189–192 (1997).
210. H. Ebendorff-Heidepriem, T.-C. Foo, R. C. Moore, W. Zhang, Y. Li, T. M. Monro, A. Hemming, and D. G. Lancaster, "Fluoride glass microstructured

optical fiber with large mode area and mid-infrared transmission," Opt. Lett. **33**, 2861–2863 (2008).
211. X. Jiang, F. Babic, T. G. Euser, T. Weiss, A. Abdolvand, M. Finger, N. Joly, M. H. Frosz, and P. S. Russell, "Recent advances in soft-glass photonic crystal fibres," in *Workshop on Specialty Optical Fibers and their Applications* (Optical Society of America, 2013), paper W2.4.
212. S. D. Jackson and D. G. Lancaster, "Fiber lasers that bridge the shortwave to midwave regions of the infrared spectrum," in *Fiber Lasers* (Wiley-VCH, 2012).
213. X. Zhu and N. Peyghambarian, "High-power ZBLAN glass fiber lasers: review and prospect," Adv. Optoelectron. **2010**, 1 (2010).
214. O. Henderson-Sapir, J. Munch, and D. J. Ottaway, "Mid-infrared fiber lasers at and beyond 3.5 μm using dual-wavelength pumping," Opt. Lett. **39**, 493–496 (2014).
215. J. Swiderski, M. Michalska, and G. Maze, "Mid-IR supercontinuum generation in a ZBLAN fiber pumped by a gain-switched mode-locked Tm-doped fiber laser and amplifier system," Opt. Express **21**, 7851–7857 (2013).
216. C. Agger, C. Petersen, S. Dupont, H. Steffensen, J. K. Lyngsø, C. L. Thomsen, J. Thøgersen, S. R. Keiding, and O. Bang, "Supercontinuum generation in ZBLAN fibers-detailed comparison between measurement and simulation," J. Opt. Soc. Am. B **29**, 635–645 (2012).
217. G. Qin, X. Yan, C. Kito, M. Liao, C. Chaudhari, T. Suzuki, and Y. Ohishi, "Ultrabroadband supercontinuum generation from ultraviolet to 6.28 μm in a fluoride fiber," Appl. Phys. Lett. **95**, 161103 (2009).
218. C. Xia, M. Kumar, O. P. Kulkarni, M. N. Islam, J. F. L. Terry, M. J. Freeman, M. Poulain, and G. Mazé, "Mid-infrared supercontinuum generation to 4.5 μm in ZBLAN fluoride fibers by nanosecond diode pumping," Opt. Lett. **31**, 2553–2555 (2006).
219. J. Swiderski and M. Michalska, "High-power supercontinuum generation in a ZBLAN fiber with very efficient power distribution toward the mid-infrared," Opt. Lett. **39**, 910–913 (2014).
220. W. Yang, B. Zhang, G. Xue, K. Yin, and J. Hou, "Thirteen watt all-fiber mid-infrared supercontinuum generation in a single mode ZBLAN fiber pumped by a 2 μm MOPA system," Opt. Lett. **39**, 1849–1852 (2014).
221. W.-Q. Yang, B. Zhang, J. Hou, K. Yin, and Z.-J. Liu, "A novel 2-μm pulsed fiber laser based on a supercontinuum source and its application to mid-infrared supercontinuum generation," Chin. Phys. B. **23**, 054208 (2014).
222. I. Kubat, C. Rosenberg Petersen, U. V. Møller, A. Seddon, T. Benson, L. Brilland, D. Méchin, P. M. Moselund, and O. Bang, "Thulium pumped mid-infrared 0.9–9 μm supercontinuum generation in concatenated fluoride and chalcogenide glass fibers," Opt. Express **22**, 3959–3967 (2014).
223. P. P. Fedorov, R. M. Zakalyukin, L. N. Ignat'eva, and V. M. Bouznik, "Fluoroindate glasses," Russ. Chem. Rev. **69**, 705–716 (2000).
224. F. Théberge, J.-F. Daigle, D. Vincent, P. Mathieu, J. Fortin, B. E. Schmidt, N. Thiré, and F. Légaré, "Mid-infrared supercontinuum generation in fluoroindate fiber," Opt. Lett. **38**, 4683–4685 (2013).
225. http://www.chgsouthampton.com/, retrieved April 1, 2015.
226. P. Houizot, C. Boussard-Plédel, A. J. Faber, L. K. Cheng, B. Bureau, P. A. Van Nijnatten, W. L. M. Gielesen, J. Pereira do Carmo, and J. Lucas,

"Infrared single mode chalcogenide glass fiber for space," Opt. Express **15**, 12529–12538 (2007).
227. S. Hocdé, C. Boussard-Plédel, G. Fonteneau, and J. Lucas, "Chalcogens based glasses for IR fiber chemical sensors," Solid State Sci. **3**, 279–284 (2001).
228. J. Sanghera, I. Aggarwal, L. Shaw, L. Busse, P. Thielen, V. Nguyen, P. Pureza, S. Bayya, and F. Kung, "Applications of chalcogenide glass optical fibers at NRL," J. Optoelectron. Adv. Mater. **3**, 627–640 (2001).
229. J. Sanghera, L. Busse, and I. Aggarwal, "Effect of scattering centers on the optical loss of As_2S_3 glass fibers in the infrared," J. Appl. Phys. **75**, 4885–4891 (1994).
230. R. C. Frye and D. Adler, "Field effect in chalcogenide glasses," Phys. Rev. B **24**, 5812 (1981).
231. A. G. Steventon, "The switching mechanisms in amorphous chalcogenide memory devices," J. Non-Cryst. Solids **21**, 319–329 (1976).
232. P. Ma, D.-Y. Choi, Y. Yu, X. Gai, Z. Yang, S. Debbarma, S. Madden, and B. Luther-Davies, "Low-loss chalcogenide waveguides for chemical sensing in the mid-infrared," Opt. Express **21**, 29927–29937 (2013).
233. N. Carlie, J. D. Musgraves, B. Zdyrko, I. Luzinov, J. Hu, V. Singh, A. Agarwal, L. C. Kimerling, A. Canciamilla, F. Morichetti, A. Melloni, and K. Richardson, "Integrated chalcogenide waveguide resonators for mid-IR sensing: leveraging material properties to meet fabrication challenges," Opt. Express **18**, 26728–26743 (2010).
234. Y. Yu, X. Gai, T. Wang, P. Ma, R. Wang, Z. Yang, D.-Y. Choi, S. Madden, and B. Luther-Davies, "Mid-infrared supercontinuum generation in chalcogenides," Opt. Mater. Express **3**, 1075–1086 (2013).
235. S. Dai, F. Chen, Y. Xu, Z. Xu, X. Shen, T. Xu, R. Wang, and W. Ji, "Mid-infrared optical nonlinearities of chalcogenide glasses in Ge-Sb-Se ternary system," Opt. Express **23**, 1300–1307 (2015).
236. A. Byrnes, R. Pant, E. Li, D.-Y. Choi, C. G. Poulton, S. Fan, S. Madden, B. Luther-Davies, and B. J. Eggleton, "Photonic chip based tunable and reconfigurable narrowband microwave photonic filter using stimulated Brillouin scattering," Opt. Express **20**, 18836–18845 (2012).
237. K. Yan, K. Vu, and S. Madden, "Internal gain in Er-doped As_2S_3 chalcogenide planar waveguides," Opt. Lett. **40**, 796–799 (2015).
238. T. Sabapathy, A. Ayiriveetil, A. K. Kar, S. Asokan, and S. J. Beecher, "Direct ultrafast laser written C-band waveguide amplifier in Er-doped chalcogenide glass," Opt. Mater. Express **2**, 1556–1561 (2012).
239. B. J. Eggleton, B. Luther-Davies, and K. Richardson, "Chalcogenide photonics," Nat. Photonics **5**, 141–148 (2011).
240. V. Ta'eed, N. J. Baker, L. Fu, K. Finsterbusch, M. R. E. Lamont, D. J. Moss, H. C. Nguyen, B. J. Eggleton, D.-Y. Choi, S. Madden, and B. Luther-Davies, "Ultrafast all-optical chalcogenide glass photonic circuits," Opt. Express **15**, 9205–9221 (2007).
241. R. J. Curry, A. K. Mairaj, C. C. Huang, R. W. Eason, C. Grivas, D. W. Hewak, and J. V. Badding, "Chalcogenide glass thin films and planar waveguides," J. Am. Ceram. Soc. **88**, 2451–2455 (2005).
242. C. C. Huang, D. Hewak, and J. Badding, "Deposition and characterization of germanium sulphide glass planar waveguides," Opt. Express **12**, 2501–2506 (2004).

243. B. F. Bowden, J. A. Harrington, and J. L. Cutrera, "Chalcogenide glass 1D photonic bandgap hollow fiber," Proc. SPIE **5691**, 66–72 (2005).
244. S. Shabahang, G. Tao, J. J. Kaufman, and A. F. Abouraddy, "Dispersion characterization of chalcogenide bulk glass, composite fibers, and robust nanotapers," J. Opt. Soc. Am. B **30**, 2498–2506 (2013).
245. J. S. Sanghera, L. B. Shaw, P. Pureza, V. Q. Nguyen, D. Gibson, L. Busse, I. D. Aggarwal, C. M. Florea, and F. H. Kung, "Nonlinear properties of chalcogenide glass fibers," Int. J. Appl. Glass Sci. **1**, 296–308 (2010).
246. R. R. Gattass, L. Brandon Shaw, V. Q. Nguyen, P. C. Pureza, I. D. Aggarwal, and J. S. Sanghera, "All-fiber chalcogenide-based mid-infrared supercontinuum source," Opt. Fiber Technol. **18**, 345–348 (2012).
247. B. Ung and M. Skorobogatiy, "Giant nonlinear optical enhancement in chalcogenide glass fibers with deep-subwavelength metallic nanowires," in *Conference on Lasers and Electro-Optics—Laser Applications to Photonic Applications*, OSA Technical Digest (CD) (Optical Society of America, 2011), paper JTuI44.
248. C. R. Petersen, U. Møller, I. Kubat, B. Zhou, S. Dupont, J. Ramsay, T. Benson, S. Sujecki, N. Abdel-Moneim, Z. Tang, D. Furniss, A. Seddon, and O. Bang, "Mid-infrared supercontinuum covering the 1.4–13.3 μm molecular fingerprint region using ultra-high NA chalcogenide step-index fibre," Nat. Photonics **8**, 830–834 (2014).
249. P. Yang, P. Zhang, S. Dai, Y. Wu, X. Wang, G. Tao, and Q. Nie, "Tapered chalcogenide–tellurite hybrid microstructured fiber for mid-infrared supercontinuum generation," J. Mod. Opt. **62**, 729–737 (2015).
250. U. Moller, Y. Yu, I. Kubat, C. R. Petersen, X. Gai, L. Brilland, D. Mechin, C. Caillaud, J. Troles, B. Luther-Davies, and O. Bang, "Multi-milliwatt mid-infrared supercontinuum generation in a suspended core chalcogenide fiber," Opt. Express **23**, 3282–3291 (2015).
251. F. Z. Cao, P. Q. Zhang, S. X. Dai, X. S. Wang, T. F. Xu, and Q. H. Nie, "Mid-infrared second-harmonic generation in chalcogenide photonic crystal fiber," Opt. Commun. **335**, 257–261 (2015).
252. W. Q. Gao, Z. C. Duan, K. Asano, T. L. Cheng, D. H. Deng, M. Matsumoto, T. Misumi, T. Suzuki, and Y. Ohishi, "Mid-infrared supercontinuum generation in a four-hole As_2S_5 chalcogenide microstructured optical fiber," Appl. Phys. B **116**, 847–853 (2014).
253. W. Q. Gao, M. El Amraoui, M. S. Liao, H. Kawashima, Z. C. Duan, D. H. Deng, T. L. Cheng, T. Suzuki, Y. Messaddeq, and Y. Ohishi, "Mid-infrared supercontinuum generation in a suspended-core As_2S_3 chalcogenide microstructured optical fiber," Opt. Express **21**, 9573–9583 (2013).
254. A. Marandi, C. W. Rudy, V. G. Plotnichenko, E. M. Dianov, K. L. Vodopyanov, and R. L. Byer, "Mid-infrared supercontinuum generation in tapered chalcogenide fiber for producing octave-spanning frequency comb around 3 μm," Opt. Express **20**, 24218–24225 (2012).
255. J. Fatome, B. Kibler, M. El-Amraoui, J. C. Jules, G. Gadret, F. Desevedavy, and F. Smektala, "Mid-infrared extension of supercontinuum in chalcogenide suspended core fibre through soliton gas pumping," Electron. Lett. **47**, 398–399 (2011).
256. J. S. Sanghera and I. D. Aggarwal, "Active and passive chalcogenide glass optical fibers for IR applications: a review," J. Non-Cryst. Solids **256–257**, 6–16 (1999).

257. J. F. Li, Y. Chen, M. Chen, H. Chen, X. B. Jin, Y. Yang, Z. Y. Dai, and Y. Liu, "Theoretical analysis and heat dissipation of mid-infrared chalcogenide fiber Raman laser," Opt. Commun. **284**, 1278–1283 (2011).
258. S. D. Jackson and G. Anzueto-Sánchez, "Chalcogenide glass Raman fiber laser," Appl. Phys. Lett. **88**, 221106 (2006).
259. P. Thielen, L. Shaw, J. Sanghera, and I. Aggarwal, "Modeling of a mid-IR chalcogenide fiber Raman laser," Opt. Express **11**, 3248–3253 (2003).
260. P. A. Thielen, L. B. Shaw, P. C. Pureza, V. Q. Nguyen, J. S. Sanghera, and I. D. Aggarwal, "Small-core As-Se fiber for Raman amplification," Opt. Lett. **28**, 1406–1408 (2003).
261. R. E. Slusher, G. Lenz, J. Hodelin, J. Sanghera, L. B. Shaw, and I. D. Aggarwal, "Large Raman gain and nonlinear phase shifts in high-purity As_2Se_3 chalcogenide fibers," J. Opt. Soc. Am. B **21**, 1146–1155 (2004).
262. M. Bernier, V. Fortin, M. El-Amraoui, Y. Messaddeq, and R. Vallée, "3.77 μm fiber laser based on cascaded Raman gain in a chalcogenide glass fiber," Opt. Lett. **39**, 2052–2055 (2014).
263. M. Bernier, V. Fortin, N. Caron, M. El-Amraoui, Y. Messaddeq, and R. Vallée, "Mid-infrared chalcogenide glass Raman fiber laser," Opt. Lett. **38**, 127–129 (2013).
264. J. Heo, "Rare-earth doped chalcogenide glasses for fiber-optic amplifiers," J. Non-Cryst. Solids **326–327**, 410–415 (2003).
265. Y. Xu, D. Chen, W. Wang, Q. Zhang, H. Zeng, C. Shen, and G. Chen, "Broadband near-infrared emission in Er^{3+}-Tm^{3+} codoped chalcohalide glasses," Opt. Lett. **33**, 2293–2295 (2008).
266. H. Guo, L. Liu, Y. Wang, C. Hou, W. Li, M. Lu, K. Zou, and B. Peng, "Host dependence of spectroscopic properties of Dy^{3+}- doped and Dy^{3+}, Tm^{3+}-codoped Ge-Ga-S-CdI_2 chalcohalide glasses," Opt. Express **17**, 15350–15358 (2009).
267. L. Feng, H. Guo, G. Tao, M. Lu, W. Wei, and B. Peng, "Dy^{3+}-doped Ge-In-S-CsI chalcohalide glasses for 1.3 μm optical fiber amplifier," J. Optoelectron. Adv. Mater. **11**, 924–928 (2009).
268. B. N. Samson, T. Schweizer, D. W. Hewak, and R. I. Laming, "Properties of dysprosium-doped gallium lanthanum sulfide fiber amplifiers operating at 1.3 μm," Opt. Lett. **22**, 703–705 (1997).
269. J. R. Hector, D. W. Hewak, J. Wang, R. C. Moore, and W. S. Brocklesby, "Quantum-efficiency measurements in oxygen-containing gallium lanthanum sulphide glasses and fibers doped with Pr^{3+}," IEEE Photon. Technol. Lett. **9**, 443–445 (1997).
270. V. Moizan, V. Nazabal, J. Troles, P. Houizot, J.-L. Adam, J.-L. Doualan, R. Moncorgé, F. Smektala, G. Gadret, S. Pitois, and G. Canat, "Er^{3+}-doped GeGaSbS glasses for mid-IR fibre laser application: synthesis and rare earth spectroscopy," Opt. Mater. **31**, 39–46 (2008).
271. F. Charpentier, F. Starecki, J. L. Doualan, P. Jóvári, P. Camy, J. Troles, S. Belin, B. Bureau, and V. Nazabal, "Mid-IR luminescence of Dy^{3+} and Pr^{3+} doped $Ga_5Ge_{20}Sb_{10}S(Se)_{65}$ bulk glasses and fibers," Mater. Lett. **101**, 21–24 (2013).
272. T. Schweizer, D. W. Hewak, B. N. Samson, and D. N. Payne, "Spectroscopy of potential mid-infrared laser transitions in gallium lanthanum sulphide glass," J. Lumin. **72–74**, 419–421 (1997).

273. G. Tao, H. Guo, L. Feng, M. Lu, W. Wei, and B. Peng, "Formation and properties of a novel heavy-metal chalcogenide glass doped with a high dysprosium concentration," J. Am. Ceram. Soc. **92**, 2226–2229 (2009).
274. W. Xu, J. Ren, Z. Zhang, G. Chen, D. Kong, C. Gu, C. Chen, and L. Kong, "Enhanced photoluminescence of Eu^{2+}-Pr^{3+} ions in Ga_2S_3 nanocrystals embedded chalcohalide glasses ceramics," J. Non-Cryst. Solids **381**, 65–67 (2013).
275. J. S. Sanghera, L. Brandon Shaw, and I. D. Aggarwal, "Chalcogenide glass-fiber-based Mid-IR sources and applications," IEEE J. Sel. Top. Quantum Electron. **15**, 114–119 (2009).
276. I. D. Aggarwal, L. B. Shaw, and J. S. Sanghera, "Chalcogenide glass fiber-based Mid-IR sources and applications," Proc. SPIE **6453**, 645312 (2007).
277. J. A. Medeiros Neto, E. R. Taylor, B. N. Samson, J. Wang, D. W. Hewak, R. I. Laming, D. N. Payne, E. Tarbox, P. D. Maton, G. M. Roba, B. E. Kinsman, and R. Hanney, "The application of Ga:La:S-based glass for optical amplification at 1.3 μm," J. Non-Cryst. Solids **184**, 292–296 (1995).
278. D. W. Hewak, R. C. Moore, T. Schweizer, J. Wang, B. Samson, W. S. Brocklesby, D. N. Payne, and E. J. Tarbox, "Gallium lanthanum sulphide optical fibre for active and passive applications," Electron. Lett. **32**, 384 (1996).
279. J. Wang, J. R. Hector, D. Brady, D. Hewak, B. Brocklesby, M. Kluth, R. Moore, and D. N. Payne, "Halide-modified Ga–La sulfide glasses with improved fiber-drawing and optical properties for Pr^{3+}-doped fiber amplifiers at 1.3 μm," Appl. Phys. Lett. **71**, 1753–1755 (1997).
280. T. Schweizer, D. Brady, and D. W. Hewak, "Fabrication and spectroscopy of erbium doped gallium lanthanum sulphide glass fibres for mid-infrared laser applications," Opt. Express **1**, 102–107 (1997).
281. T. Schweizer, F. Goutaland, E. Martins, D. W. Hewak, and W. S. Brocklesby, "Site-selective spectroscopy in dysprosium-doped chalcogenide glasses for 1.3-μm optical-fiber amplifiers," J. Opt. Soc. Am. B **18**, 1436–1442 (2001).
282. T. Schweizer, B. N. Samson, J. R. Hector, W. S. Brocklesby, D. W. Hewak, and D. N. Payne, "Infrared emission from holmium doped gallium lanthanum sulphide glass," Infrared Phys. Technol. **40**, 329–335 (1999).
283. T. Schweizer, B. Samson, R. Moore, D. Hewak, and D. Payne, "Rare-earth doped chalcogenide glass fibre laser," Electron. Lett **33**, 414–416 (1997).
284. H. Takebe, K. Yoshino, T. Murata, K. Morinaga, J. Hector, W. S. Brocklesby, D. W. Hewak, J. Wang, and D. N. Payne, "Spectroscopic properties of Nd^{3+} and Pr^{3+} in gallate glasses with low phonon energies," Appl. Opt. **36**, 5839–5843 (1997).
285. S. Sujecki, L. Sójka, E. Bere -Pawlik, Z. Tang, D. Furniss, A. B. Seddon, and T. M. Benson, "Modelling of a simple Dy^{3+} doped chalcogenide glass fibre laser for mid-infrared light generation," Opt. Quantum Electron. **42**, 69–79 (2010).
286. O. G. Pompilian, G. Dascalu, I. Mihaila, S. Gurlui, M. Olivier, P. Nemec, V. Nazabal, N. Cimpoesu, and C. Focsa, "Pulsed laser deposition of rare-earth-doped gallium lanthanum sulphide chalcogenide glass thin films," Appl. Phys. A **117**, 197–205 (2014).
287. Y. G. Choi, "Enhancing emission properties of rare earth ions in chalcogenide glass via minute compositional adjustments," J. Nonlinear Opt. Phys. Mater. **19**, 663–671 (2010).

288. Y. G. Choi and J. H. Song, "Local structural environment and intra-4f transition of rare-earth ion in chalcogenide glass: comparison between Dy-doped Ge-As-S and Ge-Ga-S glasses," J. Non-Cryst. Solids **355**, 2396–2399 (2009).
289. K. Hachiya and H. Ohashi, "Annealing process dependence of the photoluminescence in rare-earth-ion-doped chalcogenide glass," Electrochim. Acta **53**, 7–10 (2007).
290. Y. S. Tver'yanovich and A. Tverjanovich, "Rare-earth doped chalcogenide glass," in *Semiconducting Chalcogenide Glass III*, Vol. **80** of Semiconducters and Semimetals (Elsevier, 2004), pp. 169–207.
291. R. S. Quimby and B. G. Aitken, "Multiphonon energy gap law in rare-earth doped chalcogenide glass," J. Non-Cryst. Solids **320**, 100–112 (2003).
292. L. B. Shaw, B. Cole, P. A. Thielen, J. S. Sanghera, and I. D. Aggarwal, "Mid-wave IR and long-wave IR laser potential of rare-earth doped chalcogenide glass fiber," IEEE J. Quantum Electron. **37**, 1127–1137 (2001).
293. T. Schweizer, B. N. Samson, R. C. Moore, D. W. Hewak, and D. N. Payne, "Rare-earth doped chalcogenide glass fibre laser," Electron. Lett. **33**, 414–416 (1997).
294. T. Schweizer, D. W. Hewak, D. N. Payne, T. Jensen, and G. Huber, "Rare-earth doped chalcogenide glass laser," Electron. Lett. **32**, 666–667 (1996).
295. B. R. Marx, "Rare-earth-doped chalcogenide glass laser," Laser Focus World **32**, 25–26 (1996).
296. D. T. Schaafsma, L. B. Shaw, B. Cole, J. S. Sanghera, and D. Aggarwal, "Modeling of Dy^{3+}-doped GeAsSe glass 1.3-μm optical fiber amplifiers," IEEE Photon. Technol. Lett. **10**, 1548–1550 (1998).
297. B. Cole, L. B. Shaw, P. C. Pureza, R. Mossadegh, J. S. Sanghera, and I. D. Aggarwal, "Rare-earth doped selenide glasses and fibers for active applications in the near and mid-IR," J. Non-Cryst. Solids **256–257**, 253–259 (1999).
298. B. Cole, L. B. Shaw, P. C. Pureza, R. Miklos, J. S. Sanghera, and I. D. Aggarwal, "Core/clad selenide glass fiber doped with Pr^{3+} for active mid-IR applications," J. Mater. Sci. Lett. **20**, 465–467 (2001).
299. L. Sojka, Z. Tang, H. Zhu, E. Beres-Pawlik, D. Furniss, A. B. Seddon, T. M. Benson, and S. Sujecki, "Study of mid-infrared laser action in chalcogenide rare earth doped glass with Dy^{3+}, Pr^{3+} and Tb^{3+}," Opt. Mater. Express **2**, 1632–1640 (2012).
300. D. V. Martyshkin, J. T. Goldstein, V. V. Fedorov, and S. B. Mirov, "Crystalline Cr^{2+}:ZnSe/chalcogenide glass composites as active mid-IR materials," Opt. Lett. **36**, 1530–1532 (2011).
301. E. Karaksina, V. Plotnichenko, R. Mironov, R. Shaposhnikov, and L. Ketkova, "The composite materials on the basis of As_2S_3 glass containing crystals ZnS and ZnS doped with Cr^{2+}," J. Optoelectron. Adv. Mater. **13**, 1433 (2011).
302. E. V. Karaksina, L. A. Ketkova, M. F. Churbanov, and E. M. Dianov, "Preparation of mid-IR-active As_2S_3/ZnS(ZnSe):Cr^{2+} composites," Inorg. Mater. **49**, 223–229 (2013).
303. D. Lezal, M. Poulain, and J. Zavadil, "Sulphide glasses doped with rare earth elements," Ceramics **45**, 105–110 (2001).
304. Y.-S. Xu, F. Huang, B. Fan, C.-G. Lin, S.-X. Dai, L.-Y. Chen, Q.-H. Nie, H.-L. Ma, and X.-H. Zhang, "Quantum cutting in Pr^{3+}-Yb^{3+} codoped

chalcohalide glasses for high-efficiency c-Si solar cells," Opt. Lett. **39**, 2225–2228 (2014).
305. S. Bhosle, K. Gunasekera, P. Boolchand, and M. Micoulaut, "Melt homogenization and self-organization in chalcogenides-part I," Int. J. Appl. Glass Sci. **3**, 189–204 (2012).
306. J. S. Sanghera, L. B. Shaw, and I. D. Aggarwal, "Applications of chalcogenide glass optical fibers," C. R. Chim. **5**, 873–883 (2002).
307. V. S. Shiryaev, J. L. Adam, X. H. Zhang, C. Boussard-Plédel, J. Lucas, and M. F. Churbanov, "Infrared fibers based on Te–As–Se glass system with low optical losses," J. Non-Cryst. Solids **336**, 113–119 (2004).
308. F. Charpentier, J. Troles, Q. Coulombier, L. Brilland, P. Houizot, F. Smektala, C. Boussard-Plédel, V. Nazabal, N. Thibaud, and K. Le Pierres, "CO_2 detection using microstructured chalcogenide fibers," Sens. Lett. **7**, 745–749 (2009).
309. J. Keirsse, C. Boussard-Plédel, O. Loreal, O. Sire, B. Bureau, B. Turlin, P. Leroyer, and J. Lucas, "Chalcogenide glass fibers used as biosensors," J. Non-Cryst. Solids **326–327**, 430–433 (2003).
310. M.-L. Anne, C. Le Lan, V. Monbet, C. Boussard-Plédel, M. Ropert, O. Sire, M. Pouchard, C. Jard, J. Lucas, and J. L. Adam, "Fiber evanescent wave spectroscopy using the mid-infrared provides useful fingerprints for metabolic profiling in humans," J. Biomed. Opt. **14**, 054033 (2009).
311. S. Hocde, O. Lore, O. Sire, C. Boussard-Ple, B. Bureau, B. Turlin, J. Keirsse, P. Leroyer, and J. Lucas, "Metabolic imaging of tissues by infrared fiber-optic spectroscopy: an efficient tool for medical diagnosis," J. Biomed. Opt. **9**, 404–407 (2004).
312. J. Keirsse, C. Boussard-Plédel, O. Loreal, O. Sire, B. Bureau, P. Leroyer, B. Turlin, and J. Lucas, "IR optical fiber sensor for biomedical applications," Vib. Spectrosc **32**, 23–32 (2003).
313. P. Lucas, M. R. Riley, C. Boussard-Plédel, and B. Bureau, "Advances in chalcogenide fiber evanescent wave biochemical sensing," Anal. Biochem. **351**, 1–10 (2006).
314. A. B. Seddon, "A prospective for new mid-infrared medical endoscopy using chalcogenide glasses," Int. J. Appl. Glass Sci. **2**, 177–191 (2011).
315. K. Michel, B. Bureau, C. Pouvreau, J. Sangleboeuf, C. Boussard-Plédel, T. Jouan, T. Rouxel, J.-L. Adam, K. Staubmann, and H. Steinner, "Development of a chalcogenide glass fiber device for in situ pollutant detection," J. Non-Cryst. Solids **326**, 434–438 (2003).
316. J. S. Sanghera, F. H. Kung, P. C. Pureza, V. Q. Nguyen, R. E. Miklos, and I. D. Aggarwal, "Infrared evanescent-absorption spectroscopy with chalcogenide glass fibers," Appl. Opt. **33**, 6315–6322 (1994).
317. J. S. Sanghera, F. H. Kung, L. E. Busse, P. C. Pureza, and I. D. Aggarwal, "Infrared evanescent absorption spectroscopy of toxic chemicals using chalcogenide glass fibers," J. Am. Ceram. Soc. **78**, 2198–2202 (1995).
318. S. Danto, P. Houizot, C. Boussard-Pledel, X. H. Zhang, F. Smektala, and J. Lucas, "A family of far-infrared-transmitting glasses in the Ga-Ge-Te system for space applications," Adv. Funct. Mater. **16**, 1847–1852 (2006).
319. C. Conseil, V. S. Shiryaev, S. Cui, C. Boussard-Pledel, J. Troles, A. P. Velmuzhov, A. M. Potapov, A. I. Suchkov, M. F. Churbanov, and B. Bureau, "Preparation of high purity Te-rich Ge-Te-Se fibers for 5–15 μm infrared range," J. Lightwave Technol. **31**, 1703–1707 (2013).

320. H. J. Xu, Y. J. He, X. S. Wang, Q. H. Nie, P. Q. Zhang, T. F. Xu, S. X. Dai, X. H. Zhang, and G. M. Tao, "Preparation of low-loss $Ge_{15}Ga_{10}Te_{75}$ chalcogenide glass for far-IR optics applications," Infrared Phys. Technol. **65**, 77–82 (2014).
321. R. Frerichs, "New optical glasses with good transparency in the infrared," J. Opt. Soc. Am. **43**, 1153–1157 (1953).
322. N. Kapany and R. Simms, "Fiber optics. XI. Performance in the infrared region," J. Opt. Soc. Am. **55**, 963–967 (1965).
323. S. Shibata, Y. Terunuma, and T. Manabe, "Ge-P-S chalcogenide glass fibers," Jpn. J. Appl. Phys. **19**, L603 (1980).
324. T. Miyashita and Y. Terunuma, "Optical transmission loss of As–S glass fiber in 1.0–5.5 μm wavelength region," Jpn. J. Appl. Phys. **21**, L75 (1982).
325. T. Katsuyama, K. Ishida, S. Satoh, and H. Matsumura, "Low loss Ge-Se chalcogenide glass optical fibers," Appl. Phys. Lett. **45**, 925–927 (1984).
326. T. Katsuyama and H. Matsumura, "Low-loss Te-based chalcogenide glass optical fibers," Appl. Phys. Lett. **49**, 22–23 (1986).
327. T. Katsuyama, S. Satoh, and H. Matsumura, "Scattering loss characteristics of selenide-based chalcogenide glass optical fibers," J. Appl. Phys. **71**, 4132–4135 (1992).
328. T. Katsuyama and H. Matsumura, "Light transmission characteristics of telluride-based chalcogenide glass for infrared fiber application," J. Appl. Phys. **75**, 2743–2748 (1994).
329. M. Saito, M. Takizawa, S. Sakuragi, and F. Tanei, "Infrared image guide with bundled As-S glass fibers," Appl. Opt. **24**, 2304–2308 (1985).
330. M. Saito, "Optical loss increase in an As-S glass infrared fiber due to water diffusion," Appl. Opt. **26**, 202–203 (1987).
331. J. Nishii, T. Yamashita, and T. Yamagishi, "Chalcogenide glass fiber with a core-cladding structure," Appl. Opt. **28**, 5122–5127 (1989).
332. I. Inagawa, S. Morimoto, T. Yamashita, and I. Shirotani, "Temperature dependence of transmission loss of chalcogenide glass fibers," Jpn. J. Appl. Phys. **36**, 2229 (1997).
333. K. Itoh and H. Tawarayama, "Method for drawing a chalcogenide-containing glass fiber," European patent EP0850889 B1 (May 10, 2000).
334. H. Suto, "Chalcogenide fiber bundle for 3D spectroscopy," Infrared Phys. Technol. **38**, 93–99 (1997).
335. K. S. Abedin, "Brillouin amplification and lasing in a single-mode As_2Se_3 chalcogenide fiber," Opt. Lett. **31**, 1615–1617 (2006).
336. J. Nishii, T. Yamashita, and T. Yamagishi, "Low-loss chalcogenide glass fiber with core-cladding structure," Appl. Phys. Lett. **53**, 553–554 (1988).
337. J. Nishii, T. Yamashita, T. Yamagishi, C. Tanaka, and H. Sone, "Coherent infrared fiber image bundle," Appl. Phys. Lett. **59**, 2639–2641 (1991).
338. M. Asobe, K. I. Suzuki, T. Kanamori, and K. I. Kubodera, "Nonlinear refractive index measurement in chalcogenide-glass fibers by self-phase modulation," Appl. Phys. Lett. **60**, 1153–1154 (1992).
339. M. Asobe, H. Itoh, T. Miyazawa, and T. Kanamori, "Efficient and ultrafast all-optical switching using high Δn, small core chalcogenide glass fibre," Electron. Lett. **29**, 1966–1968 (1993).
340. M. Asobe, "Nonlinear optical properties of chalcogenide glass fibers and their application to all-optical switching," Opt. Fiber Technol. **3**, 142–148 (1997).

341. H. Kobayashi, H. Kanbara, M. Koga, and K. I. Kubodera, "Third-order nonlinear optical properties of As_2S_3 chalcogenide glass," J. Appl. Phys. **74**, 3683–3687 (1993).
342. G. Tao and A. F. Abouraddy, "Drawing robust infrared optical fibers from preforms produced by efficient multimaterial stacked coextrusion," Proc. SPIE **8982**, 89820F (2014).
343. M. Churbanov, "Recent advances in preparation of high-purity chalcogenide glasses in the USSR," J. Non-Cryst. Solids **140**, 324–330 (1992).
344. D. Thompson, S. Danto, J. Musgraves, P. Wachtel, B. Giroire, and K. Richardson, "Microwave assisted synthesis of high purity As_2Se_3 chalcogenide glasses," Phys. Chem. Glasses B **54**, 27–34 (2013).
345. K. Sivakumaran and C. S. Nair, "Rapid synthesis of chalcogenide glasses of Se–Te–Sb system by microwave irradiation," J. Phys. D **38**, 2476 (2005).
346. N. Prasad and A. Seddon, "First-time microwave-synthesis of $As_{40}Se_{60}$ chalcogenide glass: With potential for mid-infrared photonics," in *12th International Conference on Transparent Optical Networks (ICTON)* (IEEE, 2010).
347. T. Katsuyama, S. Satoh, and H. Matsumura, "Fabrication of high-purity chalcogenide glasses by chemical vapor deposition," J. Appl. Phys. **59**, 1446–1449 (1986).
348. M. Lines, "Scattering losses in optic fiber materials. II. Numerical estimates," J. Appl. Phys. **55**, 4058–4063 (1984).
349. M. Churbanov, "High-purity chalcogenide glasses as materials for fiber optics," J. Non-Cryst. Solids **184**, 25–29 (1995).
350. M. Churbanov, V. Shiryaev, I. Scripachev, G. Snopatin, V. Gerasimenko, S. Smetanin, I. Fadin, and V. Plotnichenko, "Optical fibers based on As–S–Se glass system," J. Non-Cryst. Solids **284**, 146–152 (2001).
351. M. Churbanov, I. Scripachev, G. Snopatin, V. Shiryaev, and V. Plotnichenko, "High-purity glasses based on arsenic chalcogenides," J. Optoelectron. Adv. Mater. **3**, 341–350 (2001).
352. M. Vlasov, G. Devyatykh, E. M. Dianov, V. Plotnichenko, I. Skripachev, V. Sysoev, and M. Churbanov, "Glassy As_2Se_3 with optical absorption of 60 dB/km," Quantum Electron. **12**, 932–933 (1982).
353. V. Shiryaev, L. Ketkova, M. Churbanov, A. Potapov, J. Troles, P. Houizot, J.-L. Adam, and A. Sibirkin, "Heterophase inclusions and dissolved impurities in $Ge_{25}Sb_{10}S_{65}$ glass," J. Non-Cryst. Solids **355**, 2640–2646 (2009).
354. V. Shiryaev, J. Troles, P. Houizot, L. Ketkova, M. Churbanov, J.-L. Adam, and A. Sibirkin, "Preparation of optical fibers based on Ge–Sb–S glass system," Opt. Mater. **32**, 362–367 (2009).
355. V. Shiryaev and M. Churbanov, "Trends and prospects for development of chalcogenide fibers for mid-infrared transmission," J. Non-Cryst. Solids **377**, 225–230 (2013).
356. E. Dianov, V. Plotnichenko, G. Devyatykh, M. Churbanov, and I. Scripachev, "Middle-infrared chalcogenide glass fibers with losses lower than 100 db km^{-1}," Infrared Phys. **29**, 303–307 (1989).
357. M. Churbanov, V. Shiryaev, A. Suchkov, A. Pushkin, V. Gerasimenko, R. Shaposhnikov, E. Dianov, V. Plotnichenko, V. Koltashev, and Y. N. Pyrkov, "High-purity As-S-Se and As-Se-Te glasses and optical fibers," Inorg. Mater. **43**, 441–447 (2007).

358. I. Chiaruttini, G. Fonteneau, X. Zhang, and J. Lucas, "Characteristics of tellurium-bromide-based glass for IR fibers optics," J. Non-Cryst. Solids **111**, 77–81 (1989).
359. X. Zhang, H. Ma, G. Fonteneau, and J. Lucas, "Improvement of tellurium halide glasses for IR fiber optics," J. Non-Cryst. Solids **140**, 47–51 (1992).
360. C. Blanchetiere, K. Le Foulgoc, H. Ma, X. Zhang, and J. Lucas, "Tellurium halide glass fibers: preparation and applications," J. Non-Cryst. Solids **184**, 200–203 (1995).
361. X. Zhang, H. Ma, C. Blanchetiere, and J. Lucas, "Low loss optical fibres of the tellurium halide-based glasses, the TeX glasses," J. Non-Cryst. Solids **161**, 327–330 (1993).
362. L. Le Neindre, F. Smektala, K. Le Foulgoc, X. Zhang, and J. Lucas, "Tellurium halide optical fibers," J. Non-Cryst. Solids **242**, 99–103 (1998).
363. F. Smektala, K. Le Foulgoc, L. Le Neindre, C. Blanchetiere, X. Zhang, and J. Lucas, "TeX-glass infrared optical fibers delivering medium power from a CO_2 laser," Opt. Mater. **13**, 271–276 (1999).
364. X. Zhang, H. Ma, and J. Lucas, "Applications of chalcogenide glass bulks and fibres," J. Optoelectron. Adv. Mater **5**, 1327–1333 (2003).
365. B. Bureau, C. Boussard, S. Cui, R. Chahal, M. L. Anne, V. Nazabal, O. Sire, O. Loréal, P. Lucas, and V. Monbet, "Chalcogenide optical fibers for mid-infrared sensing," Opt. Eng. **53**, 027101 (2014).
366. S. Maurugeon, B. Bureau, C. Boussard-Plédel, A. Faber, P. Lucas, X. Zhang, and J. Lucas, "Selenium modified $GeTe_4$ based glasses optical fibers for far-infrared sensing," Opt. Mater. **33**, 660–663 (2011).
367. V. S. Shiryaev, C. Boussard-Pledel, P. Houizot, T. Jouan, J. L. Adam, and J. Lucas, "Single-mode infrared fibers based on Te-As-Se glass system," Mat. Sci. Eng. B **127**, 138–143 (2006).
368. S. Maurugeon, C. Boussard-Pledel, J. Troles, A. J. Faber, P. Lucas, X. H. Zhang, J. Lucas, and B. Bureau, "Telluride glass step index fiber for the far infrared," J. Lightwave Technol. **28**, 3358–3363 (2010).
369. L. Busse, J. Moon, J. Sanghera, and I. Aggarwal, "Chalcogenide fibers enable delivery of mid-infrared laser radiation," Laser Focus World **32**, 143–150 (1996).
370. V. Q. Nguyen, J. S. Sanghera, P. C. Pureza, and I. D. Aggarwal, "Effect of heating on the optical loss in the As-Se glass fiber," J. Lightwave Technol. **21**, 122–126 (2003).
371. J. S. Sanghera and I. D. Aggarwal, "Development of chalcogenide glass fiber optics at NRL," J. Non-Cryst. Solids **213**, 63–67 (1997).
372. J. S. Sanghera, V. Q. Nguyen, P. C. Pureza, F. H. Kung, R. Miklos, and I. D. Aggarwal, "Fabrication of low-loss IR-transmitting $Ge_{30}As_{10}Se_{30}Te_{30}$ glass-fibers," J. Lightwave Technol. **12**, 737–741 (1994).
373. J. S. Sanghera, V. Q. Nguyen, P. C. Pureza, R. E. Miklos, F. H. Kung, and I. D. Aggarwal, "Fabrication of long lengths of low-loss IR transmitting $As_{40}S_{(60-x)}Se_x$ glass fibers," J. Lightwave Technol. **14**, 743–748 (1996).
374. R. Mossadegh, J. S. Sanghera, D. Schaafsma, B. J. Cole, V. Q. Nguyen, P. E. Miklos, and I. D. Aggarwal, "Fabrication of single-mode chalcogenide optical fiber," J. Lightwave Technol. **16**, 214–217 (1998).
375. G. M. Camilo, "Mechanical properties of chalcogenide glasses: a review," Proc. SPIE **4940**, 222–229 (2003).
376. G. G. Devyatykh, E. M. Dianov, V. G. Plotnichenko, A. Pushkin, Y. N. Pyrkov, I. Skripachev, G. Snopatin, M. F. Churbanov, and V. Shiryaev,

"Low-loss infrared arsenic-chalcogenide glass optical fibers," Proc. SPIE **4083**, 229–237 (2000).
377. S. Mitachi, S. Shibata, and T. Manabe, "Teflon FEP-clad fluoride glass fibre," Electron. Lett. **17**, 128–129 (1981).
378. G. Tao and A. F. Abouraddy, "Multimaterial fibers: a new concept in infrared fiber optics," Proc. SPIE **9098**, 90980V (2014).
379. G. Delaizir, J. C. Sangleboeuf, E. A. King, Y. Gueguen, X. H. Zhang, C. Boussard-Pledel, B. Bureau, and P. Lucas, "Influence of ageing conditions on the mechanical properties of Te-As-Se fibres," J. Phys. D **42**, 095405 (2009).
380. http://spie.org/x110821.xml, retrieved April 1, 2015.
381. J. J. Kaufman, G. M. Tao, S. Shabahang, D. S. S. Deng, Y. Fink, and A. F. Abouraddy, "Thermal drawing of high-density macroscopic arrays of well-ordered sub-5-nm-diameter nanowires," Nano Lett. **11**, 4768–4773 (2011).
382. J. Troles, L. Brilland, F. Smektala, P. Houizot, F. Désévédavy, Q. Coulombier, N. Traynor, T. Chartier, T. N. Nguyen, and J.-L. Adam, "Chalcogenide microstructured fibers for infrared systems, elaboration modelization, and characterization," Fiber Integr. Opt. **28**, 11–26 (2009).
383. P. Toupin, L. Brilland, J. Trolès, and J.-L. Adam, "Small core Ge-As-Se microstructured optical fiber with single-mode propagation and low optical losses," Opt. Mater. Express **2**, 1359–1366 (2012).
384. T. Cheng, Y. Kanou, D. Deng, X. Xue, M. Matsumoto, T. Misumi, T. Suzuki, and Y. Ohishi, "Fabrication and characterization of a hybrid four-hole $AsSe_2$-As_2S_5 microstructured optical fiber with a large refractive index difference," Opt. Express **22**, 13322–13329 (2014).
385. L. Shaw, J. Sanghera, I. Aggarwal, and F. Hung, "As-S and As-Se based photonic band gap fiber for IR laser transmission," Opt. Express **11**, 3455–3460 (2003).
386. O. Mouawad, J. Picot-Clémente, F. Amrani, C. Strutynski, J. Fatome, B. Kibler, F. Désévédavy, G. Gadret, J. C. Jules, D. Deng, Y. Ohishi, and F. Smektala, "Multioctave midinfrared supercontinuum generation in suspended-core chalcogenide fibers," Opt. Lett. **39**, 2684–2687 (2014).
387. W. Gao, M. El Amraoui, M. Liao, H. Kawashima, Z. Duan, D. Deng, T. Cheng, T. Suzuki, Y. Messaddeq, and Y. Ohishi, "Mid-infrared supercontinuum generation in a suspended-core As_2S_3 chalcogenide microstructured optical fiber," Opt. Express **21**, 9573–9583 (2013).
388. J. N. Winn, Y. Fink, S. Fan, and J. D. Joannopoulos, "Omnidirectional reflection from a one-dimensional photonic crystal," Opt. Lett. **23**, 1573–1575 (1998).
389. B. L. Scott, K. Wang, and G. Pickrell, "Fabrication of n-type silicon optical fibers," IEEE Photon. Technol. Lett. **21**, 1798–1800 (2009).
390. E. Snitzer and R. Tumminelli, "SiO_2-clad fibers with selectively volatilized soft-glass cores," Opt. Lett. **14**, 757–759 (1989).
391. J. Ballato, T. Hawkins, P. Foy, R. Stolen, B. Kokuoz, M. Ellison, C. McMillen, J. Reppert, A. Rao, and M. Daw, "Silicon optical fiber," Opt. Express **16**, 18675–18683 (2008).
392. J. R. Sparks, R. He, N. Healy, S. Chaudhuri, T. C. Fitzgibbons, A. C. Peacock, P. J. Sazio, and J. V. Badding, "Conformal coating by high pressure chemical deposition for patterned microwires of II–VI semiconductors," Adv. Funct. Mater. **23**, 1647–1654 (2013).

393. N. Healy, S. Mailis, N. M. Bulgakova, P. J. Sazio, T. D. Day, J. R. Sparks, H. Y. Cheng, J. V. Badding, and A. C. Peacock, "Extreme electronic bandgap modification in laser-crystallized silicon optical fibres," Nat. Mater. **13**, 1122–1127 (2014).
394. Y. Fink, D. J. Ripin, S. Fan, C. Chen, J. D. Joannopoulos, and E. L. Thomas, "Guiding optical light in air using an all-dielectric structure," J. Lightwave Technol. **17**, 2039 (1999).
395. K. Kuriki, O. Shapira, S. Hart, G. Benoit, Y. Kuriki, J. Viens, M. Bayindir, J. Joannopoulos, and Y. Fink, "Hollow multilayer photonic bandgap fibers for NIR applications," Opt. Express **12**, 1510–1517 (2004).
396. Z. Ruff, D. Shemuly, X. Peng, O. Shapira, Z. Wang, and Y. Fink, "Polymer-composite fibers for transmitting high peak power pulses at 1.55 microns," Opt. Express **18**, 15697–15703 (2010).
397. D. Shemuly, A. M. Stolyarov, Z. M. Ruff, L. Wei, Y. Fink, and O. Shapira, "Preparation and transmission of low-loss azimuthally polarized pure single mode in multimode photonic band gap fibers," Opt. Express **20**, 6029–6035 (2012).
398. S. Johnson, M. Ibanescu, M. Skorobogatiy, O. Weisberg, T. Engeness, M. Soljacic, S. Jacobs, J. Joannopoulos, and Y. Fink, "Low-loss asymptotically single-mode propagation in large-core OmniGuide fibers," Opt. Express **9**, 748–779 (2001).
399. M. Ibanescu, S. G. Johnson, M. Solja i , J. Joannopoulos, Y. Fink, O. Weisberg, T. D. Engeness, S. A. Jacobs, and M. Skorobogatiy, "Analysis of mode structure in hollow dielectric waveguide fibers," Phys. Rev. E **67**, 046608 (2003).
400. O. Shapira, A. F. Abouraddy, J. D. Joannopoulos, and Y. Fink, "Complete modal decomposition for optical waveguides," Phys. Rev. Lett. **94**, 143902 (2005).
401. O. Shapira, A. F. Abouraddy, Q. Hu, D. Shemuly, J. D. Joannopoulos, and Y. Fink, "Enabling coherent superpositions of iso-frequency optical states in multimode fibers," Opt. Express **18**, 12622–12629 (2010).
402. D. Shemuly, Z. M. Ruff, A. M. Stolyarov, G. Spektor, S. G. Johnson, Y. Fink, and O. Shapira, "Asymmetric wave propagation in planar chiral fibers," Opt. Express **21**, 1465–1472 (2013).
403. P. Yeh, A. Yariv, and E. Marom, "Theory of Bragg fiber," J. Opt. Soc. Am. **68**, 1196–1201 (1978).
404. A. M. Stolyarov, A. Gumennik, W. McDaniel, O. Shapira, B. Schell, F. Sorin, K. Kuriki, G. Benoit, A. Rose, and J. D. Joannopoulos, "Enhanced chemiluminescent detection scheme for trace vapor sensing in pneumatically-tuned hollow core photonic bandgap fibers," Opt. Express **20**, 12407–12415 (2012).
405. A. Yildirim, M. Vural, M. Yaman, and M. Bayindir, "Bioinspired optoelectronic nose with nanostructured wavelength-scalable hollow-core infrared fibers," Adv. Mater. **23**, 1263–1267 (2011).
406. A. Gumennik, A. M. Stolyarov, B. R. Schell, C. Hou, G. Lestoquoy, F. Sorin, W. McDaniel, A. Rose, J. D. Joannopoulos, and Y. Fink, "All-in-fiber chemical sensing," Adv. Mater. **24**, 6005–6009 (2012).
407. S. Danto, F. Sorin, N. D. Orf, Z. Wang, S. A. Speakman, J. D. Joannopoulos, and Y. Fink, "Fiber field-effect device via *in situ* channel crystallization," Adv. Mater. **22**, 4162–4166 (2010).

408. F. Sorin, O. Shapira, A. F. Abouraddy, M. Spencer, N. D. Orf, J. D. Joannopoulos, and Y. Fink, "Exploiting collective effects of multiple optoelectronic devices integrated in a single fiber," Nano Lett. **9**, 2630–2635 (2009).
409. F. Sorin, A. F. Abouraddy, N. Orf, O. Shapira, J. Viens, J. Arnold, J. D. Joannopoulos, and Y. Fink, "Multimaterial photodetecting fibers: a geometric and structural study," Adv. Mater. **19**, 3872–3877 (2007).
410. M. Bayindir, A. F. Abouraddy, J. Arnold, J. D. Joannopoulos, and Y. Fink, "Thermal-sensing fiber devices by multimaterial codrawing," Adv. Mater. **18**, 845–849 (2006).
411. D. Graham-Rowe, "Fibres get functional," Nat. Photonics **5**, 66–67 (2011).
412. R. Soref, "Silicon photonics: a review of recent literature," Silicon **2**, 1–6 (2010).
413. A. C. Peacock, J. R. Sparks, and N. Healy, "Semiconductor optical fibres: progress and opportunities," Laser Photon. Rev. **8**, 53–72 (2014).
414. A. Gumennik, L. Wei, G. Lestoquoy, A. M. Stolyarov, X. Jia, P. H. Rekemeyer, M. J. Smith, X. Liang, B. J.-B. Grena, and S. G. Johnson, "Silicon-in-silica spheres via axial thermal gradient in-fibre capillary instabilities," Nat. Commun. **4**, 2216 (2013).
415. R. He, T. D. Day, M. Krishnamurthi, J. R. Sparks, P. J. Sazio, V. Gopalan, and J. V. Badding, "Silicon p-i-n junction fibers," Adv. Mater. **25**, 1461–1467 (2013).
416. J. Ballato and P. Dragic, "Rethinking optical fiber: new demands, old glasses," J. Am. Ceram. Soc. **96**, 2675–2692 (2013).
417. S. Morris, T. Hawkins, P. Foy, J. Hudson, L. Zhu, R. Stolen, R. Rice, and J. Ballato, "On loss in silicon core optical fibers," Opt. Mater. Express **2**, 1511–1519 (2012).
418. N. Healy, J. R. Sparks, P. J. A. Sazio, J. V. Badding, and A. C. Peacock, "Tapered silicon optical fibers," Opt. Express **18**, 7596–7601 (2010).
419. S. Morris, T. Hawkins, P. Foy, J. Ballato, S. W. Martin, and R. Rice, "Cladding glass development for semiconductor core optical fibers," Int. J. Appl. Glass Sci. **3**, 144–153 (2012).
420. J. A. Harrington, "A review of IR transmitting, hollow waveguides," Fiber Integr. Opt. **19**, 211–227 (2000).
421. A. Hongo, K. Morosawa, K. Matsumoto, T. Shiota, and T. Hashimoto, "Transmission of kilowatt-class CO_2-laser light through dielectric-coated metallic hollow wave-guides for material processing," Appl. Opt. **31**, 5114–5120 (1992).
422. D. N. Su, S. Somkuarnpanit, D. R. Hall, and J. D. C. Jones, "Thermal effects in a hollow waveguide beam launch for CO_2 laser power delivery," Appl. Opt. **35**, 4787–4789 (1996).
423. J. D. Shephard, W. N. MacPherson, R. R. J. Maier, J. D. C. Jones, D. P. Hand, M. Mohebbi, A. K. George, P. J. Roberts, and J. C. Knight, "Single-mode mid-IR guidance in a hollow-core photonic crystal fiber," Opt. Express **13**, 7139–7144 (2005).
424. F. Poletti, "Nested antiresonant nodeless hollow core fiber," Opt. Express **22**, 23807–23828 (2014).
425. J. R. Hayes, F. Poletti, M. S. Abokhamis, N. V. Wheeler, N. K. Baddela, and D. J. Richardson, "Anti-resonant hexagram hollow core fibers," Opt. Express **23**, 1289–1299 (2015).

426. M. Duguay, Y. Kokubun, T. Koch, and L. Pfeiffer, "Antiresonant reflecting optical waveguides in SiO_2=-i multilayer structures," Appl. Phys. Lett. **49**, 13–15 (1986).
427. I. Garcés, F. Villuendas, J. A. Valles, C. Domínguez, and M. Moreno, "Analysis of leakage properties and guiding conditions of rib antiresonant reflecting optical waveguides," J. Lightwave Technol. **14**, 798–805 (1996).
428. N. Litchinitser, A. Abeeluck, C. Headley, and B. Eggleton, "Antiresonant reflecting photonic crystal optical waveguides," Opt. Lett. **27**, 1592–1594 (2002).
429. D. Yin, H. Schmidt, J. Barber, and A. Hawkins, "Integrated ARROW waveguides with hollow cores," Opt. Express **12**, 2710–2715 (2004).
430. E. J. Lunt, P. Measor, B. S. Phillips, S. Kühn, H. Schmidt, and A. R. Hawkins, "Improving solid to hollow core transmission for integrated ARROW waveguides," Opt. Express **16**, 20981–20986 (2008).
431. D. O. Carvalho and M. I. Alayo, "a-SiC:H anti-resonant layer ARROW waveguides," J. Opt. A Pure Appl. Opt. **10**, 104002 (2008).
432. V. Balan, C. Vigreux, A. Pradel, A. Llobera, C. Dominguez, M. Alonso, and M. Garriga, "Chalcogenide glass-based rib ARROW waveguide," J. Non-Cryst. Solids **326**, 455–459 (2003).
433. D. Yin, J. Barber, A. Hawkins, and H. Schmidt, "Waveguide loss optimization in hollow-core ARROW waveguides," Opt. Express **13**, 9331–9336 (2005).
434. A. N. Kolyadin, A. F. Kosolapov, A. D. Pryamikov, A. S. Biriukov, V. G. Plotnichenko, and E. M. Dianov, "Light transmission in negative curvature hollow core fiber in extremely high material loss region," Opt. Express **21**, 9514–9519 (2013).
435. T. Lewi, J. Ofek, and A. Katzir, "Antiresonant reflecting microstructured optical fibers for the mid-infrared," Appl. Phys. Lett. **102**, 101104 (2013).
436. N. M. Litchinitser, S. C. Dunn, B. Usner, B. J. Eggleton, T. P. White, R. C. McPhedran, and C. M. de Sterke, "Resonances in microstructured optical waveguides," Opt. Express **11**, 1243–1251 (2003).
437. P. Steinvurzel, B. Kuhlmey, T. White, M. Steel, C. de Sterke, and B. Eggleton, "Long wavelength anti-resonant guidance in high index inclusion microstructured fibers," Opt. Express **12**, 5424–5433 (2004).
438. A. Argyros, S. G. Leon-Saval, J. Pla, and A. Docherty, "Antiresonant reflection and inhibited coupling in hollow-core square lattice optical fibres," Opt. Express **16**, 5642–5648 (2008).
439. K. J. Rowland, S. Afshar V., and T. M. Monro, "Bandgaps and antiresonances in integrated-ARROWs and Bragg fibers; a simple model," Opt. Express **16**, 17935–17951 (2008).
440. A. D. Pryamikov, A. S. Biriukov, A. F. Kosolapov, V. G. Plotnichenko, S. L. Semjonov, and E. M. Dianov, "Demonstration of a waveguide regime for a silica hollow-core microstructured optical fiber with a negative curvature of the core boundary in the spectral region > 3.5 μm," Opt. Express **19**, 1441–1448 (2011).
441. N. Healy, J. Sparks, R. He, P. Sazio, J. Badding, and A. Peacock, "High index contrast semiconductor ARROW and hybrid ARROW fibers," Opt. Express **19**, 10979–10985 (2011).
442. J.-Y. Lu, C.-P. Yu, H.-C. Chang, H.-W. Chen, Y.-T. Li, C.-L. Pan, and C.-K. Sun, "Terahertz air-core microstructure fiber," Appl. Phys. Lett. **92**, 064105 (2008).

443. C.-H. Lai, B. You, J.-Y. Lu, T.-A. Liu, J.-L. Peng, C.-K. Sun, and H.-C. Chang, "Modal characteristics of antiresonant reflecting pipe waveguides for terahertz waveguiding," Opt. Express **18**, 309–322 (2010).
444. P. Jaworski, F. Yu, R. R. Maier, W. J. Wadsworth, J. C. Knight, J. D. Shephard, and D. P. Hand, "Picosecond and nanosecond pulse delivery through a hollow-core negative curvature fiber for micro-machining applications," Opt. Express **21**, 22742–22753 (2013).
445. A. Hartung, J. Kobelke, A. Schwuchow, K. Wondraczek, J. Bierlich, J. Popp, T. Frosch, and M. A. Schmidt, "Double antiresonant hollow core fiber—guidance in the deep ultraviolet by modified tunneling leaky modes," Opt. Express **22**, 19131–19140 (2014).
446. F. Yu, W. J. Wadsworth, and J. C. Knight, "Low loss silica hollow core fibers for 3–4 μm spectral region," Opt. Express **20**, 11153–11158 (2012).
447. W. Belardi and J. C. Knight, "Hollow antiresonant fibers with low bending loss," Opt. Express **22**, 10091–10096 (2014).
448. W. Belardi and J. C. Knight, "Hollow antiresonant fibers with reduced attenuation," Opt. Lett. **39**, 1853–1856 (2014).
449. A. F. Kosolapov, A. D. Pryamikov, A. S. Biriukov, V. S. Shiryaev, M. S. Astapovich, G. E. Snopatin, V. G. Plotnichenko, M. F. Churbanov, and E. M. Dianov, "Demonstration of CO_2-laser power delivery through chalcogenide-glass fiber with negative-curvature hollow core," Opt. Express **19**, 25723–25728 (2011).
450. K. D. Laakmann and M. B. Levy, "Hollow lightpipe and lightpipe tip using a low refractive index inner layer," U.S. patent 5,005,944 A (April 9, 1991).
451. M. Miyagi, A. Hongo, Y. Aizawa, and S. Kawakami, "Fabrication of germanium-coated nickel hollow waveguides for infrared transmission," Appl. Phys. Lett. **43**, 430–432 (1983).
452. P. Bhardwaj, O. Gregory, C. Morrow, G. Gu, and K. Burbank, "Performance of a dielectric-coated monolithic hollow metallic waveguide," Mater. Lett. **16**, 150–156 (1993).
453. Y. Matsuura and M. Miyagi, "Er: YAG, CO, and CO_2 laser delivery by ZnS-coated Ag hollow waveguides," Appl. Opt. **32**, 6598–6601 (1993).
454. H. Machida, Y. Matsuura, H. Ishikawa, and M. Miyagi, "Transmission properties of rectangular hollow waveguides for CO_2 laser light," Appl. Opt. **31**, 7617–7622 (1992).
455. S. J. Saggese, J. A. Harrington, and G. H. Sigel, "Attenuation of incoherent infrared radiation in hollow sapphire and silica waveguides," Opt. Lett. **16**, 27–29 (1991).
456. M. Saito, Y. Matsuura, M. Kawamura, and M. Miyagi, "Bending losses of incoherent light in circular hollow waveguides," J. Opt. Soc. Am. A **7**, 2063–2068 (1990).
457. A. Hongo, S. Sato, A. Hattori, K. Iwai, T. Hiroyuki, and M. Miyagi, "AgI-coated silver-clad stainless steel hollow waveguides for infrared lightwave transmission and their applications," Appl. Opt. **51**, 1–7 (2012).
458. D. J. Haan and J. A. Harrington, "Hollow waveguides for gas sensing and near-IR applications," Proc. SPIE **3596**, 43–49 (1999).
459. D. A. Pinnow, A. L. Gentile, A. G. Standlee, A. J. Timper, and L. M. Hobrock, "Polycrystalline fiber optical-waveguides for infrared transmission," Appl. Phys. Lett. **33**, 28–29 (1978).

460. E. Rave, P. Ephrat, M. Goldberg, E. Kedmi, and A. Katzir, "Silver halide photonic crystal fibers for the middle infrared," Appl. Opt. **43**, 2236–2241 (2004).
461. S. Sakuragi, T. Morikawa, J. Shimada, M. Saito, Y. Kubo, K. Imagawa, and H. Kotani, "KRS-5 optical fibers capable of transmitting high-power CO_2 laser beam," Opt. Lett. **6**, 629–631 (1981).
462. T. Lewi, A. Tsun, A. Katzir, J. Kaster, and F. Fuchs, "Silver halide single mode fibers for broadband middle infrared stellar interferometry," Appl. Phys. Lett. **94**, 261105 (2009).
463. V. Artyushenko, A. Bocharnikov, T. Sakharova, and I. Usenov, "Mid-infrared fiber optics for 1–18 μm range," Opt. Photon. **9**, 35–39 (2014).
464. N. Granzow, M. Schmidt, W. Chang, L. Wang, Q. Coulombier, J. Troles, P. Toupin, I. Hartl, K. Lee, and M. Fermann, "Mid-infrared supercontinuum generation in As_2S_3-silica 'nano-spike' step-index waveguide," Opt. Express **21**, 10969–10977 (2013).
465. S. R. Xie, F. Tani, J. C. Travers, P. Uebel, C. Caillaud, J. Troles, M. A. Schmidt, and P. S. J. Russell, "As_2S_3-silica double-nanospike waveguide for mid-infrared supercontinuum generation," Opt. Lett. **39**, 5216–5219 (2014).
466. M. A. Schmidt, N. Granzow, N. Da, M. Peng, L. Wondraczek, and P. St. J. Russell, "All-solid bandgap guiding in tellurite-filled silica photonic crystal fibers," Opt. Lett. **34**, 1946–1948 (2009).
467. N. Granzow, P. Uebel, M. A. Schmidt, A. S. Tverjanovich, L. Wondraczek, and P. S. J. Russell, "Bandgap guidance in hybrid chalcogenide–silica photonic crystal fibers," Opt. Lett. **36**, 2432–2434 (2011).
468. M. Karim, B. Rahman, and G. P. Agrawal, "Mid-infrared supercontinuum generation using dispersion-engineered $Ge_{11.5}As_{24}Se_{64.5}$ chalcogenide channel waveguide," Opt. Express **23**, 6903–6914 (2015).
469. T. Cheng, L. Zhang, X. Xue, D. Deng, T. Suzuki, and Y. Ohishi, "Broadband cascaded four-wave mixing and supercontinuum generation in a tellurite microstructured optical fiber pumped at 2 μm," Opt. Express **23**, 4125–4134 (2015).
470. C. Kneis, B. Donelan, A. Berrou, I. Manek-Hönninger, B. Cadier, T. Robin, M. Poulain, F. Joulain, M. Eichhorn, and C. Kieleck, "4.5 W mid-infrared supercontinuum generation in a ZBLAN fiber pumped by a Q-switched mode-locked Tm^{3+}- doped fiber laser," Proc. SPIE **9342**, 93420B (2015).
471. B. Zhang, W. Guo, Y. Yu, C. Zhai, S. Qi, A. Yang, L. Li, Z. Yang, R. Wang, D. Tang, G. Tao, and B. Luther-Davies, "Low loss, high NA chalcogenide glass fibers for broadband mid-infrared supercontinuum generation," J. Am. Ceram. Soc. (to be published).
472. W. Kim, V. Nguyen, L. Shaw, L. Busse, C. Florea, D. Gibson, R. Gattass, S. Bayya, F. Kung, and G. Chin, "Recent progress in chalcogenide fiber technology at NRL," J. Non-Cryst. Solids (to be published).
473. H. Saghaei, M. Ebnali-Heidari, and M. K. Moravvej-Farshi, "Midinfrared supercontinuum generation via As_2Se_3 chalcogenide photonic crystal fibers," Appl. Opt. **54**, 2072–2079 (2015).
474. T. Udem, R. Holzwarth, and T. W. Hansch, "Optical frequency metrology," Nature **416**, 233–237 (2002).
475. T. Ideguchi, S. Holzner, B. Bernhardt, G. Guelachvili, N. Picque, and T. W. Hansch, "Coherent Raman spectro-imaging with laser frequency combs," Nature **502**, 355–358 (2013).

476. B. R. Washburn, S. A. Diddams, N. R. Newbury, J. W. Nicholson, M. F. Yan, and C. G. Jrgensen, "Phase-locked, erbium-fiber-laser-based frequency comb in the near infrared," Opt. Lett. **29**, 250–252 (2004).
477. J.-C. Beugnot, R. Ahmad, M. Rochette, V. Laude, H. Maillotte, and T. Sylvestre, "Reduction and control of stimulated Brillouin scattering in polymer-coated chalcogenide optical microwires," Opt. Lett. **39**, 482–485 (2014).
478. M. Karlowatz, M. Kraft, E. Eitenberger, B. Mizaikoff, and A. Katzir, "Chemically tapered silver halide fibers: an approach for increasing the sensitivity of mid-infrared evanescent wave sensors," Appl. Spectrosc. **54**, 1629–1633 (2000).
479. D. T. Schaafsma, J. A. Moon, J. S. Sanghera, and I. D. Aggarwal, "Fused taper infrared optical fiber couplers in chalcogenide glass," J. Lightwave Technol. **15**, 2242–2245 (1997).
480. Z. Chen, A. J. Taylor, and A. Efimov, "Coherent mid-infrared broadband continuum generation in non-uniform ZBLAN fiber taper," Opt. Express **17**, 5852–5860 (2009).
481. N. Bozinovic, Y. Yue, Y. Ren, M. Tur, P. Kristensen, H. Huang, A. E. Willner, and S. Ramachandran, "Terabit-scale orbital angular momentum mode division multiplexing in fibers," Science **340**, 1545–1548 (2013).

Guangming Tao received his B.Eng. in 2006 from Shandong University, M.Sc. in 2009 from Fudan University, and Ph.D. in 2014 from the University of Central Florida in optics/optoelectronics. He was a visiting scholar at the Chinese Academy of Science (2007, 2008) and the Massachusetts Institute of Technology (2012) and an infrared material engineer at LightPath Technologies (2012, 2013). He is a Research Scientist at CREOL, The College of Optics & Photonics, the University of Central Florida. He has been awarded several scholarships/honors from The Optical Society (OSA), the International Society of Optical Engineering (SPIE), and the American Ceramic Society (ACerS), and was awarded the *Extraordinary Potential Prize* of the Chinese Government Award for Outstanding Self-financed Students Abroad (2013). Dr. Tao is also a cofounder and CTO of Lambda Photonics LLC (2014), an IR fiber startup company that developed out of his Ph.D. work. He has years of research experience in sciences and engineering in academia, industry, and government institutes with expertise in the areas of infrared material, infrared fiber and fiber laser, in-fiber nanofabrication, in-fiber energy devices, and novel smart fibers with unique functionalities.

Heike Ebendorff-Heidepriem received the Ph.D. degree in chemistry from the University of Jena, Germany, in 1994, where she continued her research on optical glasses until 2000. During 2001–2004 she was with the Optoelectronics Research Centre at the University of Southampton, UK, working on novel photosensitive glasses and soft-glass microstructured optical fibers with record high nonlinearity. Since 2005, she has been with the University of

Adelaide, Australia. Currently, she is one of the leaders of the Optical Materials & Structures Theme at the Institute for Photonics & Advanced Sensing at The University of Adelaide. She was awarded the Woldemar A. Weyl International Glass Science Award and a prestigious EU Marie Curie Individual Fellowship in 2001. Her research focuses on the development of mid-infrared, high-nonlinearity and active glasses; glass, preform and fiber fabrication techniques; and surface functionalization of glass.

Alexander M. Stolyarov received a Ph.D. in Applied Physics from Harvard University in 2012. His doctoral and postdoctoral research was conducted in the group of Prof. Yoel Fink at MIT, where he worked on novel multi-material fiber structures, including microfluidic fiber lasers, liquid crystal fiber devices, chemical sensing fibers, and hollow-core photonic bandgap fibers for high-power laser transmission. Alexander has coauthored 15 journal publications and holds two U.S. patents. Currently, he is a member of the technical staff in the Chemical, Microsystem, and Nanoscale Technologies Group at MIT Lincoln Laboratory.

Sylvain Danto received his Ph.D. in Materials Science from the University of Rennes (France) in 2005 where he worked on tellurium-based glasses for data storage and infrared optics. Next he joined the group of Prof. Y. Fink at MIT, where he developed the *in-fiber* glass/crystal phase-change capability for fiber-based optoelectronics, and then the group of Prof. K. Richardson at Clemson University in 2011. He is currently working at the University of Bordeaux, where he continues his research on glasses for applications in optics and photonics.

John V. Badding is a professor in the Chemistry Department and the Department of Physics & Astronomy at Pennsylvania State University. He received his doctorate from U.C. Berkeley in 1989. After postdoctoral work in high-pressure science as a Carnegie Fellow at the Geophysical Laboratory of the Carnegie Institution of Washington, he moved to Penn State in 1991. He visited the Optoelectronics Research Center at the University of Southampton for a year in 2001. His research interests are in the area of materials chemistry relevant to fields such as photonics, carbon nanomaterials, semiconductor nanomaterials, and polymers. His group has pioneered the high-pressure chemical vapor deposition approach to the fabrication metal and semiconductor optical fibers for applications such as solar fabrics, high-speed in-fiber junction detectors, and very-high-power infrared fibers and lasers. Both unary semiconductors and compound semiconductors that are difficult to draw in pure form can be deposited by this method. He is the author of 190 publications and has received both NSF and David and Lucile Packard Foundation fellowships.

Yoel Fink is a professor of materials science and engineering and Director of the Research Laboratory of Electronics (RLE) at the Massachusetts Institute of Technology (MIT). Professor Fink received a B.Sc. in Chemical Engineering (1994) and a B.A. degree in Physics (1995) from the Technion, Haifa. In 2000 he was awarded a Ph.D. degree in Materials Science from MIT. That same year, he joined the faculty of the MIT Materials Science and Engineering Department, and in 2011 he became a joint professor of electrical engineering and computer science. He was a recipient of the Weizmann Institute Amos De-Shalit Foundation Scholarship in 1992, was awarded the Hershel Rich Technion Innovation Competition in 1994, was a recipient of the Technology Review Award for the 100 Top Young Innovators in 1999, and was awarded the National Academy of Sciences Initiatives in Research Award for 2004. In 2006 he won the Joseph Lane Award for Excellence in Teaching, and in 2007 was named one of the MIT MacVicar Fellows, an award given in recognition of outstanding teaching abilities. Professor Fink's research group has pioneered the field of multimaterial multifunctional fibers. His research focuses on extending the frontiers of fiber materials from optical transmission to encompass electronic, optoelectronic, and even acoustic properties. Professor Fink is a co-founder of OmniGuide Inc. (2000) and served as its chief executive officer from 2007 to 2010; he is currently an active member the Board. He is the coauthor of over 75 scientific journal articles, and holds 44 issued U.S. patents on photonic fibers and devices.

John Ballato is Vice President for Economic Development at Clemson University. A professor of materials science and engineering and electrical and computer engineering, he founded and directed for 14 years the Center for Optical Materials Science and Engineering Technologies (COMSET). Dr. Ballato has published 300 archival scientific papers, holds over 25 U.S. and foreign patents, has given in excess of 150 keynote/invited lectures, and has co-organized 70 national and international conferences and symposia. He has been a Principal Investigator on more than $46 million worth of sponsored programs. Among numerous other honors, he is a Fellow of The Optical Society (OSA), the International Society of Optical Engineering (SPIE), and the American Ceramic Society (ACerS).

Ayman F. Abouraddy received the B.S. and M.S. degrees from Alexandria University, Alexandria, Egypt, in 1994 and 1997, respectively, and the Ph.D. degree from Boston University, Boston, Massachusetts, in 2003, all in electrical engineering. In 2003 he joined the Massachusetts Institute of Technology (MIT), Cambridge, as a postdoctoral fellow working with Prof. Yoel Fink and Prof. John D. Joannopoulos, and then became a Research Scientist at the Research Laboratory of Electronics in 2005. At MIT he pursued research on novel multimaterial optical fiber structures, photonic bandgap fibers,

nanophotonics, fiber-based optoelectronic devices, and mid-infrared nonlinear fiber optics. He is the coauthor of more than 60 journal publications and 130 conference presentations, holds seven patents, and has three patents pending. He joined CREOL, The College of Optics & Photonics, at the University of Central Florida as an assistant professor in September 2008, where he has since established facilities for fabricating new classes of polymer and soft-glass fibers for applications ranging from mid-infrared optics to solar energy concentration.